Studies on the epithelial injury-related molecules inducing the urinary system disorders in animals

（動物の泌尿器異常を導く上皮障害関連分子の研究）

Takashi NAMBA

Contents

Abbreviations

Actb: beta, actin
Ac-lysine: acetylated lysine
AKI: acute kidney injury
AP-1: activator protein 1
α-SMA: alpha smooth muscle actin
BrdU: bromodeoxyuridine
BSA: bovine serum albumin
BUN: blood urea nitrogen
B6: C57BL/6N
CD: cluster of differentiation
COL17A1: collagen 17A1
CK: cytokeratin
CKD: chronic kidney disease
Cr: creatinine
CXCL: C-X-C motif chemokine ligand
d: day
dsDNA: double stranded DNA
FGF: fibroblast growth factor
FOS: Fos proto-oncogene, AP-1 transcription factor subunit
GCN5: general control non-depressible 5
GO: gene ontology
h: hour
HNF-4α: hepatic nuclear factor 4, alpha
IBA-1: ionized calcium-binding adapter molecule
IF: immunofluorescence
IHC: immunohistochemistry
IL: interleukin
IL-1RAPL1: IL-1R accessory protein-like 1
IL-1RL2: IL-1R like 2
IRI: ischemic reperfusion injury
ISH: *in situ* hybridization
Itgam: integrin alpha M
JUN: Jun proto-oncogene, AP-1 transcription factor subunit
KO: knockout
LN: lupus nephritis
MAPK: mitogen-activated protein kinase
MRL/lpr: MRL/MpJ-*Fas*$^{lpr/lpr}$
MRL/+: MRL/MpJ
NBF: neutral buffered formalin
NF-κB: nuclear factor kappa B
NLRP3: nucleotide- binding oligomerization domain-like receptor family pyrin domain containing 3
OCLN: occludin
PAS-H: periodic acid Schiff-hematoxylin
PBS: phosphate-buffered saline
PDGFRα: platelet-derived growth factor R alpha
qPCR: quantitative polymerase chain reaction
R: receptor
Ra: receptor antagonist
rh: recombinant human
SE: standard error
Sham: sham-operation
SLE: systemic lupus erythematosus
S/B ratio: weight ratio of spleen to body
TEM: transmission electron microscopy
TJP: tight junction protein
TNF-α: tumor necrosis factor alpha
uACR: urinary albumin to creatinine ratio
UEB: urine-epithelium barrier
Upk2: uroplakin 2
UTALS: urinary tract associated lymphoid structure
UUO: unilateral ureteral obstruction
WT: wild-type
ZO-1: zonula occludens-1

Preface

Kidneys have key roles in regulating systemic homeostasis in animal bodies, such as eliminating extra fluid and wastes, adjusting serum mineral level, and contributing to hematopoiesis; therefore, chronic kidney disease (CKD) is one of the major causes of death in mammals. In 2017, over 1.2 million people died from CKD throughout the world, and its mortality rate increased by 41.5% since 1990. Moreover, CKD prevalence at all ages was around 9.1%, and more than 10 million people suffered from the disease in 12 countries including Japan [13]. In veterinary medicine, it is also reported that approximately 4.2% and 12.1% of dogs and cats die from renal disorders in UK, respectively [74,96]. Importantly, 80.9% of cats over 15-year-old develop CKD [84]. However, the pathological features in CKD differ among disease causes and animals; cats mainly manifest tubulointerstitial lesions rather than glomerular lesions, and the opposite is true in dogs [58]. For both animals and humans, it is still challenging to diagnose CKD at the early stage to prevent the further disease progression.

CKD is defined as functional, morphological, or both abnormalities of the kidneys that persist for more than 3 months, regardless of the underlying causes [129]. CKD is also developed in more than 20% of the patients with acute kidney injury (AKI), which mainly is divided into three pathophysiology; pre-, intrinsic-, and post-renal injuries [7,82,101]. Pre-renal injury indicates that decreased blood-supply into kidneys, caused by dehydration, bleeding, and heart failure, results in impaired excretion of waste products through blood [82]. In intrinsic-renal injuries, glomeruli, tubulointerstitium, and vasculatures in the kidneys are injured by aging, autoimmune diseases, polyarteritis nodosa, several drugs, and ischemia [82]. Obstruction of urine outflow from kidneys caused by anatomical defect, urolithiasis, bacterial infection, cystitis, and neoplasia induces post renal injury characterized by the dilation of urinary tracts upstream from the obstructed area, including hydroureteronephrosis with tubulointerstitial lesions [82].

Urinary system includes kidneys, renal pelvis, ureters, urinary bladder, and urethra, and produces and eliminates urine. They are lined by epithelial cells, such as renal epithelial cells and urothelial cells, and these epithelial cells form urine-epithelium barriers (UEBs) which function as the borders between urine and tissue parenchyma in urinary system. In renal epithelial cells, podocytes with glomerular basement membrane and endothelial cells have a function for blood filtration barrier [87]. Then, tubular and collecting duct epithelial cells reabsorb or secrete water, glucose, and mineral ions from or into the primitive urine. Urothelial cells covering renal pelvis to urethra accommodate a large change of urine amount by stretchable and impermeable characteristics, and UEB protects tissues under the urothelium, regardless of germ layer origins [68]; the urothelial cells from kidneys including renal pelvis to ureters are mainly derived from mesoderm, while those from urinary bladder to urethra are from endoderm.

CKD causes renal epithelial cell injuries in the kidney and urinary tracts, resulting in UEB disruptions. Briefly, albumin is hyper-filtrated from glomeruli with injured podocytes, and parietal epithelial cells move to the glomerular tuft with damaged podocytes and seal the disrupted filtration barrier, leading to glomerular sclerotic lesion development [40]. Further, some of damaged tubular epithelial cells undergo epithelial-mesenchymal transition, leading to chronic fibrosis [44]. In urothelial cells of chronic nephritis, UEB disruptions in renal pelvis with altered expression of tight junction proteins (TJPs) allow urine to penetrate into the parenchyma from the renal pelvis lumen, contributing to development of urinary tract associated lymphoid structures (UTALSs), which are tertiary lymphoid structures formed under the urothelium [54]. These UEB disruptions by renal epithelial cell injuries are involved in inflammatory mediators such as interleukin 1β (IL-1β), tumor necrosis factor α (TNF-α), and interferon γ (IFN-γ), and collagen family [61,103,104]. Importantly, those produced by the epithelial cells can be therapeutic targets and be detectable from urine as diagnosis markers.

Recently, it is reported that IL-36α belonging to IL-1 family is upregulated in injured distal tubular epithelial cells of the kidneys in CKD- or AKI-developing mice as well as human patients with the renal diseases [28,94]. Although its specific receptor, IL-36 receptor (R) has another four ligands, including IL-36β, IL-36γ, IL-36 receptor antagonist (Ra), and IL-38, those expression and localization in kidneys in addition to the interactions with each other have not yet examined [45]. Furthermore, a recent study reported that the renal pelvis in mice and human kidneys with CKD presents ectopic overexpression of collagen 17A1 (COL17A1) in the urothelial cells covering UTALSs [54]. For skin studies, COL17A1 is constitutively expressed in keratinocytes as a hemidesmosome component, while it can be an autoantigen for bullous pemphigoid [121]; however, its functions in urothelial cells are still unclear. Thus, these molecules have a potential for UEB disruption-related disease markers, but they have not been investigated in veterinary fields.

In the thesis, the author analyzes injured renal epithelial and urothelial cell-associated pathological molecules to evaluate UEB disruptions. The first and second chapters focus on IL-36 family and examine the altered expression and localization of IL-36R and its ligands by using the spontaneous nephritis model mice. In the third chapter, the author focuses on COL17A1 functions in the urinary system of mouse showing obstructive uropathy. Moreover, both IL-36R and COL17A1 expression are analyzed in the urinary organs of humans and/or cats. Thus, the present study provides novel findings to understand the pathological mechanism of UEB disruption-related diseases and develop their marker molecules applicable in animals and humans.

Notes

Contents of this thesis are partially published in the following article list. The number of each article is corresponding to chapter number.

Consist of this research

1. Namba T, Ichii O, Nakamura T, Masum MA, Otani Y, Hosotani M, Elewa YHA, Kon Y. Compartmentalization of interleukin 36 subfamily according to inducible and constitutive expression in the kidneys of a murine autoimmune nephritis model. Cell Tissue Res 386(1):59-77, 2021.
2. Namba T, Ichii O, Okamura T, Nakano K, Nakamura T, Otani Y, Kon Y. Ameliorated renal pathological feature in MRL/MpJ-*Fas*$^{lpr/lpr}$ background interleukin-36 receptor deficient mice. Microsc Microanal, in press.
3. Namba T, Ichii O, Natsuga K, Nakamura T, Otani Y, Kon Y. Collagen 17A1 in the urothelium regulates epithelial cell integrity and local immunological responses in obstructive uropathy. Under review.

Chapter 1

Interleukin 36 receptor pathway deteriorates renal epithelial injuries in autoimmune disease-mediated nephritis

Introduction

Renal epithelial cells, such as podocytes as well as proximal and distal tubular epithelial cells, have various roles in renal physiology including UEB formations. In CKD pathology, the renal epithelial cells show morpho-functional alterations including proliferation and injuries, leading to glomerular and tubulointerstitial lesions [129]. Several studies report that the latter lesions are closely associated with renal disfunction rather than the former, and tubular epithelial cells are regarded as inflammation- and fibrosis-inducer cells [16,77,80]. CKD is caused by several factors such as hypertension, drug use, and certain infections as well as immunological alternations presenting tubulointerstitial lesions [25,129]. For example, a complication of nephritis is frequently observed in systemic lupus erythematosus (SLE), a chronic autoimmune disease characterized by damaged systemic organs including the skin, spleen, kidneys, and/or central nervous system in conjunction with autoantibody production [139]. It has been reported that renal disorder due to lupus nephritis (LN) is diagnosed in approximately 50% of human, cat and dog patients with SLE [6,43,53]. Importantly, CKD development is strongly mediated by inflammatory cytokines and chemokines such as IL-1, TNF-α, and IFN-γ, and these factors are primarily produced by renal epithelial cells and hematopoietic cells recruited during inflammation [61,103].

The IL-1 family plays crucial roles in acute and chronic inflammation. In humans, this family is composed of 7 agonists (IL-1α, IL-1β, IL-18, IL-33, IL-36α, IL-36β, and IL-36γ) and 4 antagonists (IL-1Ra, IL-36Ra, IL-37, and IL-38), while mice lack IL-37 function [45]. Although these cytokines are produced in response to inflammation, some of the IL-1 family members are constitutively expressed in the mesenchymal cells and epithelial cells of several organs [45,83]. Briefly, IL-1α and IL-33 localize to type 2 alveolar and intestinal epithelial cells, respectively [83]. The IL-1 family is regulated through protein processing and by maintaining a balance between IL-1 family agonists and antagonists. Thus, an imbalance in IL-1 family members is induced during pathological development due to inflammation and genetic mutation, ultimately leading to disease progression [83].

A previous study revealed that IL-36α was overexpressed in injured epithelial cells of the distal tubules in several murine models of nephritis [55,56]. The IL-36 subfamily of the IL-1 family is comprised of IL-36α, IL-36β, IL-36γ, and IL-36Ra, which are also known as IL-1F6, IL-1F8, IL-1F9, and IL-1F5, respectively. All of the members of the IL-36 subfamily can bind to the IL-36R (known as IL-1R like 2 [IL-1RL2]) [45]. IL-36α, IL-36β, and IL-36γ function as agonists for IL-36R, and IL-36Ra in turn functions as their antagonist. Additionally, IL-38 (known as IL-1F10) is the putative antagonist for IL-36R, as it can bind to IL-36R and inhibit IL-36R signaling [45,102]. It has been reported that IL-36 agonists promote inflammatory responses in the lungs, skin, kidneys, and joints by activating mitogen-activated protein kinase (MAPK) and nuclear factor kappa B (NF-κB), and all IL-36R ligands in the skin and IL-36γ in the intestine are constitutively

expressed to facilitate the host response to infection [4,102]. In the kidneys, IL-36α expression positively correlates with the progression of tubulointerstitial lesions, including cell death, cell infiltration, and fibrosis in the murine kidneys with unilateral ureteral obstruction (UUO). *In vitro* experiments have shown that IL-36α production is induced in distal tubular epithelial cells by lipopolysaccharide, a toll-like receptor ligand [55]. Another study revealed that tubulointerstitial lesions were ameliorated in an IL-36R knockout (KO) mouse model with UUO or with renal ischemia-reperfusion injury (IRI) [28,94]. Furthermore, IL-36α levels were also increased in the kidneys and urine of patients with both acute kidney injury and CKD [28,94]. In regard to IL-38 function in the kidney, the injection improved the glomerular damage in MRL/MpJ-*Fas*$^{lpr/lpr}$ (MRL/lpr) mice, which are representative autoimmune disease-prone mice that are characterized by severe lymphadenopathy, splenomegaly, and nephritis; however, it must be noted that the presence of IL-38-producing cells remains undetermined in the kidney [29,32]. These studies suggest that the IL-36R ligands are involved in the development of renal disorders and has potential for use as a novel target for the treatment and diagnosis of various renal diseases.

In other tissues, the molecular crosstalk between IL-36R ligands and disease development has been more thoroughly characterized. Psoriasis is an immune-mediated inflammatory skin condition that exhibits an upregulation of IL-36α, IL-36β, IL-36γ, and IL-36Ra primarily in the keratinocytes of human patients and mouse models [14,15,62]. Furthermore, IL-36Ra-KO-mice presented with a more severe phenotype of psoriatic skin [15]. In patients with SLE, the serum levels of IL-36α and IL-36γ were positively correlated with the SLE disease activity index, although that of IL-36Ra was decreased [30,81]. Therefore, the expression patterns of the IL-36R ligands appear to differ among disease types. Additionally, it has been reported that IL-1 family members can induce production of other family members, as IL-1α can stimulate IL-36α to induce inflammation in the skin [45,88]. Although it is possible that IL-36R ligands closely interact with each other in the kidneys, their fine localization and biological functions remain unclear.

In this chapter, the author investigated MRL/lpr and MRL/MpJ (MRL/+) as a murine model of spontaneous nephritis and a healthy control, respectively, to elucidate the renal pathogenesis focusing on epithelial cell injuries. This study revealed differences in the localization of IL-36R ligands; specifically, IL-36γ and IL-36Ra were constitutively expressed in murine kidneys, while IL-36α, IL-36β, IL-36Ra, and IL-38 were induced in renal epithelial cells and mesenchymal cells of MRL/lpr mice. Moreover, the localization of IL-36R mRNA was common to the kidneys of mice and cats, which frequently develop CKD manifesting tubulointerstitial lesions [58,84]. These finding suggest that the IL-36R ligands are associated with both homeostasis and inflammation in the kidneys.

Material and Methods

Ethics statement

All animal experimentation was approved by the Institutional Animal Care and Use Committee of the Faculty of Veterinary Medicine, Hokkaido University (approved by the Association for Assessment and Accreditation of Laboratory Animal Care International, approval No. 16-0124, 20-0012 for mice).

Cat sample analysis

Feline kidneys showing normal histology was obtained from autopsied case in Faculty of Veterinary Medicine, Hokkaido University. Specimens were fixed with 10% neutral buffered formalin (NBF), and histological sections were used for *in situ* hybridization (ISH) of *IL-1RL2*.

Mouse sample preparation

Male and female MRL/+ and MRL/lpr mice at 3-7 months were purchased from Japan SLC, Inc. (Hamamatsu, Japan) and were housed in an air-conditioned animal room at 22 ± 4°C with a relative humidity of 50 ± 20% under specific pathogen-free conditions, with a 12 hour (h) light/dark cycle (07:00−19:00/19:00−07:00). All mice were fed a standard rodent CE-2 diet (CLEA Japan, Inc., Tokyo, Japan) and had ad libitum access to water.

Urine was collected by pressure urination and stored at -30°C. Under deep anesthesia using a mixture of medetomidine (0.3 mg/kg), midazolam (4 mg/kg), and butorphanol (5 mg/kg), body weight was measured, and blood samples were collected from the femoral arteries. The mice were then euthanized by cervical dislocation. The weights of the spleens were measured, and then the weight ratio of spleen to body (S/B ratio) was calculated.

Serological analysis and urinalysis

Serum levels of anti-double stranded DNA (dsDNA) antibody were measured as an index of systemic autoimmune condition using an LBIS Anti-dsDNA-Mouse ELISA Kit (FUJIFILM Wako Pure Chemical Corporation, Osaka, Japan) according to the manufacturer's instructions. Serum concentrations of creatinine (Cr) and blood urea nitrogen (BUN) were determined using a Fuji Dri-Chem 7000v instrument (FUJIFILM Medical Co., Ltd., Osaka, Japan) according to the manufacturer's instructions. Urinary levels of Cr and albumin were measured using a Urinary Creatinine Assay Kit (Detroit R&D, Inc., Detroit, MI, USA) and an LBIS Mouse Albumin ELISA Kit (FUJIFILM Wako Pure Chemical Corporation), respectively, and the urinary albumin-to-creatinine ratio (uACR) was then calculated.

Histological analysis

Murine kidneys were fixed overnight using 10% NBF at room temperature or 4% paraformaldehyde at 4°C. Specimens were routinely dehydrated using ethanol and then embedded in paraffin. Paraffin sections (2-μm thick) fixed with 10% NBF were prepared and stained with periodic acid Schiff-hematoxylin (PAS-H) to analyze renal histopathology.

Immunohistochemistry (IHC) and immunofluorescence (IF)

IHC and/or IF analyses for B220, cluster of differentiation 3 (CD3), ionized calcium-binding adapter molecule 1 (IBA-1), Gr-1, CD138, CD44, alpha smooth muscle actin (α-SMA), tyrosine hydroxylase, calbindin-D28k, hepatic nuclear factor 4 alpha (HNF-4α), and phosphorylated (p)-NF-κB-p65 were performed to detect B cells, T cells, macrophages, neutrophils, plasma cells, activated parietal epithelial cells, smooth muscle cells, sympathetic neurons, distal convoluted tubules, proximal tubules, and activated NF-κB-p65, respectively. Similar assays for IL-36α, IL-36β, IL-36γ, IL-36Ra, and IL-38 were also performed for the localization analysis. Paraffin sections (2-μm thick) fixed with 4% paraformaldehyde were deparaffinized and then antigen retrieved. To block internal peroxidase activity for IHC, the sections were soaked in methanol containing 0.3% H_2O_2 for 20 min at room temperature. After washing three times in phosphate-buffered saline (PBS), the sections were incubated with blocking serum for 1 h at room temperature to block the non-specific sites. Then, sections were incubated with primary antibodies overnight at 4°C. Subsequently, the sections were washed three times in PBS and were then incubated with secondary antibodies for 30 min at room temperature. After washing three times in PBS, the sections for IHC were incubated with streptavidin-conjugated horseradish peroxidase (SABPOI kit; Nichirei, Tokyo, Japan) for 30 min at room temperature and subsequently washed three times in PBS. Then, the immunopositive reaction was visualized using 3,3'-diaminobenzidine tetrahydrochloride-H_2O_2 solution. Finally, the sections were lightly stained with hematoxylin. For IF, the tissue sections were incubated with Hoechst 33342 (1:500; FUJIFILM Wako Pure Chemical Corporation) for nuclear staining at room temperature for 30 min and then washed three times. This was followed by examinations under an All-in-one Fluorescence Microscope BZ-X710 (Keyence, Osaka, Japan). The details of the antibodies, antigen retrieval, blocking and combination of multiple IF are listed in Table 1-1.

ISH

For ISH, NBF-fixed paraffin-embedded sections were assessed using an RNAscope 2.5 assay following the manufacturer's instructions, and all reagents and equipment for hybridization was purchased from Advanced Cell Diagnostics, Inc. (Hayward, CA, USA). Paraffin sections (5-μm thick) were air-dried overnight and then baked in HybEZ II oven for 1 h at 60°C. All procedures for ISH were performed using RNAscope 2.5 HD Reagent Kit-BROWN (#322300;

Advanced Cell Diagnostics, Inc.) following the manufacturer's instructions. RNAscope Target probe-Mm-*Il1rl2* (Mouse, #403761) and custom-ordered probe-Fc-*IL1RL2* (Cat, #1118131-C1) were used. Further, the author performed ISH for *Il1rl2* followed by PAS-H staining to distinguish between proximal and distal tubules in mice.

Histoplanimetry

In PAS-H stained sections, 30 glomeruli that showed a vascular and/or urinary pole were selected, and the number of nuclei in the glomerulus, the size, and the area ratio of PAS^+ mesangium to glomerulus were all measured and calculated using NDP. view2 (Hamamatsu Photonics Co., Ltd., Hamamatsu, Japan) and a BZ-X Analyzer (Keyence). To evaluate infiltrated cells, including $B220^+$ B cells, $CD3^+$ T cells, IBA-1^+ macrophages, and Gr-1^+ neutrophils, the number was counted within 30 glomeruli with a vascular and/or urinary pole using NDP.view2. These cells were also counted in 20 tubulointerstitial areas at 400× magnification, which were first selected in the renal cortex at 4× magnification and then replaced to exclude glomeruli, and the averages per area were then calculated. For quantification of IL-36α, the number of IL-36α^+ tubules and renal corpuscles in the cortex area was calculated in 3 sections from each mouse. Then, the number of IL-36α^+ tubules was divided by the cortex area, and the ratio of IL-36α^+ renal corpuscle number to total renal corpuscle number was calculated. In 25 renal corpuscles from each male MRL/lpr mice at 6-7 months, the IL-36α^+ parietal epithelial cell ratio was examined in $CD44^+$ or $CD44^-$ parietal epithelial cells using a BZ-X Analyzer. To evaluate IL-38, the number of positive cells was counted in 20 tubulointerstitial areas at 400x magnification using NDP. view2, and the averages per area were then calculated.

Quantitative polymerase chain reaction (qPCR)

Kidneys were soaked in RNA later solution (#R0901; Merck KgaA, Darmstadt, Germany) at 4°C and then stored at -80°C after the solution was removed. Total RNA from kidneys was purified using TRIzol reagent (#15596018; Thermo Fisher Scientific) following the manufacturer's instructions. The purified total RNA was treated as a template to synthesize cDNA using ReverTra Ace qPCR RT Master Mix (#FSQ-301; Toyobo Co., Ltd., Osaka, Japan). qPCR analysis was performed on the cDNA (20 ng/μl) using THUNDERBIRD® SYBR® qPCR Mix (#QPS-101; Toyobo Co., Ltd.), gene-specific primers (Table 1-2) and a real-time thermal cycler (CFX Connect; BIO-RAD, Santa Rosa, CA, USA). The qPCR cycling conditions were as follows: 95°C for 1 min, (95°C for 15 s, 60°C for 45 s [40 cycles]). The data were normalized according to the values of beta, actin (*Actb*), and those of female MRL/+ mice at 3 months using the delta-delta Ct method.

Microarray analysis

Similar to the qPCR analysis, total RNA was isolated from the kidneys of female MRL/+ and MRL/lpr mice at 6 months (n= 3). RNA integrity was validated using an Agilent 2100 Bioanalyzer II (Agilent Technologies, Santa Clara, CA, USA), and complementary RNA was synthesized using a Low Input Quick Amp Labeling Kit (Agilent Technologies). Gene expression was analyzed using an Agilent Technologies Microarray Scanner and SurePrint G3 Mouse 8x60K v2.0 (Agilent Technologies), and the raw data were normalized through the use of a 75Percentile shift (GeneSpring; Agilent Technologies). Toppgene Suite (https://toppgene.cchmc.org/) and Morpheus (https://software.broadinstitute.org/morpheus/) were used for gene ontology (GO) analysis and heatmap preparation, respectively.

Statistical analysis

The results were expressed as the mean ± standard error (SE) and statistically analyzed in a non-parametric manner. The significance between two groups was analyzed using the Mann-Whitney *U*-test ($P < 0.05$). As an exception, the values in the microarray analysis were compared using the Student's t-test ($P < 0.05$). The correlation between two parameters was analyzed using Spearman's correlation test ($P < 0.05$).

Results

Development of nephritis in MRL/lpr mice

First, autoimmune disease and nephritis in MRL/lpr mice at 3 and 6-7 months were evaluated using serological and urinary analyses (Table 1-3). In regard to indices of autoimmune disease, male and female MRL/lpr mice, regardless of age, showed significantly higher values in the S/B ratio and the serum level of anti-dsDNA antibody compared to those in each sex of MRL/+ mice that served as healthy controls. Furthermore, in MRL/lpr mice, the S/B ratio in both sexes and the serum level of anti-dsDNA antibody in males was significantly increased with age. For renal function indices at 6-7 months, only BUN levels were significantly higher in both sexes of MRL/lpr mice compared to those values in MRL/+ mice.

Meanwhile, there was significant differences in renal histopathology between MRL/+ and MRL/lpr mice (Fig.1-1-3). At 6-7 months, both sexes of the MRL/lpr mice exhibited significantly higher values of nuclei in a glomerulus, glomerular size, the area ratio of mesangium to glomerulus, and the number of infiltrated cells such as $B220^+$ B cells, $CD3^+$ T cells, IBA-1^+ macrophages, and Gr-1^+ neutrophils in glomeruli and tubulointerstitium compared to those in MRL/+ mice (Table 1-3). In MRL/lpr mice, the majority of the histopathological indices, with the exception of the mesangial area ratio in the male, were significantly increased with age (Table 1-3). Based on these findings, the author confirmed the development of autoimmune disease followed by nephritis in MRL/lpr mice and classified both strains of mice at 3 and 6-7 months as early and late stage of nephritis, respectively.

Enhanced mRNA expression of Il1f6 among the IL-36R ligands in MRL/lpr kidneys

The mRNA expression of the IL-1F members including IL-36R ligands in the kidneys was evaluated using qPCR (Fig. 1-4). Among the IL-1 family members expressed in the late stage of nephritis, *Il1f6* coding IL-36α was the most upregulated in both sexes of MRL/lpr mice, and the mRNA levels of *Il1f6*, *Il1b*, and *Il1rn* in MRL/lpr mice were significantly higher than those in MRL/+ mice. However, other IL-36R ligands did not show any common alterations between males and females in MRL/lpr mice among strains, sexes, or in regard to disease development. For *Il1f8* coding of IL-36β, female MRL/+ mice exhibited significantly decreased expression with age. For *Il1f9* of coding IL-36γ, female MRL/lpr mice at the late stage exhibited significantly higher expression levels compared to those of the female and male mice at the early and late stages, respectively. For *Il1f5* coding of IL-36Ra, female MRL/+ mice and male MRL/lpr mice exhibited decreased expression with aging, and there were sex differences in MRL/+ and MRL/lpr mice at the early and late stages, respectively, and these differences were more pronounced in female mice than in male mice. For *Il1f10* coding of IL-38, there was no significant difference among strains, stages, or disease stages. Thus, as described in previous reports, *Il1f6* in both sexes

of MRL/lpr mouse kidneys was the most remarkably upregulated and was most associated with the progression of nephritis among the IL-36R ligands [55,56].

IL-36α overexpression in renal tubules of MRL/lpr mice

Using immunostaining, the localization of the IL-36R ligands in kidneys was examined. Initially, IL-36α$^+$ reactions appeared in renal tubules from the early stage of nephritis, and these tubules tended to be increased in number in MRL/lpr mice as disease development progressed (Fig. 1-5A). IL-36α$^+$ reactions localized to the cytoplasm and nucleus of renal tubular epithelial cells and appeared first in the segment close to macula densa, and IL-36α$^+$ tubules frequently exhibited dilated tubular lumens and urinary casts at the late stage, as reported in previous studies (Fig. 1-5B) [55,56]. As shown in Fig. 1-5C, the number of IL-36α$^+$ tubules was significantly increased in all groups as disease progression occurred, and those in both sexes at the late stage were significantly higher in MRL/lpr mice compared to these values in MRL/+ mice. According to double IF staining for IL-36α and calbindin-D28k (a distal tubule marker), IL-36α primarily localized to distal tubular epithelial cells; however, several IL-36α$^+$ tubular epithelial cells did not show calbindin-D28k$^+$ reactions in IL-36α$^+$ tubules (Fig. 1-5D). Furthermore, IL-36α$^+$ tubular epithelial cells were also observed in HNF-4α$^+$ proximal tubule; however, this number was quite low (Fig. 1-5E).

CD44$^+$ activated parietal epithelial cells expressing IL-36α in male MRL/lpr mice

IL-36α also localized to parietal epithelial cells in Bowman's capsules, and these were more frequently observed in male MRL/lpr mice at the late stage (Fig. 1-5A and 6A). In female mice, only MRL/lpr mice at the late stage also possessed a small number of IL-36α$^+$ parietal epithelial cells that exhibited cuboidal shapes. For histoplanimetry, both male strains exhibited a significantly higher ratio of IL-36α$^+$ renal corpuscles to total ones compared to that of the female strains at the late stage, and this ratio was the highest in male MRL/lpr mice (Fig. 1-6B).

Next, the author performed double IF for IL-36α and CD44, a marker for activated parietal epithelial cells that is indicative of their proliferation, migration, and matrix production [114]. CD44 was observed on the cell membranes of parietal epithelial cells and infiltrated cells in renal corpuscles, and IL-36α and CD44 were frequently co-localized in parietal epithelial cells (Fig. 1-6C). The author then counted and calculated the ratio of IL-36α$^+$ parietal epithelial cells in CD44 positive or negative parietal epithelial cells in male MRL/lpr mouse cells at the late stage. As shown in Fig. 1-6D, IL-36α was significantly and highly co-localized with CD44 in parietal epithelial cells.

Localization of IL-36β and IL-36γ in plasma cells and sympathetic nerves, respectively

Next, the localization of other IL-36R agonists (IL-36β and IL-36γ) was analyzed in the kidneys. IL-36β localized to the cytoplasm of $CD138^+$ plasma cells in both sexes of MRL/lpr mice at the late stage but not at the early stage (Fig. 1-7A and B). However, the number of positive cells was low in the kidneys, with one or two positive cells observed in each kidney section.

IL-$36\gamma^+$ reactions appeared at the peri-vessels and peri-glomeruli of all groups (Fig. 1-7C). According to double IF assays, IL-36γ was co-localized with tyrosine hydroxylase, a marker for peripheral sympathetic neurons (Fig. 1-7D). Interestingly, there were IL-36γ positive and negative axons in the kidneys of all groups; however, the author could not identify constant localization patterns of IL-36γ among sexes, strains, or disease stages (Fig. 1-7D).

Localization of IL-36Ra in smooth muscle cells, distal tubular and parietal epithelial cells

The author also examined the localization of IL-36R antagonists in the kidneys. For IL-36Ra, all groups exhibited positive reactions in the intrarenal arteries and arterioles, and IL-36Ra was localized in the cytoplasm of α-SMA^+ smooth muscle cells within the tunica media (Fig. 1-8A and B). However, in vasculitis lesions in MRL/lpr mice, the IL-$36Ra^+$ reaction was defective in a subset of these lesions with transmural cell infiltration (Fig. 1-8C). Both sexes of MRL/lpr mice at the late stage possessed IL-$36Ra^+$ parietal epithelial cells that exhibited both flat and cuboidal shapes (Fig. 1-8D). However, the author could not determine obvious sex differences in IHC, unlike the IL-36α expression in parietal epithelial cells. In both strains at the late stage, granular IL-$36Ra^+$ reactions were observed in the apical portion of tubular epithelial cells (Fig. 1-8E). Although female MRL/+ and male MRL/lpr mice exhibited age-related decreases in *Il1f5* expression (Fig. 1-4), a similar tendency was not observed in regard to protein expression. According to IF or IHC using serial sections, IL-36Ra co-localized with calbindin-D28k but not with HNF-4α, thus indicating its expression in distal tubules (Fig. 1-8F and G). Furthermore, several tubular epithelial cells co-expressed IL-36Ra and IL-36α (Fig. 1-8H).

IL-38 overexpression in the plasma cells of MRL/lpr mice

Another IL-36R antagonist, IL-38, localized to the cytoplasm of renal interstitial cells in all groups, and the expression appeared to be abundant in both sexes of MRL/lpr mice at the late stage compared to that of the other groups (Fig. 1-9A). Using serial sections followed by IHC, $CD138^+$ plasma cells were positive for IL-38^+ reactions (Fig. 1-9B). In disagreement with the mRNA analysis, both sexes of MRL/lpr mice showed that the number of IL-38^+ cells significantly increased with the progression of nephritis, and at the late stage, the number of IL-38^+ cells of MRL/lpr mice tended to be higher than that of MRL/+ mice (Fig. 1-9C). These IL-38^+ cells did not directly contact the IL-$36\alpha^+$ tubules (Fig. 1-9D).

Overexpression of IL-36α and IL-38 is positively correlated with nephritis

The protein expression of IL-36α and IL-38 at the late stage of nephritis was enhanced in MRL/lpr mice compared to that in MRL/+ mice among the IL-36R ligands (Fig.1-5, 6 and 9). Thus, the author analyzed correlations between the parameters of IL-36α and IL-38 and indices for autoimmune disease, renal function, and histopathology in both sexes of MRL/lpr mice (Table 1-4). In regard to the number of IL-36α$^+$ tubules, there were significant positive correlations with serum levels of anti-dsDNA antibody, uACR, the number of all infiltrated cells, particularly CD3$^+$ T cells and IBA-1$^+$ macrophages, into the tubulointerstitium. Furthermore, IL-36α$^+$ tubules were significantly and positively correlated with BUN in females and with S/B ratio in males. In regard to the IL-36α$^+$ renal corpuscle ratio, male MRL/lpr mice exhibited significant and positive correlations with all indices for autoimmune disease, glomerular lesionand uACR. In contrast, the IL-36α$^+$ renal corpuscle ratio of female MRL/lpr mice was significantly and positively correlated with BUN, uACR, glomerular size, glomerular nucleus number, and mesangial area ratio. Characteristically, both sexes of MRL/lpr mice showed a significantly positive correlation between the IL-36α$^+$ renal corpuscle ratio and Gr-1$^+$ neutrophil number among infiltrated cells in the glomerulus. Additionally, there was a significantly positive correlation between the number of IL-36α$^+$ tubules and the renal corpuscle ratio in both sexes.

In regard to the IL-38$^+$ cell number, both sexes of MRL/lpr mice exhibited significantly positive correlations with the values of anti-dsDNA antibody, uACR, CD3$^+$ T cells in tubulointerstitium, and IL-36α$^+$ tubules. In female MRL/lpr mice, there were also significant positive correlations between IL-38$^+$ cells and the indices for BUN, Cr, and other infiltration cells into the tubulointerstitium.

Ubiquitous mRNA expression of Il1rl2 in murine kidneys

According to a previous study, IL-36R was localized in podocytes, proximal and distal tubules in healthy kidneys, whereas it was observed in interstitial cells and platelets in unilateral ureteral obstruction kidneys [55]. To identify the localization and induction of the IL-36R mRNA *Il1rl2*, the author performed ISH assays in MRL/+ and MRL/lpr mice at the late stage. *Il1rl2* localized to tubular epithelial cells, mesangial cells, podocytes, parietal epithelial cells, interstitial cells, urothelial cells, smooth muscle cells, and endothelial cells in the kidneys of both strains from the cortex to the medulla (Fig. 1-10A). In the kidneys of both sexes of MRL/lpr mice, *Il1rl2* was induced in tubular epithelial cells, parietal epithelial cells, and infiltrated immune cells in glomerular and tubulointerstitial lesions and vasculitis, and positive signals in parietal epithelial cells tended to be higher in male MRL/lpr mice than in female mice, similar to the localization pattern of IL-36α (Fig. 1-10A). As shown in Fig. 1-10B, *Il1rl2*$^+$ signals were primarily localized in distal tubular epithelial cells, and MRL/lpr exhibited localization in the cells in close proximity

to the vascular pole, including the juxtaglomerular complex. However, qPCR analysis revealed that there was no difference in mRNA levels of *Il1rl2* among the groups (Fig. 1-10C).

Upregulation of IL-1 family signaling in MRL/lpr kidneys

Stimulation of IL-36R induces IL-1 family signaling, including MAPK and NF-κB [120]. To detect the significant GO associated with these signaling pathways, gene expression in the kidneys at the late stage was comprehensively compared between female MRL/+ and MRL/lpr mice by microarray focusing on 2-fold upregulated genes in the latter (Fig. 1-11A and B). As shown in Fig. 1-11A, 25 genes associated with positive regulation of MAPK activity (GO: 0043406) were significantly upregulated in MRL/lpr mice. Furthermore, in the genes related to positive regulation of NF-κB transcription factor activity (GO: 0051092), MRL/lpr mice possessed 11 genes that were significantly upregulated compared to levels in MRL/+ mice (Fig. 1-11B). To confirm the activation of the NF-κB pathway, the author performed IHC for p-NF-κB-p65, the effective component of NF-κB (Fig. 1-11C). Positive reactions appeared in the nuclei of tubular and parietal epithelial cells, and especially infiltrated cells in all groups at the late stage, and the number was abundant in both sexes of MRL/lpr mice. Therefore, IL-1 family signaling, including that of IL-36R, was upregulated in MRL/lpr mice.

mRNA expression of IL1RL2 in the cat kidneys

Reportedly, distal tubular and parietal epithelial cells express IL-36α in the human patients with CKD [28]. To elucidate a potential of IL-36R ligands for clinical investigation of renal diseases in animals, the author examined *IL1RL2* localization in the kidneys of cats, presenting a high susceptibility to CKD with tubulointerstitium-dominant lesions [58,84]. The cat kidneys showed that *IL1RL2* was mainly localized in tubular epithelial cells, especially distal ones, as well as parietal epithelial cells with dilated Bowman's capsule, podocytes, and urothelial cells (Figure 1-12), indicating that IL-36R signaling roles in the kidneys are common between mice and cats.

Discussion

The present study demonstrated the localization of the IL-36R ligands in murine kidneys (Table 1-5). In regard to mRNA expression, both sexes of MRL/lpr mice manifested autoimmune disease-mediated nephritis, and the present results demonstrated that IL-36α coded by *Il1f6* was the most overexpressed in the kidneys of MRL/lpr mice, especially in the renal epithelial cells, among the IL-1 family members at the late stage as previously reported [55,56]. In contrast, no common alteration was observed in the mRNA expression of other IL-36R ligands between male and female MRL/lpr mice. In previous studies, murine kidney injury models created by UUO and folic acid injection revealed the downregulation of *Il1f5* and *Il1f8* in the kidney, while Nishikawa *et al*. reported that the mRNA expression of IL-36α, IL-36β, and IL-36γ was upregulated in murine kidneys with IRI [55,94]. Importantly, a disease-specific expression pattern of the IL-36R ligands was also reported in other organs. In mice, collagen-induced arthritis increased the mRNA levels of all members of this family; however, only *Il1f6*, *Il1f9*, and *Il1f5* were upregulated in antigen-induced arthritis [18]. Thus, these gene expression analyses indicated that IL-36α contributes to the progression of various kidney diseases, while the expression of other members may depend upon disease type.

The author investigated the localization of IL-36R ligands, and IL-36α was mainly localized to distal tubular epithelial cells. Characteristically, some IL-36α$^+$ tubular epithelial cells exhibited decreased specific marker expression for each renal tubule, indicating an alternation of morpho-functional phenotypes. Furthermore, parietal epithelial cells also expressed IL-36α during disease progression in MRL/lpr mice, and this was abundant in males. Chi *et al*. reported the presence of IL-36α$^+$ parietal epithelial cells in human patients with a pathologic diagnosis of tubulointerstitial lesions in nephritis or diabetic nephropathy [28]. Importantly, IL-36α$^+$ parietal epithelial cells frequently presented with a cuboidal and not squamous morphology and a positive reaction for CD44, an activated parietal epithelial cell marker. CD44 is a glycoprotein involved in cell-cell interactions, cell adhesion, and cell migration [11,114]. Reportedly, those parietal epithelial cells are observed with renal UEB disruption; they move to the tuft with damaged podocytes and seal the disrupted filtration barrier, leading to glomerular sclerotic lesion development [40]. Furthermore, IL-36α$^+$ parietal epithelial cell number was positively correlated with neutrophil infiltration into the glomerulus in MRL/lpr mice. Neutrophil-secreting enzymes, including elastase, cathepsin G, and proteinase 3, play crucial roles in processing and activating IL-36R agonists, thus suggesting that neutrophils in glomeruli are involved in IL-36α production in parietal epithelial cells [31]. In mice, female parietal epithelial cells are squamous, while male parietal epithelial cells are composed of squamous to cuboidal cells under the control of sex-hormones. Furthermore, several glomerular lesions, including focal segmental glomerular sclerosis, are more severe in males than those in females of mice as well as humans [3,69,112]. Thus, induced IL-36α expression appeared to

be associated with the morpho-functional changes of epithelial cells as tubular and parietal epithelial cells and contribute to the pathogenesis of nephritis.

In MRL/lpr mouse kidneys, CD138$^+$ plasma cells expressed IL-36β and IL-38, an agonist and antagonist of IL-36R signaling, respectively. Plasma cells produce antibodies in addition to immunosuppressive and pro-inflammatory cytokines such as IL-10 and IL-17, respectively [34]. It has been reported that IL-36α, IL-36β, IL-36γ, and IL-36Ra are expressed in plasma cells, indicating that these cells might be one of the main producers of IL-36R ligands [18]. In another report, IL-36β$^+$ plasma cells were observed in the synovium and colonic mucosa of human patients with rheumatoid arthritis and Crohn's disease, respectively, and the number of IL-36β$^+$ cells was increased in the former only [18]. In contrast, IL-36β$^+$ cells were rarely observed in the tubulointerstitium of MRL/lpr mice at the late stage only. Therefore, the author concluded that the contribution of IL-36β to the pathogenesis of nephritis in MRL/lpr mice was relatively low compared to that of other members.

In contrast, IL-38$^+$ plasma cells were significantly increased in MRL/lpr mice during the progression of nephritis; however, the mRNA level was not altered. SLE patients possessed high serum levels of IL-38 that were associated with the risk of LN and central nervous system lupus [105]. In MRL/lpr mice and another SLE model mouse induced by pristane, IL-38 injection ameliorated skin inflammation and nephritis and reduced proteinuria [29,134]. Additionally, *in vitro* experiments demonstrated that IL-38 inhibited T helper 17 cell responses such as the production of IL-17 and IL-22 that were activated by IL-36R signaling [29,122]. In the present study, infiltration of IL-38$^+$ plasma cells into the tubulointerstitium was relatively mild compared to that observed in T cells and in macrophages. However, the IL-38$^+$ cell number in the tubulointerstitium exhibited a positive correlation with certain indices for tubulointerstitial lesions such as IL-36α$^+$ tubule number. Therefore, these results indicated that IL-38 was induced by IL-36α upregulation and was involved in tubulointerstitial lesions as an antagonist.

The author found that IL-36γ and IL-36Ra were constitutively expressed in murine kidneys. IL-36γ was localized to sympathetic nerves in the kidney, as observed previously in the intestine. Another study also revealed that IL-36γ was expressed and upregulated in spinal nerves of a mouse model of chronic inflammatory pain induced by injection of complete Freund's adjuvant [75]. However, in the kidney, IL-36γ was also expressed under healthy conditions. Similar to IL-36γ localization, IL-1α, a member of the IL-1 family, is expressed in rat peripheral nerves in accordance with the distribution of noradrenergic innervation of organs such as the colon and pancreas [9]. Cytokines exert several physiological functions in the nervous system. For example, TNF-α is produced by neurons, astrocytes, and microglia and contributes to the development of the hippocampus, ionic homeostasis, and synaptic plasticity and also to the initiation and progression of some neuronal diseases [99]. Further investigation is required to elucidate the

physiological functions of IL-36γ in the kidneys through the function of nerves, and these studies should particularly focus on representative sympathetic nerve activity such as the regulation of renal blood flow [111].

Under healthy conditions, IL-36Ra was expressed in smooth muscle cells of the tunica media of arteries and arterioles and was partially absent in the cells with vasculitis in MRL/lpr mice. It has been reported that IL-36Ra was expressed in keratinocytes, in various immune cells such as B cells, macrophages, and dendritic cells, and in perivascular cells surrounding the fetal blood vessels of human placentas [102,116]. Further, blood vessels in the tumor and tonsil of patients with colon carcinoma express IL-36Ra with IL-36γ, and there has been a positive correlation between IL-36Ra expression and the upregulation of immune checkpoint markers such as programmed cell death 1, programmed cell death ligand 1, and cytotoxic T-lymphocyte associated protein 4 [130]. Additionally, distal tubular and parietal epithelial cells also expressed IL-36Ra in accordance with IL-36α localization, and both of them were at least partially co-expressed in distal tubular epithelial cells. Therefore, IL-36Ra induction might be associated with IL-36α overexpression in injured renal epithelial cells to regulate inflammation, and this has been reported as a positive correlation between the mRNA and protein levels in synovial tissues of patients with rheumatoid arthritis [18].

The present ISH study revealed that the mRNA of IL-36R, *Il1rl2*, was ubiquitously expressed in murine kidneys. It has been previously reported that IL-36R is expressed in immune and non-immune cells; the former are dendritic cells, T cells, and macrophages and the latter are the epithelial cells of renal tubules and bronchioles, keratinocytes, and fibroblasts [55,102]. Additionally, the nephritis models exhibited induction of *Il1rl2* in renal lesions, including tubular epithelial cells of dilated tubules and proliferative cells, and this induction was markedly present in mesangial cells and parietal epithelial cells. In MRL/lpr mice at the late stage, the microarray analysis and IHC for p-NF-κB-p65 showed the upregulation of genes associated with MAPK and NF-κB pathways, which are common to the IL-1 family, including IL-36α [120]. In IL-36R-expressing cells, these pathways promote inflammatory responses through the production of cytokines and chemokines, including IL-6, IL-8, TNF-α, C-X-C motif chemokine ligand 1 (CXCL1), and CXCL8, suggesting that renal inflammation with the renal epithelial cell injuries in MRL/lpr mice was activated by IL-36α [102].

Reportedly, patients with SLE show high serum levels of IL-36α, IL-36γ, and IL-38 and a low level of IL-36Ra, and peripheral blood mononuclear cells are suspected to be their origin [81,105]. However, the levels of these proteins have not yet been investigated in MRL/lpr mice. In mice, systemic autoimmune disease is caused by *lpr* mutation, a defect in the expression of FAS antigen, which is involved in T cell apoptosis to eliminate autoreactive cells under normal conditions [47]. Furthermore, MRL/lpr mice showed increased expression of *Il1b* and *Ifng* in

spleens and lymph nodes before the onset of autoimmune disease, suggesting that *lpr* mutation might be associated with the upregulation of cytokines [72]. In the kidneys, the author considered that the gene mutation might regulate the IL-36R ligand expression through indirect pathways; the progression of autoimmune disease might induce renal inflammation, leading to overexpression of IL-36α, which exacerbates the symptoms of nephritis.

IL-36α is expressed in distal tubular and parietal epithelial cells of human patients with CKD and AKI in addition to the mouse models [28,94]. The present study focused on cats which mainly manifest tubulointerstitial lesions rather than glomerular lesions, frequently develop CKD (incidence, 80.9%, over 15 year-old), and show renal disorders at 57% under SLE [53,58,84]. As distal tubular and parietal epithelial cells express both IL-36α and IL-36R in the examined mice, the cat kidneys showed the similar localization pattern of IL-36R gene-expressing cells; however, IL-36α coding gene in cats and dogs has not been annotated yet (Ensembl; https://asia.ensembl.org/index.html, UCSC Genome Browser; https://genome.ucsc.edu/index.html). Thus, further investigations are needed to elucidate whether IL-36R agonists have the similar pathological roles in cat kidneys, contributing to a novel approach dependent on IL-36R signaling for CKD diagnosis and treatment in veterinary and human medicine.

In conclusion, the author demonstrated the functional compartmentalization of the IL-36R ligands in murine kidneys, and each member exhibited constitutive or induced expression in renal epithelial cells and interstitial cells. Importantly, IL-36R gene localization in mice coincided with that of cats. Although further studies are required to elucidate the functions of each member of this family in the kidneys, the present study strongly suggested that a balance of IL-36R agonists and antagonists was maintained under health conditions; however, inflammatory conditions cause an IL-36α-dominant imbalance in renal epithelial cells, leading to deterioration and increased renal pathology with UEB disfunctions. Therefore, redressing the balance, particularly IL-36α inhibition, may play a key role in the development of novel therapeutic strategies targeting kidney disease.

Summary

The IL-36R ligands belongs to the IL-1 family and is comprised of agonists (IL-36α, IL-36β, IL-36γ) and antagonists (IL-36Ra, IL-38). A previous report have showed IL-36α overexpression in renal tubules of chronic nephritis mice. To understand the localization status and biological relationships among each member of the IL-36R ligands in the renal epithelium, MRL/lpr mice were investigated as spontaneous nephritis models using pathology-based techniques. MRL/lpr mice exhibited disease onset from 3 months and severe nephritis at 6-7 months (early and late stages, respectively). Briefly, IL-36γ and IL-36Ra were constitutively expressed in murine kidneys, while the expression of IL-36α, IL-36β, IL-36Ra, and IL-38 was induced in MRL/lpr mice. IL-36α expression was significantly increased and localized to injured tubular epithelial cells. $CD44^{+}$-activated parietal epithelial cells also exhibited higher IL-36α positive rates, particularly in males. IL-36β and IL-38 are expressed in interstitial plasma cells. Quantitative indices for IL-36α and IL-38 positively correlated with nephritis severity. Similar to IL-36α, IL-36Ra localized to tubular and parietal epithelial cells at the late stage; however, MRL/lpr and healthy MRL/+ mice possessed $IL\text{-}36Ra^{+}$ smooth muscle cells in kidney arterial tunica media at both stages. IL-36γ was constitutively expressed in renal sympathetic axons regardless of strain and stage. IL-36R gene was ubiquitously expressed in the kidneys and was induced especially in renal epithelial cells proportional to disease severity. MRL/lpr mouse kidneys possessed significantly upregulated IL-36R downstream candidates, including NF-κB- or MAPK-pathway organizing molecules. Moreover, IL-36R gene in cat kidneys was localized in distal tubular and parietal epithelial cells, in accordance with IL-36R and IL-36α localization in the mouse kidneys. Thus, the IL-36R ligands contributes to homeostasis and inflammation in the kidneys, and especially, an IL-36α-dominant imbalance in renal epithelial cells could strongly impact nephritis deterioration.

Tables and Figures

Table 1-1. List of antibodies used in this study

Primary and secondary antibodies	Host	Dilution	Source	Antigen retrieval	Blocking serum	
					IHC	IF
B220	Rat	1:1,600	Cedarlane, Burlington, Canada	Tris	10% NGS	
CD3	Rabbit	1:200	Nichirei, Tokyo, Japan	Tris	10% NGS	
IBA-1	Rabbit	1:1200	Wako, Tokyo, Japan	Tris	10% NGS	
Gr-1	Rat	1:800	R and D system, Minneapolis, MN, USA	Pepsin	10% NGS	
CD138	Rat	1:300	Biolegend, San Diego, CA, USA	Tris	10% NGS	5% NDS
CD44	Rat	1:800	BD Biosciences, Franklin Lakes, NJ, USA	Tris		5% NDS
α-SMA	Rabbit	1:3,000	Abcam, Cambridge, UK	Tris		5% NDS
Tyrosine hydroxylase	Rabbit	1:1,000	Abcam, Cambridge, UK	Tris		5% NDS
Calbindin-D28k	Rabbit	1:1,000	Proteintech, Rosemont, IL, USA	Tris		5% NDS
HNF-4α	Rabbit	1:1,000	Cell signaling, Danvers, MA, USA	Tris		5% NDS
IL-36*α*	Goat	1:400	R and D system, Minneapolis, MN, USA	CB	5% NDS	5% NDS
IL-36β	Goat	1:2,000	R and D system, Minneapolis, MN, USA	Tris	5% NDS	5% NDS
IL-36γ	Mouse	1:1,600	Abcam, Cambridge, UK	Tris	Mouse stain Kit	5% NDS
IL-36Ra	Rat	1:200	R and D system, Minneapolis, MN, USA	Pepsin	10% NGS	5% NDS
IL-38	Rat	1:1,500	R and D system, Minneapolis, MN, USA	Pepsin	10% NGS	5% NDS
Rat IgG-biotin	Goat	1:400	Biolegend, San Diego, CA, USA			
Rabbit IgG-biotin	Goat	Undiluted	SABPO(R)Kit, Nichirei, Tokyo, Japan			
Goat IgG-biotin	Donkey	1:200	Santa Cruz Biotechnology, Santa Cruz, CA, USA			
Mouse IgG-biotin	Goat	Undiluted	Mouse stain Kit, Nichirei, Tokyo, Japan			
Rabbit IgG-Alexa Fluor 488/546	Donkey	1:500	Thermo Fisher Scientific, Waltham, MA, USA			
Rat IgG-Alexa Fluor 488/546	Donkey	1:500	Thermo Fisher Scientific, Waltham, MA, USA			
Goat IgG-Alexa Fluor 488/546	Donkey	1:500	Thermo Fisher Scientific, Waltham, MA, USA			
Mouse IgG-Alexa Fluor 488	Donkey	1:500	Thermo Fisher Scientific, Waltham, MA, USA			

Tris: 20mM Tris-HCl buffer (pH9.0) at 110°C for 15min. CB: 10mM citrate buffer (pH6.0) at 110°C for 15min. Pepsin: 0.1% pepsin. NDS: Normal donkey serum NGS: Normal goat serum.

Table 1-2. List of primers used in this study

Gene symbol (Gene ID)	Primer sequence (5′-3′) F: Forward, R: Reverse		Product size (bp)
Actb (11461)	F: TGTTACCAACTGGGACGACA	R: GGGGTGTTGAAGGTCTCAAA	165
Il1f6 (54448)	F: TCCTGCAGAACAATATCCTCAC	R: GTTCGTCTCAAGAGTGTCCAGA	104
Il1f8 (69677)	F: GTTCCTGCTAGCAACAATGTCA	R: CCATCTCAACACAGCAGAAGC	142
Il1f9 (215257)	F: CCAGTCAGCGTGACTATCCTC	R: ATGGCTTCATTGGCTCAGG	193
Il1f5 (54450)	F: GAAGGATTCAGCCTTGAAGGTA	R: CCGATTTGGGACAACACTG	112
Il1f10 (215274)	F: TGGGAGACCCTGATTCAGACA	R: TCTTTACACACGCCAGGCAG	132
Il1rl2 (107527)	F: AGACACCTTAGAGTTCACCAGGAC	R: CCATGGAAGAGTCACACCAG	163
Il1a (16175)	F: AGATGACCTGCAGTCCATAACC	R: GACAAACTTCTGCCTGACGAG	121
Il1b (16176)	F: TTCCAGGATGAGGACATGAGC	R: AATGGGAACGTCACACACCAG	111
Il1rn (16181)	F: TTGTGCCAAGTCTGGAGATG	R: TTCTCAGAGCGGATGAAGGTA	111
Il18 (16173)	F: AGTAAGAGGACTGGCTGTGACC	R: AACTCCATCTTGTTGTGTCCTG	174
Il33 (77125)	F: GCTGATGGTGAACATGAGTCC	R: CTCCTATGTAAGTGCCAGGAAG	188

Table 1-3. Indices of autoimmune disease, renal functions, and renal histopathology

		Early stage of nephritis (3 months)				Late stage of nephritis (6-7 months)			
		Female		Male		Female		Male	
	Index	MRL/+	MRL/lpr	MRL/+	MRL/lpr	MRL/+	MRL/lpr	MRL/+	MRL/lpr
Autoimmune disease	S/B ratio (%)	0.26 ± 0.01†	0.69 ± 0.07*	0.20 ± 0.01	0.59 ± 0.08*	0.25 ± 0.02	2.29 ± 0.53**§§	0.22 ± 0.01	1.54 ± 0.23**§
	dsDNA (U/mL)	7.56 ± 0.94	406.31 ± 74.99*	3.77 ± 1.58	201.71 ± 39.23*	8.70 ± 3.95	807.90 ± 88.02*	11.46 ± 3.67	632.48 ± 95.29**§§
Renal function	BUN (mg/dL)	20.83 ± 2.14	28.23 ± 5.42	28.28 ± 1.77	31.93 ± 4.97	26.60 ± 2.08	52.63 ± 3.33*	21.13 ± 1.64	36.81 ± 4.53*
	Cr (mg/dL)	0.38 ± 0.06	0.28 ± 0.03	0.34 ± 0.10	0.32 ± 0.04	0.29 ± 0.06	0.51 ± 0.15	0.70 ± 0.39	1.13 ±0.80
	uACR (μg/mg)	NE				29.40 ± 10.43†	345.021 ± 133.42	42.03 ± 9.94	463.14 ± 118.14
Renal histopathology	Glo. Nucleus (No.)	41.95 ± 0.41	45.4 ± 0.20*†	42.33 ± 1.11	47.63 ± 0.54*	45.65 ± 0.96§	78.64 ± 5.59**§§	43.08 ± 0.37	62.74 ± 5.13**§
	Glo. Size (×10^{3}μm^2)	2.18 ± 0.03†	2.24 ± 0.07†	2.54 ± 0.05	2.82 ± 0.10*	2.94 ± 0.19†§	5.54 ± 0.63**§§	2.58 ± 0.03	4.51 ± 0.42**§
	Mesangial area (%)	34.89 ± 1.07	40.10 ± 0.79*	36.23 ± 0.95	38.61 ± 0.74*	37.33 ± 1.40§	47.08 ± 2.17*†§	34.32 ± 0.88	46.10 ± 1.92**
	Glo. B220 (No./Glo.)	0.03 ± 0.02	0.03 ± 0.03	0.03 ± 0.02	0.08 ± 0.02	0.03 ± 0.02	1.46 ± 0.43**§§	0.08 ± 0.03	0.90 ± 0.17**§§
	Glo. CD3 (No./Glo.)	0.11 ± 0.03	0.18 ± 0.06	0.10 ± 0.04	0.17 ± 0.04	0.11 ± 0.03	1.95 ± 0.38**§§	0.13 ± 0.02	1.21 ± 0.23**§§
	Glo. IBA-1 (No./Glo.)	0.01 ± 0.01	0.02 ± 0.01	0.01 ± 0.01	0.12 ± 0.06	0.17 ± 0.13	1.65 ± 0.18*§§	0.03 ± 0.02	0.74 ± 0.10**§§
	Glo. Gr-1 (No./Glo.)	0.11 ± 0.02	0.12 ± 0.04	0.09 ± 0.05	0.21 ± 0.08	0.28 ± 0.13†	0.81 ± 0.10*§§	0.13 ± 0.03	1.03 ± 0.31**§
	Ti. B220 (No./mm^2)	5.42 ± 2.19	10.38 ± 2.78	7.08 ± 2.20	13.92 ± 2.99	10.38 ± 3.49	52.70 ± 11.04*§§	14.15 ± 1.76	45.60 ± 4.05**§§
	Ti. CD3 (No./mm^2)	13.21 ±1.72	93.16 ± 1.56*	23.35 ± 4.08	86.79 ± 3.11*	24.76 ± 10.29	296.43 ± 32.25**§§	40.33 ± 4.45§	196.22 ±27.35**§§
	Ti. IBA-1 (No./mm^2)	3.99 ± 1.42	26.52 ± 6.42*	17.34 ± 14.16	38.28 ± 10.67	127.12 ± 21.46§	386.15 ± 50.66**§§	159.20 ± 11.71§	289.18 ± 21.88**§§
	Ti. Gr-1 (No./mm^2)	2.83 ± 1.02	7.55 ± 1.85	3.77 ± 0.39	9.43 ± 1.02*	13.21 ± 4.92§	23.46 ± 2.58*§	14.39 ± 1.05§	20.21 ± 2.33*§§

Each value represents the mean ± SE (n= 4-9, except for Cr; n=3-8). *: Significant difference in MRL/lpr against MRL/+ mice of the same sex at the same stage (*: $P < 0.05$, **: $P < 0.01$). † Significant difference in female versus male mice of the same strain at the same stage (†: $P < 0.05$, ††: $P < 0.01$). §: Significant difference at the late stage against the early stage in the same mouse strains of the same sex (§: $P < 0.05$, §§: $P < 0.01$). Mann-Whitney *U*-test. S/B ratio: weight ratio of spleen to body, dsDNA: serum anti-double-stranded DNA antibody level, BUN: blood urea nitrogen, Cr: serum creatinine level, uACR: urinary albumin to creatinine ratio, Glo: glomerulus, Ti: tubulointerstitium, No: number, NE: not examined.

Table 1-4. Correlation analysis between parameters of IL-36α and IL-38 and indices for lupus nephritis in MRL/lpr

Index		IL36α$^+$ tubules		IL36α$^+$ PECs		Ti. IL-38$^+$ cells	
		Female	Male	Female	Male	Female	Male
Autoimmune disease	S/B ratio	0.500	0.681*	0.121	0.736**	0.401	0.391
	dsDNA	0.782**	0.698**	0.528	0.714**	0.646*	0.624*
Renal function	BUN	0.636*	0.413	0.674*	0.487	0.668*	0.157
	Cr	0.517	-0.191	0.429	0.036	0.633*	-0.014
	uACR	0.943**	0.967**	0.845*	0.800*	0.671*	0.680*
Renal histopathology	Glo. Nucleus	0.927**	0.791**	0.674*	0.923**	0.691*	0.737**
	Glo. Size	0.918**	0.819**	0.674*	0.918**	0.807**	0.770**
	Mesangial area	0.818**	0.791**	0.661*	0.709**	0.673*	0.704**
	Glo. B220$^+$ cells	0.615*	0.736**	0.122	0.711**	0.474	0.415
	Glo. CD3$^+$ cells	0.659*	0.797**	0.231	0.758**	0.480	0.523
	Glo. IBA-1$^+$ cells	0.548	0.865**	0.190	0.901**	0.375	0.728**
	Glo. Gr-1$^+$ cells	0.888**	0.802**	0.676*	0.906**	0.624*	0.632*
	Ti. B220$^+$ cells	0.718*	0.652*	0.283	0.465	0.636*	0.277
	Ti. CD3$^+$ cells	0.918**	0.857**	0.674*	0.758**	0.880**	0.597*
	Ti. IBA-1$^+$ cells	0.900**	0.808**	0.674*	0.648*	0.737**	0.370
	Ti. Gr-1$^+$ cells	0.679*	0.731**	0.392	0.736**	0.610*	0.404
	IL-36α$^+$ tubules	-	-	0.674*	0.885**	0.820**	0.737**
	IL-36α$^+$ PECs	0.674*	0.885**	-	-	0.547	0.779**
	Ti. IL-38$^+$ cells	0.820**	0.737**	0.547	0.779**	-	-

Values indicate Spearman's correlation coefficient (ρ; n= 6-13, * $P < 0.05$, ** $P < 0.01$). S/B ratio: weight ratio of spleen to body, dsDNA: serum anti-double-stranded DNA antibody level, BUN: blood urea nitrogen, Cr: serum creatinine level, uACR: urinary albumin to creatinine ratio, Glo: glomerulus, Ti: tubulointerstitium, PECs: parietal epithelial cells.

Table 1-5. Localization of IL-36R ligands in murine kidneys

	IL-36α	IL-36β	IL-36γ	IL-36Ra	IL-38
TEC	I	-	-	I	-
PEC	I	-	-	I	-
Plasma cell	-	I	-	-	I
Sympathetic axon	-	-	C	-	-
Smooth muscle cell	-	-	-	C	-

I: Induced expression in lupus nephritis, C: Constitutive expression, TEC: tubular epithelial cell, PEC: Parietal epithelial cell.

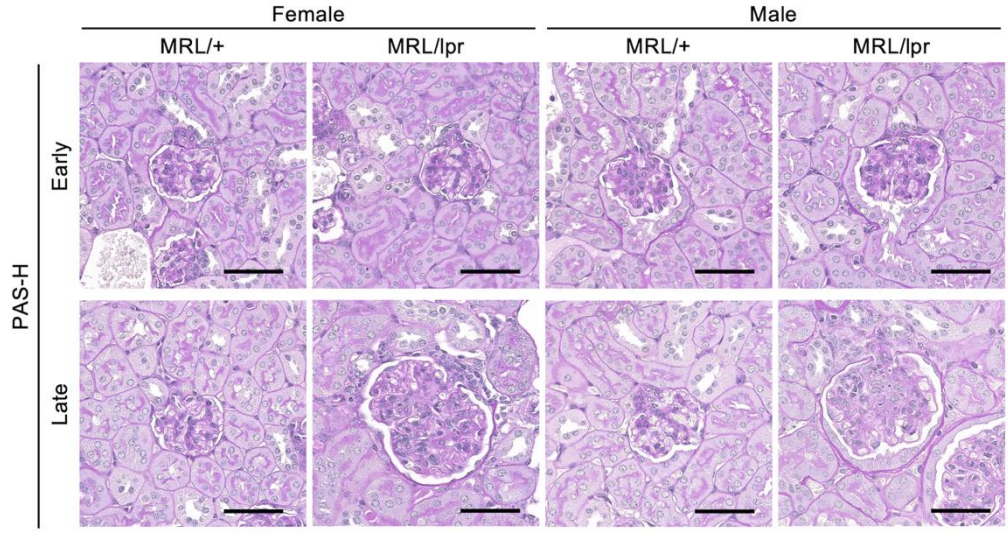

Figure 1-1. Histopathology of glomeruli in the murine kidneys

PAS-H staining images for all groups. Glomerular hypercellularity and hypertrophy as well as mesangial matrix expansion are clearly observed in both sexes of MRL/lpr mice at the late stage of spontaneous nephritis. Bars = 50 μm. PAS-H: periodic acid Schiff-hematoxylin, Early: early stage of nephritis (3 months), Late: late stage of nephritis (6-7 months).

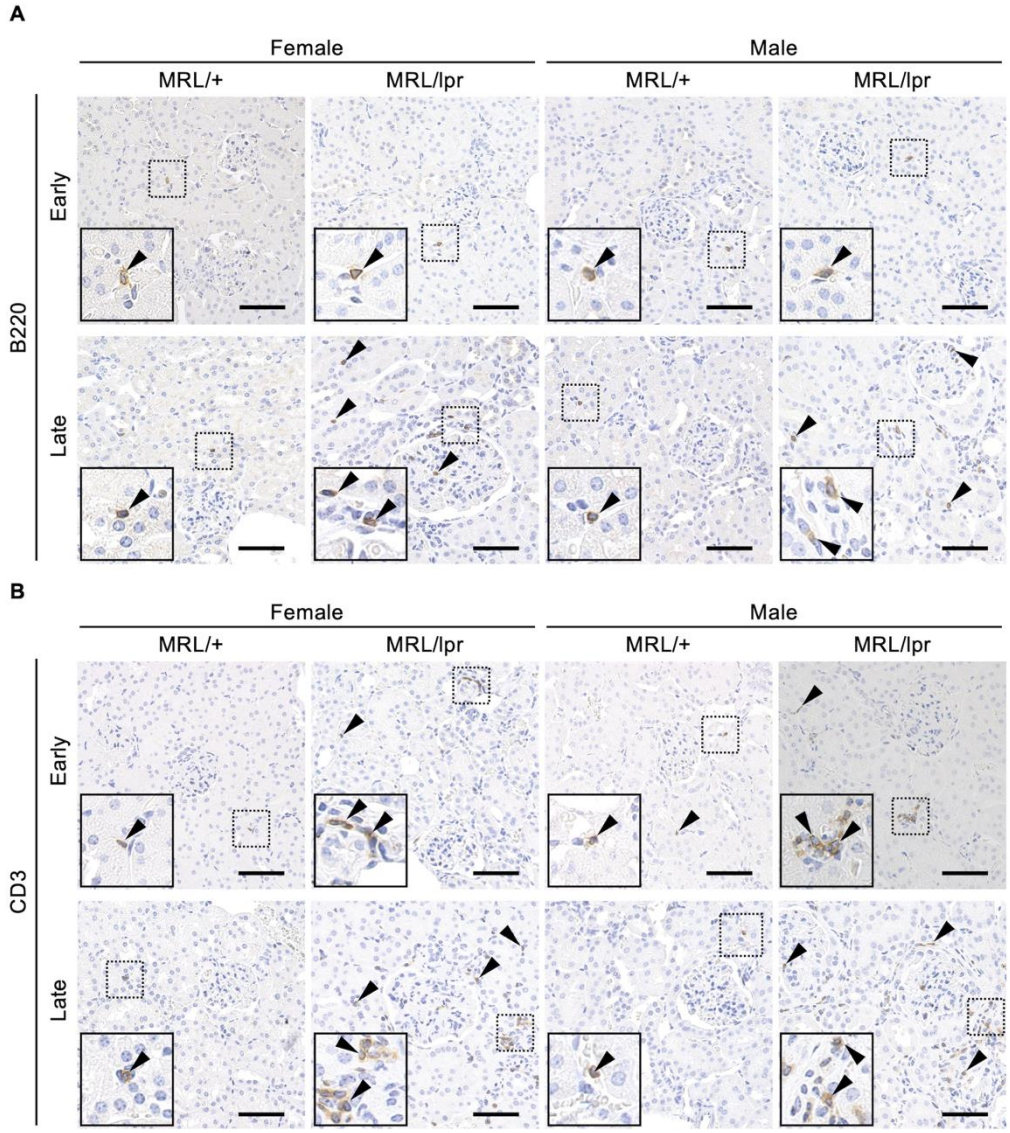

Figure 1-2. Infiltration of B cells and T cells in the murine kidneys

(A and B) IHC images for B220 (B cell marker, panel A) and CD3 (T cell marker, panel B), respectively. Both $B220^+$ B cells and $CD3^+$ T cells are abundant in the glomeruli and tubulointerstitium of both sexes of MRL/lpr mice at the late stage of spontaneous nephritis. Arrowheads indicate immune-positive cells. Insets indicate high magnification images of the areas marked by the black squares. Bars = 50 μm. Early: early stage of nephritis (3 months), Late: late stage of nephritis (6-7 months).

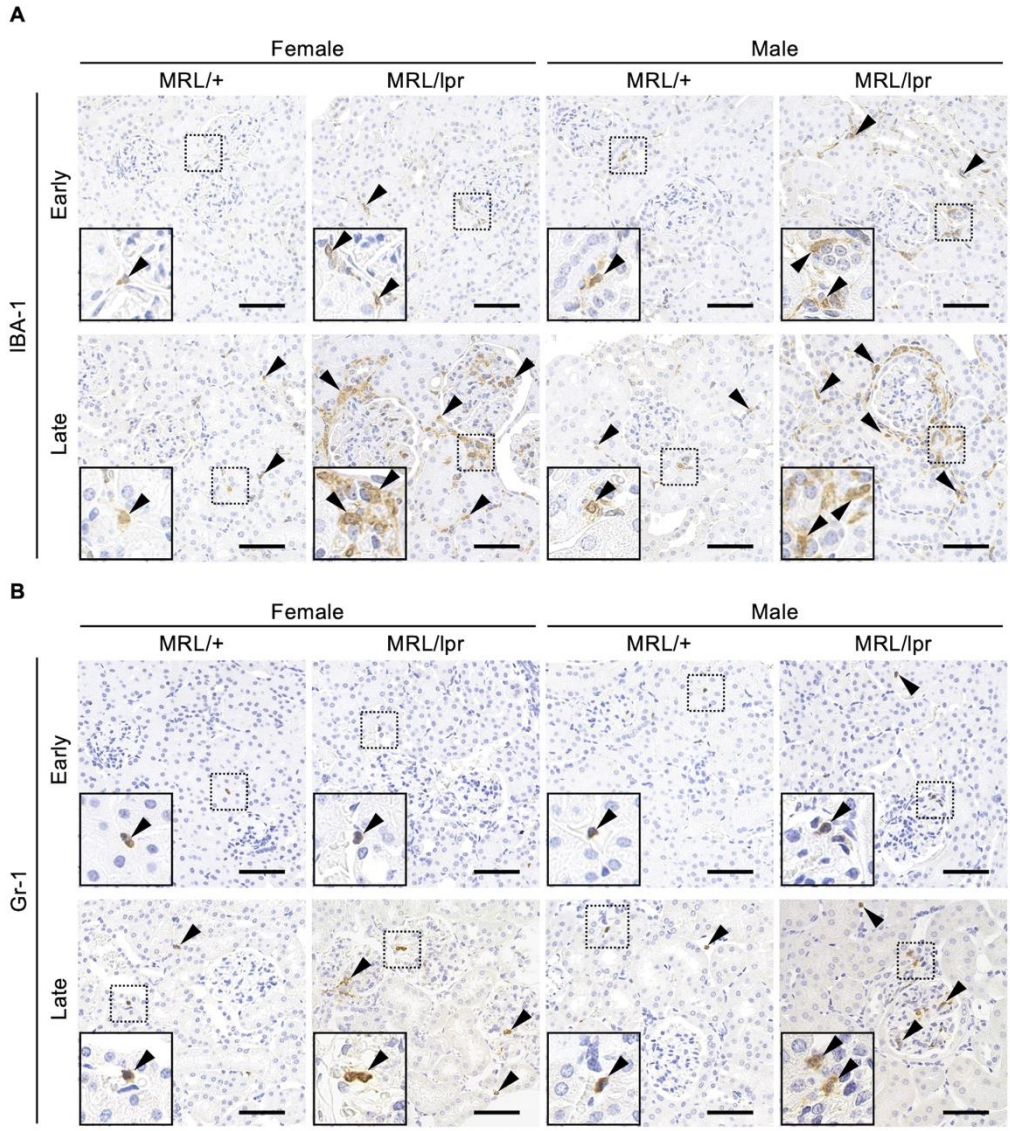

Figure 1-3. Infiltration of macrophages and neutrophils in the murine kidneys

(A and B) IHC images for IBA-1 (macrophage marker, panel A) and Gr-1 (neutrophil marker, panel B), respectively, for all groups. IBA-1$^+$ macrophages and Gr-1$^+$ neutrophils are abundant in the glomeruli and tubulointerstitium of both sexes of MRL/lpr mice at the late stage of spontaneous nephritis. Arrowheads indicate immune-positive cells. Insets indicate high magnification images of the areas marked by the black squares. Bars = 50 μm. Early: early stage of nephritis (3 months), Late: late stage of nephritis (6-7 months).

	Early				Late			
	F		M		F		M	
	MRL/+	MRL/lpr	MRL/+	MRL/lpr	MRL/+	MRL/lpr	MRL/+	MRL/lpr
Il1a	1.431	0.742	0.923	0.728	0.840	0.760	0.591	0.677
Il1b	1.037†	1.554	0.619	0.922	0.932†	2.282*	0.511	1.098*
Il1rn	1.217	1.079	0.778	1.966	1.112	11.323**§	0.682	5.569*
Il18	1.124	1.414	1.178	0.870	0.905	1.758	1.203	1.382
Il1f5 (IL-36Ra)	1.023†	0.434	0.284	0.496	0.337	0.306†	0.247	0.106§
Il1f6 (IL-36α)	1.113	1.130	0.538	0.879	1.023	12.022**§§	1.300	9.332**§
Il1f8 (IL-36β)	1.093	0.581	0.378	0.202	0.312§	0.447	0.533	0.228
Il1f9 (IL-36γ)	1.493	0.429	0.431	0.849	0.855	1.056††§	1.392	0.301
Il1f10 (IL-38)	1.504	0.918	0.258	0.554	0.668	0.513	0.289	0.392
Il33	1.099	0.948	0.550	0.782	1.139†	1.842	0.624	0.537

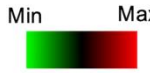

Figure 1-4. mRNA expression of IL-1 family members in the murine kidneys

Heatmap for relative mRNA expression levels of *Il1a*, *Il1b*, *Il1rn*, *Il18*, *Il1f5*, *Il1f6*, *Il1f8*, *Il1f9*, *Il1f10*, and *Il33* in the kidneys. The expression levels are normalized to the values of *Actb* of female MRL/+ mice at the early stage of spontaneous nephritis. Each value represents the mean (n= 4-11). *: Significant difference in MRL/lpr mice against MRL/+ mice of the same sex at the same stage (*: $P < 0.05$, **: $P < 0.01$). †: Significant difference in female against male mice of the same strain at the same stage (†: $P < 0.05$, ††: $P < 0.01$). §: Significant difference at the late stage against the early stage in the same mice strains of the same sex (§: $P < 0.05$, §§: $P < 0.01$). Mann-Whitney *U*-test, qPCR analysis. F: female, M: male, Early: early stage of nephritis (3 months), Late: late stage of nephritis (6-7 months).

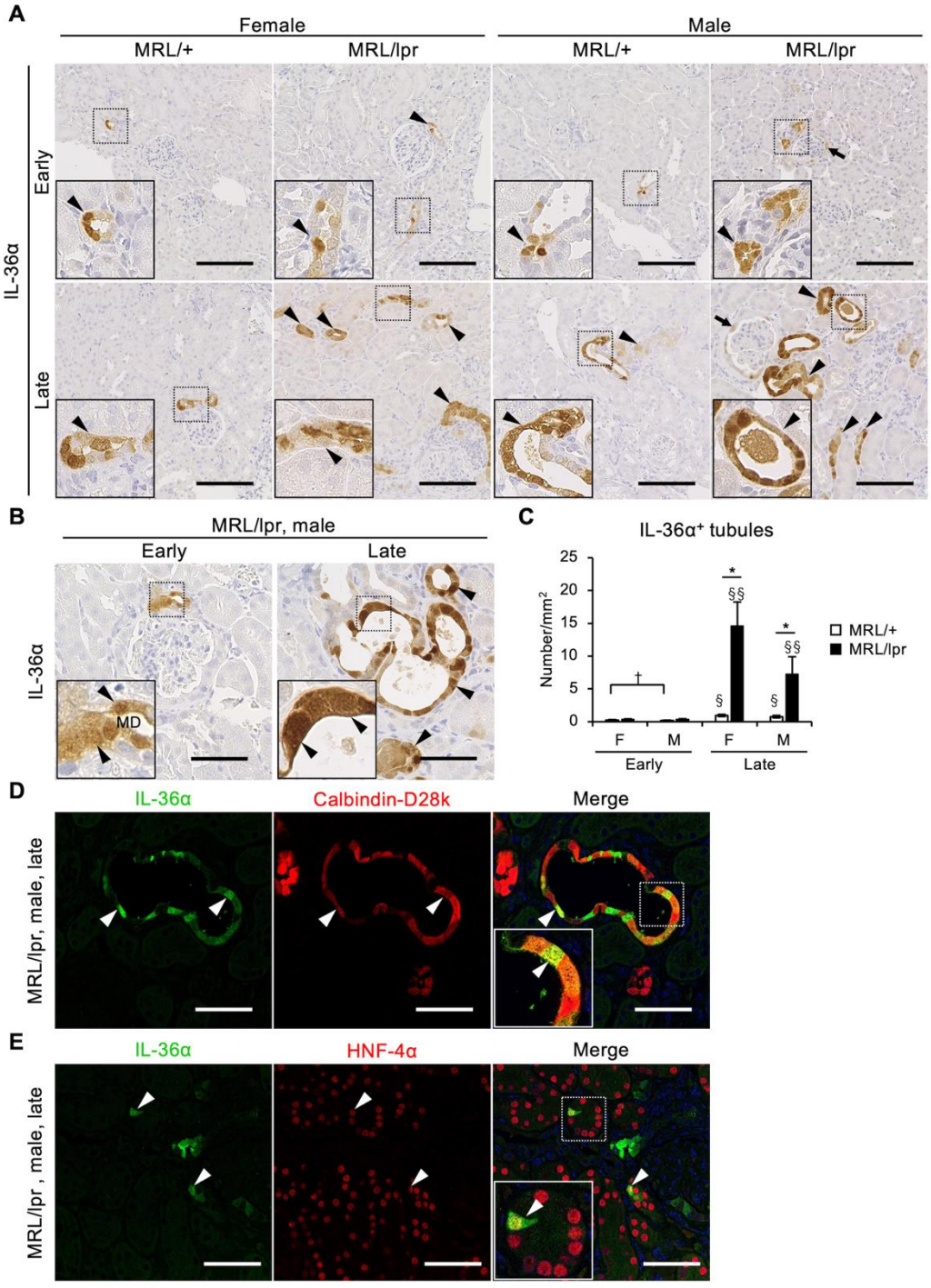
A
Female
Male
MRL/+
MRL/lpr
MRL/+
MRL/lpr
IL-36α
Early
Late
B
MRL/lpr, male
Early
Late
IL-36α
MD
C
IL-36α⁺ tubules
Number/mm²
25
20
15
10
5
0
MRL/+
MRL/lpr
F
M
F
M
Early
Late
D
IL-36α
Calbindin-D28k
Merge
MRL/lpr, male, late
E
IL-36α
HNF-4α
Merge
MRL/lpr , male, late

Figure 1-5. IL-36α localization in the renal tubules of the murine kidneys

(A) IHC images for IL-36α. IL-36α$^+$ renal tubules (arrowheads) are observed in all groups at the early stage of spontaneous nephritis, and those numbers tend to increase in both sexes of MRL/lpr mice as they age. Meanwhile, IL-36α$^+$ renal corpuscles (arrows) are frequently found in male MRL/lpr mice at the late stage. Bars = 100 μm. **(B)** Representative IHC images for IL-36α in male MRL/lpr mice at the early and late stages. IL-36α$^+$ reactions (arrowheads) are observed in the cytoplasm and nucleus of tubular epithelial cells, including a segment of MD and dilated tubules with urinary cast. Bars = 50 μm. **(C)** The number of IL-36α$^+$ renal tubules. Each bar represents the mean ± SE (n= 4-9). *: Significant difference in MRL/lpr against MRL/+ mice of the same sex at the same stage (*: $P < 0.05$). †: Significant difference in female against male mice of the same strain at the same stage (†: $P < 0.05$). §: Significant difference at the late stage against the early stage in the same mouse strains of the same sex (§: $P < 0.05$, §§: $P < 0.01$). Mann-Whitney *U*-test. **(D and E)** Representative double IF images for IL-36α (green) with calbindin-D28k (red, distal tubule marker) or HNF-4α (red, proximal tubule marker) in male MRL/lpr mice at the late stage. IL-36α$^+$ cells are mainly observed in calbindin-D28k$^+$ distal tubules (panel D), while the number of these cells in HNF-4α$^+$ proximal tubules is quite few (panel E). Arrowheads indicate IL-36α$^+$, calbindin-D28k$^+$, or HNF-4α$^+$ cells. The nucleus is stained by Hoechst (blue). Insets indicate high magnification images of areas marked by the white squares. Bars = 50 μm. F: female, M: male, Early: early stage of nephritis (3 months), Late: late stage of nephritis (6-7 months), MD: macula densa.

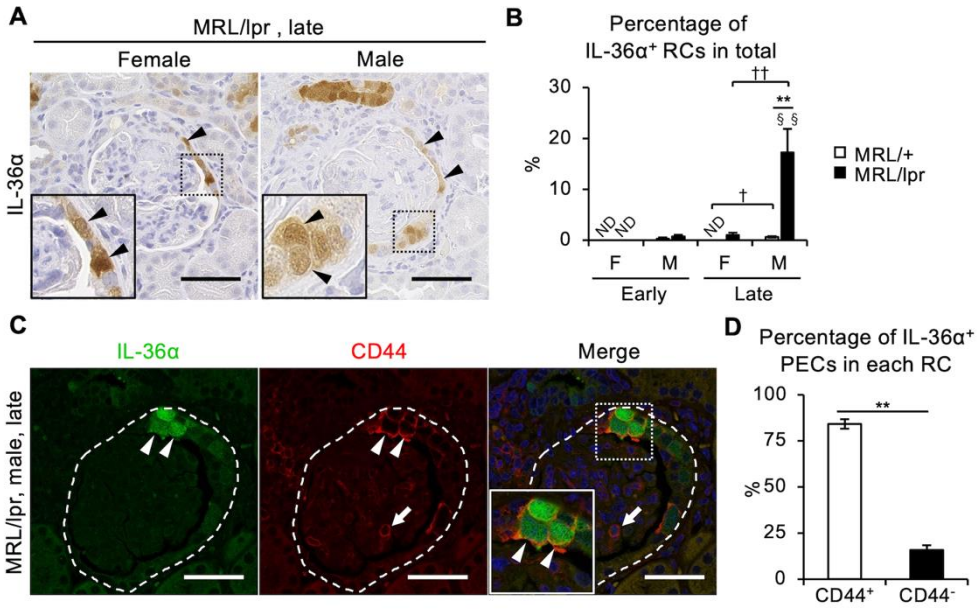

Figure 1-6. IL-36α localization in parietal epithelial cells of the murine kidneys

(A) Representative IHC images for IL-36α in female and male MRL/lpr mice at the late stage of spontaneous nephritis. IL-36α$^+$ reactions (arrowheads) are observed in the cytoplasm and nucleus of cuboidal parietal epithelial cells. Bars = 50 μm. **(B)** Percentage of the number of IL-36α$^+$ renal corpuscles to that of total ones. Each bar represents the mean ± SE (n= 4-9). *: Significant difference in MRL/lpr against MRL/+ mice of the same sex at the same stage (**: P <0.01). †: Significant difference in female against male mice of the same strain at the same stage (†: P < 0.05, ††: P <0.01). §: Significant difference at the late stage against the early stage in the same mouse strains of the same sex (§§: P <0.01). Mann-Whitney U-test. **(C)** Representative double IF images for IL-36α (green) and CD44 (red) in male MRL/lpr mice at the late stage. IL-36α is frequently co-expressed in CD44$^+$ parietal epithelial cells (arrowheads). Arrows indicate infiltrated CD44$^+$ cells. The nucleus is stained by Hoechst (blue). Dotted lines indicate renal corpuscles. Inset indicates high magnification image of area marked by the white square. Bars = 50 μm. **(D)** Percentage of IL-36α$^+$ parietal epithelial cells in CD44 positive and negative parietal epithelial cells in male MRL/lpr mice at the late stage. Each bar represent the mean ± SE (n= 5). *: Significant difference in CD44$^+$ parietal epithelial cells against CD44$^-$ parietal epithelial cells (Mann-Whitney U-test, ** P < 0.01). F: female, M: male, Early: early stage of nephritis (3 months), Late: late stage of nephritis (6-7 months), RC: renal corpuscle, PEC: parietal epithelial cell, ND: not detected.

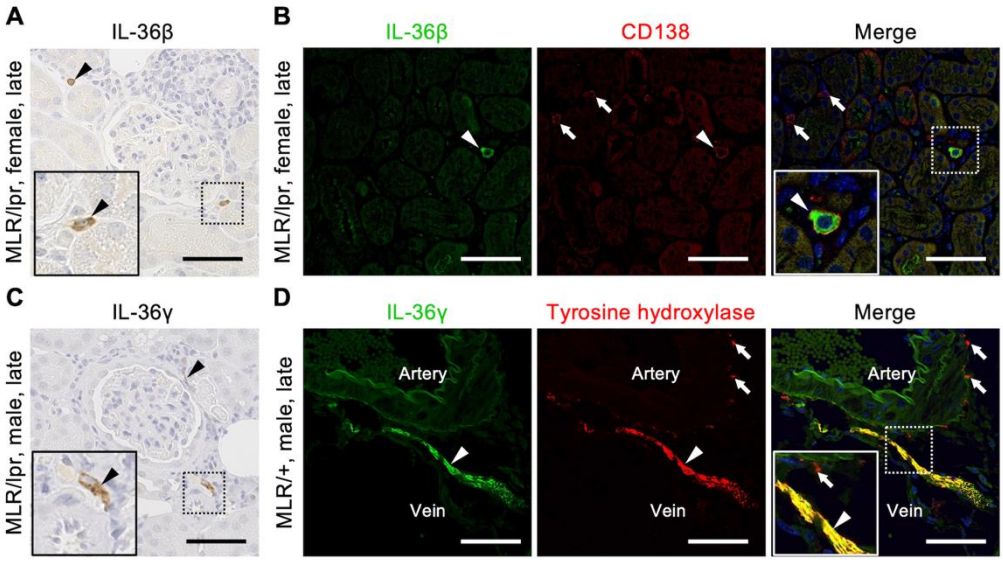

Figure 1-7. Localization of IL-36β and IL-36γ in the murine kidneys

(A) Representative IHC image for IL-36β in female MRL/lpr mice at the late stage of spontaneous nephritis. IL-36β^{+} reactions (arrowheads) are rarely observed in the cytoplasm of interstitial cells. Bars = 50 μm. **(B)** Representative double IF images for IL-36β (green) and CD138 (red, plasma cell marker) in female MRL/lpr mice at the late stage. IL-36β is expressed in CD138^{+} plasma cells (arrowheads). Arrows indicate IL-36β^{-} CD138^{+} cells. The nucleus is stained by Hoechst (blue). Inset indicates high magnification image of the area marked by the white square. Bars = 50 μm. **(C)** Representative IHC image for IL-36γ in male MRL/lpr mice at the late stage. IL-36γ^{+} reactions (arrowheads) are found mainly in the interstitium surrounding the vessels or renal corpuscles. Bars = 50 μm. **(D)** Representative double IF images for IL-36γ (green) and tyrosine hydroxylase (red, sympathetic nerve marker) in male MRL/+ mice at the late stage. Tyrosine hydroxylase^{+} sympathetic axons exhibit IL-36γ positive and negative reactions (arrowheads and arrows, respectively). The nucleus is stained by Hoechst (blue). Inset indicates high magnification image of the area marked by the white square. Bars = 50 μm. Late: late stage of nephritis (6-7 months).

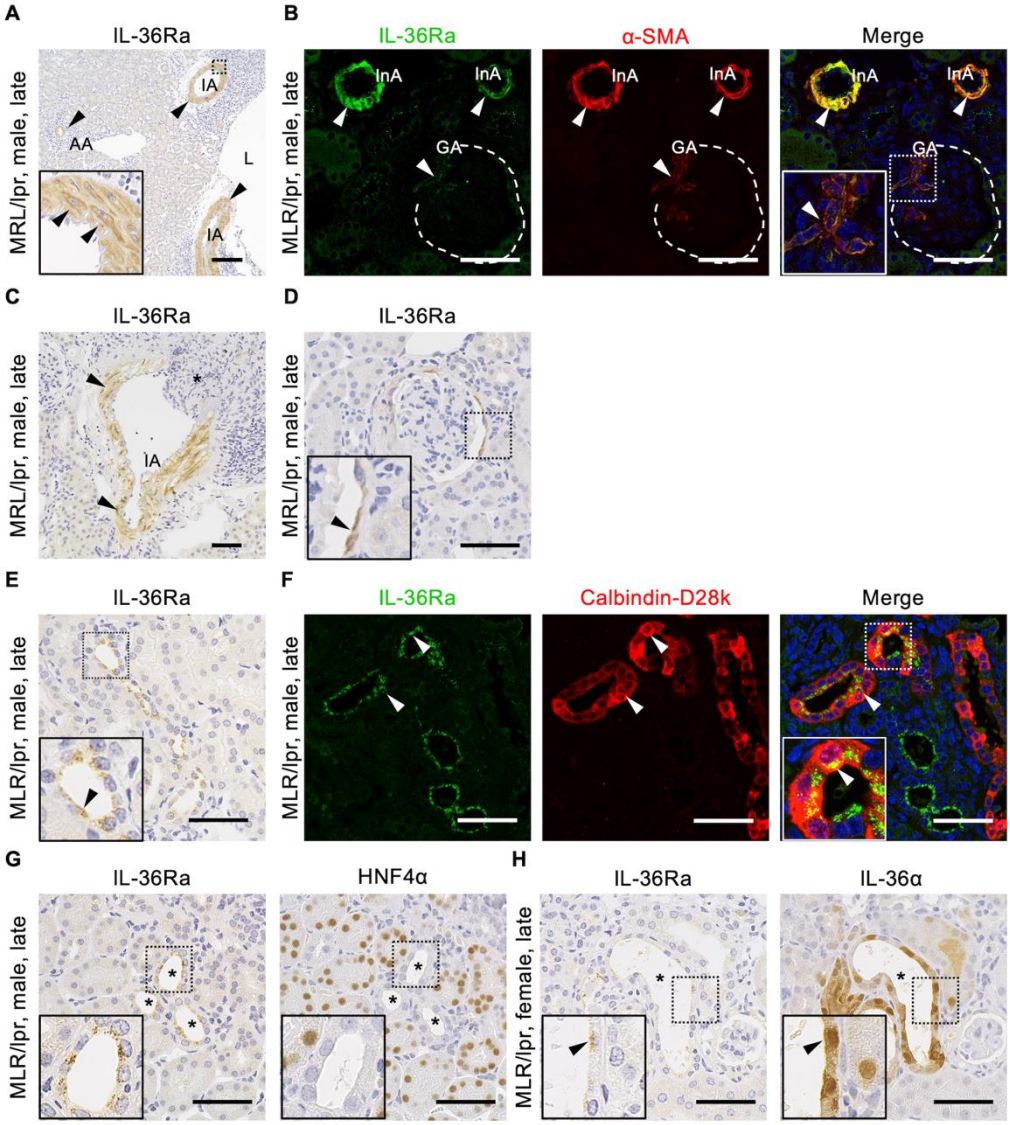
A
IL-36Ra
MRL/lpr, male, late
IA
AA
L
IA
B
IL-36Ra
α-SMA
Merge
MLR/lpr, male, late
InA
InA
GA
C
IL-36Ra
MRL/lpr, male, late
IA
D
IL-36Ra
MRL/lpr, male, late
E
IL-36Ra
MLR/lpr, male, late
F
IL-36Ra
Calbindin-D28k
Merge
MLR/lpr, male, late
G
IL-36Ra
HNF4α
MLR/lpr, male, late
H
IL-36Ra
IL-36α
MLR/lpr, female, late

Figure 1-8. Localization of IL-36Ra in the murine kidneys

(A) Representative IHC image for IL-36Ra in male MRL/lpr mice at the late stage of spontaneous nephritis. IL-36Ra$^+$ reactions (arrowheads) are observed in the tunica media of arteries. Bars = 100 μm. **(B)** Representative double IF images for IL-36Ra (green) with α-SMA (red, smooth muscle cell marker) in male MRL/lpr mice at the late stage. IL-36Ra$^+$ reactions are observed in the cytoplasm of smooth muscle cells of arteries and arterioles. Arrowheads indicate IL-36Ra$^+$ or α-SMA$^+$ cells. The nucleus is stained by Hoechst (blue). Dotted lines represent renal corpuscles. Inset indicates high magnification image of the area marked by the white square. Bars = 50 μm. **(C-E)** Representative IHC images for IL-36Ra in male MRL/lpr mice at the late stage. The IL-36Ra$^+$ reaction in smooth muscle cells with vasculitis (asterisk) is partially defective (panel C). IL-36Ra$^+$ reactions are observed in parietal and tubular epithelial cells (panel D and E, respectively). Arrowheads indicate IL-36Ra$^+$ reactions. Insets indicate high magnification images of the areas marked by the black squares. Bars = 50 μm. **(F)** Representative double IF images for IL-36Ra (green) and calbindin-D28k (red, distal tubule marker) in male MRL/lpr mice at the late stage. The granular IL-36Ra$^+$ reactions are expressed in the apical portion of distal tubular epithelial cells. Arrowheads indicate IL-36Ra$^+$ or calbindin-D28k$^+$ cells. The nucleus is stained by Hoechst (blue). Insets indicate high magnification images of areas marked by the black squares. Bars = 50 μm. **(G)** Representative serial sections followed by IHC for IL-36Ra and HNF-4α (proximal tubule marker) in male MRL/lpr mice at the late stage. The IL-36Ra$^+$ reaction is not observed in HNF-4α$^+$ proximal tubules. Asterisks indicate IL-36Ra$^+$ HNF-4α$^-$ tubules. Bars = 50 μm. **(H)** Representative serial sections followed by IHC for IL-36Ra and IL-36α in female MRL/lpr mice at the late stage. A portion of the tubular epithelial cells co-express IL-36Ra and IL-36α (arrowheads). Asterisks indicate the same tubules. Insets indicate high magnification images of the areas marked by the black squares. Bars = 50 μm. Late: late stage of nephritis (6-7 months), L: lumen of renal pelvis, IA: interlobar artery, AA: arcuate artery, InA: intralobular artery, GA: glomerular arteriole.

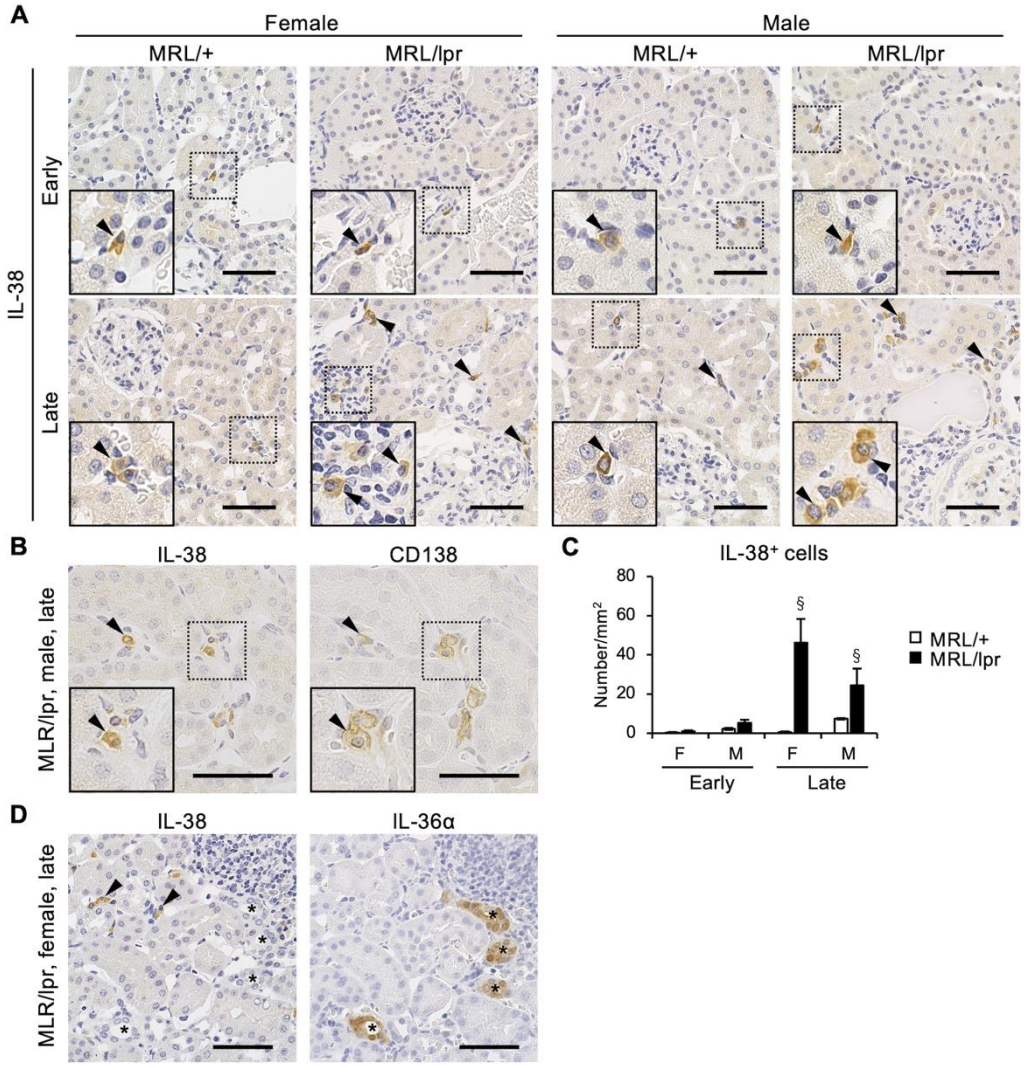

Figure 1-9. Localization of IL-38 in the murine kidneys

(A) IHC images for IL-38. IL-38$^+$ cells are found in the tubulointerstitium of all groups, and that number is abundant in both sexes of MRL/lpr mice at late stage of spontaneous nephritis compared to those observed in the others. Bars = 50 μm. **(B)** Representative serial sections followed by IHC for IL-38 and CD138 (plasma cell marker) in male MRL/lpr mice at the late stage. IL-38 is expressed in CD138$^+$ plasma cells (arrowheads). Bars = 50 μm. **(C)** The number of IL-38$^+$ cells in the tubulointerstitium. Each bar represents the mean ± SE (n= 4-9). §: Significant difference at the late stage against the early stage in the same mouse strains of same sex (§: $P < 0.05$). Mann-Whitney *U*-test. **(D)** Representative serial sections followed by IHC for IL-38 and IL-36α in female MRL/lpr mice at the late stage. IL-38$^+$ cells (arrowheads) are not surrounding IL-36α$^+$ renal tubules (asterisks). Bars = 50 μm. F: female, M: male, Early: early stage of nephritis (3 months), Late: late stage of nephritis (6-7 months).

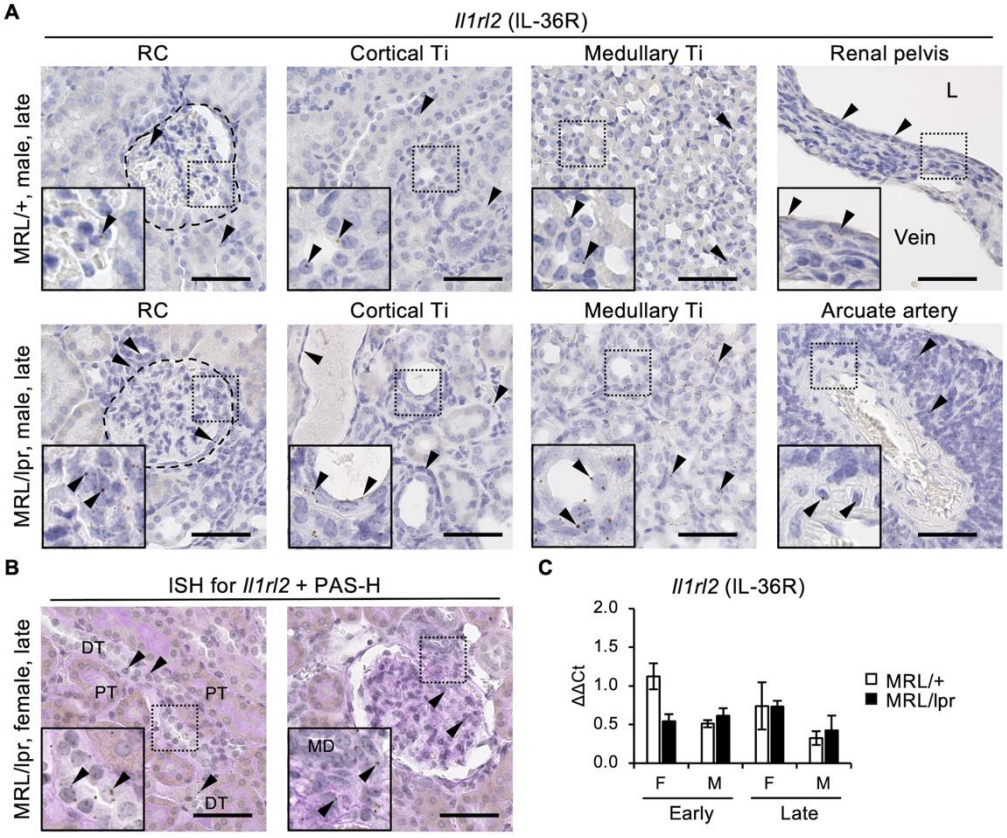

Figure 1-10. *Il1rl2* localization in the murine kidneys

(A) Representative ISH images for *Il1rl2* in male MRL/+ and MRL/lpr mice at the late stage of spontaneous nephritis. *Il1rl2*$^{+}$ reactions (arrowheads) are observed in glomeruli, tubulointerstitium, and vasculature from cortex to medulla in both strains, and this expression is induced in glomerular and tubulointerstitial lesions of MRL/lpr mice. Dotted lines indicate renal corpuscles. Insets indicate high magnification images of the areas marked by the black squares. Bars = 50 μm. **(B)** Representative ISH for *Il1rl2* images followed by PAS-H staining in female MRL/lpr mice at the late stage. *Il1rl2*$^{+}$ reaction (arrowheads) is observed in PAS^{-} distal tubules and not in PAS^{+} proximal tubules. The positive cells are in close proximity to the vascular pole in MRL/lpr mice at the late stage. Insets indicate high magnification images of the areas marked by the black squares. Bars = 50 μm. **(C)** mRNA expression of *Il1rl2* coding IL-36R in kidneys. The expression levels are normalized to the values of *Actb*, and those of female MRL/+ mice at the early stage. Each bar represents the mean ± SE (n= 4-11). F: female, M: male, Early: early stage of nephritis (3 months), Late: late stage of nephritis (6-7 months), RC: renal corpuscle, Ti: tubulointerstitium, L: lumen of renal pelvis, PAS-H: periodic acid Schiff-hematoxylin, DT: distal tubule, PT: proximal tubule, MD: macula densa.

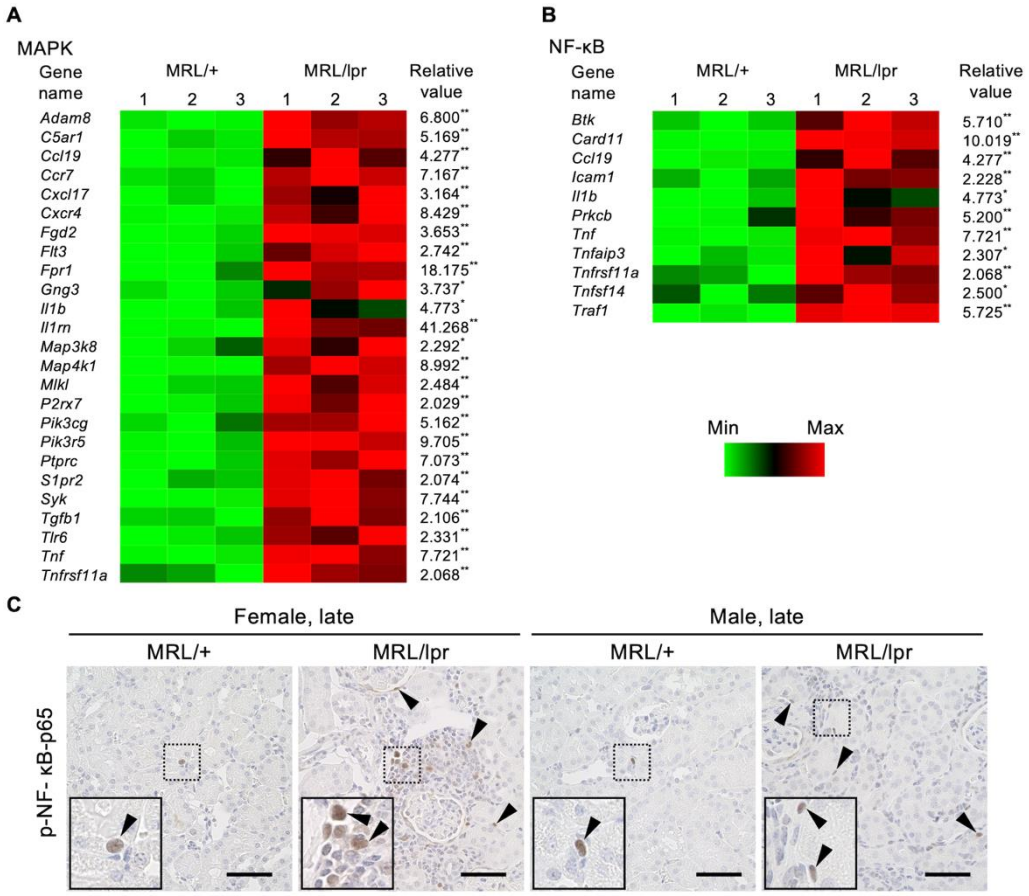

Figure 1-11. Upregulated downstream-genes involved in IL-1 family signaling and localization of p-NF-κB in the murine kidneys

(A and B) GO analysis for positive regulation of MAPK activity (GO: 0043406; panel A) and of NF-κB transcription factor activity (GO: 0051092; panel B) in the kidneys of female MRL/lpr mice at the late stage of spontaneous nephritis compared to those values in female MRL/+ mice at the same stage. MRL/lpr mice possess 25 genes associated with positive regulation of MAPK activity (panel A) and 11 genes associated NF-κB transcription factor activity (panel B) that are upregulated more than 2-fold compared to those of MRL/+ mice. Each value represents the relative mRNA level of MRL/lpr mice against MRL/+ mice (n =3). *: Significant difference in female MRL/lpr mice at the late stage against the same sexes of MRL/+ mice at the same stage (Student *t*-test, * $P < 0.05$, ** $P < 0.01$). **(C)** Representative IHC images for p-NF-κB. p-NF-κB^{+} nuclei (arrowheads) are observed in tubular and parietal epithelial cells, and infiltrated cells of all groups at the late stage of nephritis, and that number is abundant in both sexes of MRL/lpr mice compared to MRL/+. Insets indicate high magnification images of the areas marked by the black squares. Bars = 50 μm. Min: minimum expression of mRNA, Max: maximum expression of mRNA, Early: early stage of spontaneous nephritis (3 months), Late: late stage of spontaneous nephritis (6-7 months).

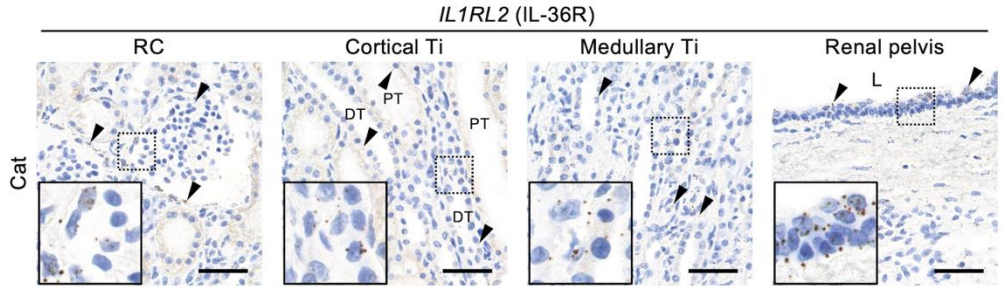

Figure 1-12. *IL1RL2* localization in the cat kidneys

Representative ISH images for *IL1RL2* in cat kidneys. *IL1RL2*$^{+}$ reactions (arrowheads) are observed in parietal epithelial cells, podocytes, mesangial cells, and tubular epithelial cells, interstitial cells from cortex to medulla as well as urothelium. In renal tubules, the positive reactions are dominant in distal tubules compared with proximal tubules. Insets indicate high magnification images of the areas marked by the black squares. Bars = 50 μm. RC: renal corpuscle, Ti: tubulointerstitium, L: lumen of renal pelvis, PT: proximal tubule, DT: distal tubule.

Chapter 2

Interleukin 36 receptor deficiency ameliorates the renal lesions in autoimmune disease-mediated nephritis

Introduction

In Chapter 1, the author described that IL-36R ligands are associated with the development and progression of glomerular and tubulointerstitial lesions showing renal epithelial cell damages in spontaneous nephritis of MRL/lpr mice. The IL-36α, IL-36β, and IL-36γ act as agonists and induce NF-κB and MAPK signaling, while IL-36Ra and IL-38 bind to IL-36R and prevent the formation of IL-1R accessory protein. In the kidneys of MRL/lpr mice, IL-36R ligands show constitutive and induced expression. In normal kidneys, IL-36γ and IL-36Ra are localized in sympathetic axons and smooth muscle cells, respectively, while IL-36α, IL-36β, IL-36Ra, and IL-38 are ectopically induced in renal tissues, such as renal epithelial cells and mesenchymal cells. In particular, the nephritis show overexpression of IL-36α in parietal and distal tubular epithelial cells, and IL-38 in plasma cells. Since IL-36R-KO mice present the amelioration of CKD and AKI pathology [28,94], the author next analyzed renal phenotypes of MRL/lpr mice with IL-36R deficiency in this chapter.

Immune-mediated nephritis, such as LN, is closely associated with progression of systemic and local immune conditions, which are mediated by IL-36R signaling. Serum levels of IL-36α, IL-36γ, and IL-38 are increased in patients with SLE, whereas IL-36Ra levels are decreased [30,81]. Furthermore, IL-36R ligands are associated with the development of inflammatory diseases in other organs; rheumatoid arthritis, psoriasis, inflammatory bowel disease, neuromyelitis, Sjögren's syndrome, and systemic sclerosis [26]. Constitutively, they are produced in dendritic cells and epithelial cells in sites including the skin and intestine, and have a function in innate immunity. However, their overexpression under disease conditions is induced in T cells, B cells, and monocytes, leading to exacerbation of their pathology [4,102]. Although injection of IL-38, an IL-36R antagonist, inhibits skin and kidney lesions in MRL/lpr mice, IL-38 can bind to other receptors, including IL-1R and IL-1R accessory protein-like 1 (IL-1RAPL1) [29,46]. Thus, it remains unclear whether IL-36R deficiency affects systemic immune abnormality followed by the development and progression of nephritis.

In the local immunity, tertiary lymphoid structures, which develop under chronic inflammation, contribute to renal pathology. They are formed in the renal parenchyma and are involved in the progression of nephritis including an increase in IL-36α$^+$ injured renal tubules [24,71,109,110,117,137]. Previous studies using MRL/lpr mice revealed that autoimmunity also induces the development of tertiary lymphoid structures in the kidneys, UTALSs beneath the urothelium, and perivascular tertiary lymphoid structures in the surrounding arteries [54,85]. Regardless of IL-36R ligand expression in several lymphoid organs, including bone marrow and spleen [123], a relation between IL-36R signaling and local tertiary lymphoid structures in kidneys have not been revealed.

In this chapter, the author examined alterations in the immunological status and renal

phenotypes, especially the renal epithelial cell injuries, in IL-36R deficient MRL/lpr mice. Lack of IL-36R signaling partially ameliorated the glomerular and tubulointerstitial lesions without expression changes of IL-36R ligands. Moreover, the collective findings support the possibility of IL-36R-independent IL-36α signaling pathway.

Materials and Methods

Research ethics

All animal experimentation was approved by the Institutional Animal Care and Use Committee of the Faculty of Veterinary Medicine, Hokkaido University (approved by the Association for Assessment and Accreditation of Laboratory Animal Care International, approval No. 16-0124, 20-0012, 21-0008).

IL-36R-KO mice

Two single-guide RNA designed for the target sequences (5'-3') and *Cas9* mRNA were prepared as described previously [95]. An single-guide RNA expression vector for target sequence with a T7 promoter was chemically synthesized (Operon Biotechnologies, Tokyo, Japan), and transcribed *in vitro* using the MEGAshortscript Kit (#AM1354; Life Technologies, Carlsbad, CA, USA). *hCas9* mRNA was synthesized using the mMESSAGE mMACHINE T7 Kit (#AM1344; Life Technologies) and polyadenylated with a Poly(A) Tailing Kit (#AM1350; Life Technologies). Purified *hCas9* mRNAs at 100 ng/mL and each single-guide RNA at 50 ng/mL targeting exon 3 for *Il1rl2* (encoding IL-36R) were co-injected into the cytoplasm of pronuclear stage eggs from C57BL/6N (B6; Japan SLC, Inc.). The eggs were transferred into the oviduct of pseudopregnant ICR (Japan SLC, Inc.) female mice. The target sequences containing protospacer adjacent motif (PAM) sequences for intron 2 and intron 3 of *Il1rl2* gene were as follows: 5'-TCTAAATGACTGGGCTAGTTTGG-3' ; 5'- CAGGGCAGCCTTGAACTGGCAGG-3', respectively. Founders were genotyped using primer pairs spanning the CRISPR/Cas9 cleaved site. The *Il1rl2* mutation was confirmed by sequencing. To minimize the risk of off-target effects, the resulting founder mouse was backcrossed with B6 mice for more than two generations. The progeny were crossed with MRL/lpr mice for six generations. Homozygous IL-36R-KO and wild-type (WT) of MRL/lpr mice were used in this study. The genotype of the obtained littermates was confirmed by genotyping PCR analysis using primers specific for the *Il1rl2* mutation (Table 2-1). Six-month-old male and female IL-36R-KO and WT mice were used and were maintained under the conditions as described in chapter 1.

Anesthesia, urine and blood collection, and S/B ratio calculation were performed as described in chapter 1.

Cell culture

Spleens were isolated from WT or IL-36R-KO mice and minced in culture dishes. Ten milliliters of 1× PBS- (#164-25511; FUJIFILM Wako Pure Chemical Corporation) was added, the sample was filtered using 100-μm cell strainers (#352360; Corning Inc., Corning, NY, USA), and centrifuged at 200 g for 5 min. Following aspiration of the supernatant, the cells were

resuspended, incubated with 10 mL 0.017 M Tris buffer containing 0.75% ammonium chloride (pH 7.65) for 5 min, and washed with 10 mL PBS. This solution was filtered using 40-μm cell strainers (#352340; Corning Inc.) and centrifuged at 200 g for 5 min. After washing twice with PBS, the collected cells were resuspended in antibiotic-free, L-glutamine-containing RPMI 1640 (#189-02025; FUJIFILM Wako Pure Chemical Corporation) and harvested in 12-well culture plates (#92424; Techno Plastic Products, Trasadingen, Switzerland).

The cells were stimulated with recombinant mouse IL-36α (#7059-ML-010; R&D Systems, Minneapolis, MN, USA) at 0, 20, and 200 ng/mL in PBS. After incubation at 37 °C for 5 h, the culture medium and cells were collected for RNA analysis.

Serological analysis and urinalysis

Serum levels of dsDNA antibody, serum concentration of Cr, BUN and uACR were measured as performed in chapter 1.

Histopathology

Kidneys were fixed overnight in 10% NBF at room temperature or 4% paraformaldehyde at 4 °C. The specimens were dehydrated using ethanol and embedded in paraffin. Paraffin sections (2-μm thick) were fixed with 10% NBF and stained with PAS-H or picrosirius red to analyze renal histopathology.

IHC and/or IF analyses for IBA-1, CD3, IL-36α, IL-38, acetylated lysine (Ac-lysine), and general control non-depressible 5 (GCN5) were performed to detect macrophages, T cells, injured distal tubules, IL-36 subfamily associated plasma cells, acetylated histone, and acetyl transferase in nuclei. IHC and IF were performed as done in Chapter 1. Details of the antibodies, antigen retrieval, and blocking are listed in Table 1-1 and 2-2.

All specimens were randomly analyzed. IL-36α^{+} tubules and renal corpuscles, IL-38^{+} cells in tubulointerstitium, the number of nuclei in the glomerulus, size, and area ratio of PAS^{+} mesangium to glomerulus, infiltrated IBA-1^{+} macrophages and CD3^{+} T cells in tubulointerstitium, were measured as done in Chapter 1. For picrosirius red staining, the positive fiber area was measured in more than 10 tubulointertstitial areas in the cortex and outer medulla at 200× magnification using a BZ-X analyzer and the positive area ratio was calculated.

qPCR

qPCR analysis was performed as done in Chapter 1 by using gene-specific primers (Table 1-2 and 2-1). The data were normalized according to the values of *Actb*, and those of female WT mice using the delta-delta Ct method.

Statistical analyses

The results are expressed as the mean ± SE and statistically analyzed in a non-parametric manner. The significance between the two groups was analyzed using the Mann-Whitney *U*-test ($P < 0.05$). The correlation between the two parameters was analyzed using Spearman's correlation test ($P < 0.05$).

Results

No altered systemic autoimmunity in IL-36R-KO mice

The author established IL-36R-KO mice on a spontaneous nephritis model mouse, MRL/lpr background (Fig. 2-1A and B). In WT mice, the mRNA level of *Il1rl2*, which encodes IL-36R, was higher in the kidneys of female mice than in those of male mice (Fig. 2-1B). To clarify the deficiency of IL-36R signaling, spleen cells derived from WT and IL-36R-KO male mice were stimulated with IL-36α, and *Cxcl2*, the downstream molecule, was analyzed [63]. Following IL-36α stimulation at 200 ng/mL, *Cxcl2* levels in spleen cells from IL-36R-KO mice were significantly lower than those in WT mice (Fig. 2-1C). Thus, the author confirmed a lack of IL-36R function in the mice.

Previous studies in addition to the results shown in Chapter 1 have revealed that IL-36R ligands are expressed in immune cells, such as plasma cells and T cells, under hyperimmune reactivity [102]. Thus, systemic autoimmune conditions were presently examined in MRL/lpr mice according to IL-36R deficiency. Both sexes of IL-36R-KO mice showed no difference compared with WT mice in the indices of S/B ratio and serum anti-dsDNA antibody level. However, anti-dsDNA antibody levels in female WT mice were significantly higher than those in male mice (Fig. 2-1D and E). Therefore, IL-36R dysfunction did not affect systemic autoimmune abnormalities in the MRL/lpr mice.

No altered IL-36R ligand expression in the kidneys of IL-36R-KO mice

To clarify whether IL-36R ligand expression is affected by IL-36R deficiency, the author examined the mRNA levels of IL-36R ligands in the kidneys using qPCR analysis. There was no difference between IL-36R-KO and WT mice or between sexes (Fig. 2-2A). As show in Chapter 1, the author revealed that IL-36α and IL-38, which are agonists and antagonists of IL-36R, respectively, are overexpressed in the kidneys of MRL/lpr mice with the nephritis progression. Thus, those protein localization and levels were also analyzed by IHC. IL-36α was localized in the cytoplasm and nuclei of distal tubular epithelial cells with dilated tubular lumen and/or urinary cast. IL-36α was also found in parietal epithelial cells, especially in male mice (Fig. 2-2B). Importantly, the localization of IL-36α$^+$ reactions in these cells was not altered by IL-36R deficiency. Furthermore, IL-38$^+$ plasma cells were observed in tubulointerstitium (Fig. 2-2C). The histological scores showed that IL-36α expression in renal corpuscles was higher in male mice than in female mice with or without IL-36R deficiency. The IL-36α$^+$ renal corpuscle ratio, number of IL-36α$^+$ renal tubules, and IL-38$^+$ cells in tubulointerstitium were comparable between WT and IL-36R-KO mice (Fig. 2-2D-F). Thus, the lack of IL-36R signaling did not alter the expression of IL-36R ligands in mouse kidneys with the nephritis.

Ameliorated glomerular lesions in IL-36R-KO mice

Next, the author examined the renal function using serological analysis and urinalysis. BUN, Cr, and uACR levels were comparable among all groups, although some female WT mice showed high values (Fig. 2-3A-C).

The author also analyzed glomerular histopathology in IL-36R-KO mice. All groups manifested glomerular hypercellularity, hypertrophy, and mesangial matrix expansion (Fig. 2-3-D). In terms of histopathological scores, glomerular size tended to be larger in male mice than in female mice, although there was no difference in size between WT and IL-36R-KO mice (Fig. 2-3E). In terms of the number of nuclei in the glomerulus and the area ratio of mesangium to glomerulus, male and female IL-36R-KO mice showed less tendency compared with WT mice of the same sex. Moreover, there were significant differences in the nuclei number of female and in the mesangial area of both sexes (Fig. 2-3F and G). The findings indicate that IL-36R deficiency ameliorated histopathological glomerular injury.

Partially inhibited tubulointerstitial fibrosis in IL-36R-KO mice

The author also evaluated tubulointerstitial lesions histopathologically. All groups showed cell infiltration into the tubulointerstitium with the development of tertiary lymphoid structures, such as perivascular tertiary lymphoid structures and UTALSs under the urothelium. These observations were comparable among the groups (Fig. 2-4A). Furthermore, IL-38$^+$ cells were also localized in tertiary lymphoid structures, although there was no significance in their expression (Fig. 2-4B). IBA-1$^+$ macrophages and CD3$^+$ T cells, which are involved in tubulointerstitial lesions with IL-36R ligands, were also evaluated. Both immune cells located in the tubulointerstitium and surrounding renal corpuscles and IBA-1$^+$ macrophages were more abundant than CD3$^+$ T cells (Fig. 2-4C and D). These numbers were comparable between WT and IL-36R-KO mice, independent of sex (Fig. 2-4E and F). Correlation analysis showed that the number of IL-36α$^+$ renal tubules in WT mice was positively correlated with the scores of CD3$^+$ T cells ($\rho = 0.770$, $P < 0.01$) and IBA-1$^+$ macrophages ($\rho = 0.624$, $P = 0.052$). However, IL-36R-KO mice did not show any correlation (Table 2-3), indicating that cell infiltration was not affected by IL-36α in IL-36R-KO mice.

Picrosirius red staining was performed to evaluate tubulointerstitial fibrosis. All groups featured more collagen fibers in the outer medulla than in the cortex (Fig. 2-5A). The histological scores in the outer medulla, but not the cortex, were significantly lower in female IL-36R-KO mice than in WT mice. However, there was no difference between the other groups (Fig. 2-5B). The mRNA levels of cytokines associated with inflammation and/or fibrosis were also examined. Only *Il10* levels in both female mice were significantly higher than those in male mice, while that in female IL-36R-KO mice was significantly downregulated compared with that in WT mice (Fig.

2-5C).

IL-36α translocation into the nuclei of renal epithelial cells independent of IL-36R

The author focused on IL-36α expression, which showed localization in the cytoplasm and nuclei of renal epithelial cells regardless of IL-36R expression (Fig. 2-2B). IL-1α, an IL-1 family member, functions in the nucleus as a transcriptional factor by lysine acetylation, but not through IL-1R, inducing IL-6 and IL-8 [98]. Thus, the author hypothesized that histones are acetylated in IL-36α$^+$ nuclei. In the kidneys with severe nephritis, Ac-lysine was mainly expressed in distal tubular and parietal epithelial cells, as well as myeloid cells. The positive nuclei were more abundant than in mild nephritis (Fig. 2-6A). In both WT and IL-36R-KO mice, Ac-lysine was localized in both IL-36α positive and negative nuclei. However, most IL-36α$^+$ nuclei co-expressed Ac-lysine (Fig. 2-6B). Moreover, the expression of lysine acetyltransferase 2A (also known as GCN5), which is a histone acetyltransferase and an IL-1α counterpart in the nuclei, was histologically examined. Both IL-36α and GCN5 were detected in the nuclei of distal tubular epithelial cells and were partially co-localized (Fig. 2-6C), indicating that histones were acetylated in nuclei expressing IL-36α.

Discussion

The present study clarified the prevention of IL-36R signaling pathway-modified renal epithelial cell injuries in spontaneous nephritis-prone MRL/lpr mice. IL-36R deficiency did not affect renal function, systemic autoimmune diseases, or local tertiary lymphoid structure formation in the mice. However, the histopathology of the nephritis, including glomerular and tubulointerstitial lesions, was partially ameliorated in IL-36R-KO mice. Moreover, IL-36α localized in the nuclei of renal epithelial cells was associated with histone acetylation.

In systemic autoimmune diseases, autoantibodies form immune complexes, which are deposited in the glomeruli, leading to glomerulonephritis. Moreover, the author have reported that systemic autoimmune abnormalities in MRL/lpr mice are one of the causes of the development of UTALSs and perivascular tertiary lymphoid structures in the kidneys, which are also formed in humans with CKD [54,85,109]. Some IL-36R ligands are expressed in immune cells, such as B cells, T cells, and monocytes, and are involved in immunological functions in healthy and disease conditions [102]. Dendritic cells and $CD4^+$ T cells in primary and secondary lymphoid tissues, such as the bone marrow and spleen, express IL-36R ligands contribute to cell maturation and activation, leading to the production of IL-1β and IL-6 proinflammatory cytokines [123]. In clinical cases, it has been reported that SLE severity in human patients is positively correlated with serum levels of IL-36α and IL-36γ [15]. However, in the present study, the author did not find any alteration in the systemic or local immune condition due to IL-36R deficiency, except for a decrease in *Il10* levels in the kidneys of female IL-36R-KO mice. IL-10, a major immunosuppressive cytokine, has various functions in the pathogenesis of autoimmune disease-mediated nephritis. IL-10-KO MRL/lpr mice exhaust skin lesions and glomerulonephritis, while $CD4^+$ helper T cell-producing IL-10 induces autoantibody production, leading to pathogenesis [21,107,138]. Further investigations are needed to elucidate the contribution of IL-36R signaling to IL-10 function in the nephritis development and progression. In contrast, major inflammatory cytokines, such as IL-1β, IL-6, and IFN-γ, which are abundantly produced under hyper-immuno-activating conditions, such as autoimmune disease, are comparable in the kidneys between genotypes [22,41,61,103]. Thus, IL-36R deficiency in MRL/lpr mice might not have crucial effects on immune reactivity because of hyperactivation of another immunological pathway in this strain.

Lack of IL-36R signaling also did not affect the gene and protein expression levels of IL-36R ligands, including IL-36α and IL-38, which were major molecules associated with pathological progression in mouse kidneys with autoimmune disease-mediated nephritis as shown in Chapter 1. However, glomerular and tubulointerstitial lesions were partially ameliorated in IL-36R-KO mice. IL-36α was localized in injured distal tubular and parietal epithelial cells in kidneys with the nephritis. A previous *in vitro* experiment revealed that lipopolysaccharide, a toll-like receptor ligand, induces IL-36α expression in distal tubular epithelial cells [55]. Furthermore,

IL-36α is associated with activation of the nucleotide-binding oligomerization domain-like receptor family pyrin domain containing 3 (NLRP3) inflammasome and IL-23/IL-17 signaling to facilitate inflammation and fibrosis [28]. IL-36R-KO mice with UUO display inhibited activation of the NLRP3 inflammasome and decreased infiltration of macrophages and T cells [28]. Moreover, tubular necrosis, apoptosis, and renal function, including BUN and serum Cr levels, were ameliorated in the AKI model of IL-36R-KO mice with IRI [94].

In this study, infiltration of $CD3^+$ cells and IBA-1^+ macrophages into tubulointerstitium was not altered by IL-36R deficiency. However, the number of IL-36α^+ tubules was positively correlated with cell infiltration in WT mice, but not in IL-36R-KO mice, indicating that alternative inflammatory cytokines might contribute to inflammation in IL-36R-KO mice. Tubulointerstitial fibrosis was also ameliorated in female IL-36R-KO mice, but not in male mice, compared with fibrosis in WT mice. Moreover, both sexes of IL-36R-KO mice showed inhibition of mesangial matrix expansion, although male mice showed abundant IL-36α^+ parietal epithelial cells compared with female mice. As one pathological mechanism, podocyte injuries cause renal UEB disruption with glomerular sclerosis; the study in Chapter 1 revealed that IL-36α^+ parietal epithelial cells co-express CD44, a marker of activated parietal epithelial cells, during proliferation and migration to the glomerulus in response to podocyte injury [114]. The pathology of autoimmune disease-mediated nephritis is formed by autoimmune reactivity, chronic tissue inflammation, and pathological response of kidney composing cells. In humans, females tend to develop SLE more easily than males; however, it is reported that the male patients show more severe pathology including typical skin lesions, serositis, and nephritis [79,112,135]. In MRL/lpr mice, the sex differences are still controversial. Some studies have reported that females present more sever nephritis with more autoantibody production [106,118], while another ones have showed that there is no significance between sexes in the disease severity [8,89,126]. In the present study, although female WT possessed higher level of autoantibody production compared with that in male, the renal lesions were comparable between sexes, indicating that autoantibody level, an index for SLE development, is not always correlated with LN severity. Moreover, the author found that expression of *Il1rl2* coding IL-36R was higher in the kidney of female WT than that of male. Sex-related mechanism regulating IL-36R expression is still unclear; however, downstream signaling in IL-36R^+ cells might be more strongly affected in female than male. Interestingly, distal tubular and parietal epithelial cells express IL-36R as well as estrogen and androgen receptors in rodents [12,59,66,97]. Therefore, the sex differences shown in the present study might be affected by sex-related molecules regulating IL-36R expression in renal epithelial cells, although further analysis is needed to elucidate the relations between IL-36R signaling and sex hormones in kidneys.

As shown in Chapter 1, plasma cells overexpressed IL-38 in MRL/lpr cells with the progression of renal lesions. In this chapter, IL-38 expression did not change with IL-36R

expression. IL-38 injection in MRL/lpr mice was reported to ameliorate pathological severity, including skin and kidney lesions [29], while IL-38 deficiency exacerbated renal pathology with an increase in autoantibody production [133]. Both IL-36Ra and IL-38 bind to IL-36R and cannot recruit IL-1R accessory protein; however, IL-38 can bind to other receptors, IL-1R and IL-1RAPL1 [46,132]. The affinity of IL-38 to IL-1R, whose agonists are IL-1α and IL-1β, is lower than that of IL-1Ra. Yet, IL-38 can prevent the formation of IL-1R with the co-receptor, similar to IL-1Ra [10,46]. Another IL-38 receptor, IL-1RAPL1, is expressed mainly in the brain, heart, and skin [17]. *In vitro* experiments revealed that this receptor is overexpressed in human macrophages cultured in a medium with apoptotic conditions, and that IL-38 produced in apoptotic cells antagonizes the IL-1RAPL1 signaling pathway [90]. In the present study, IL-38$^+$ plasma cells, one of the cells comprising perivascular tertiary lymphoid structures and UTALSs, were comparable between WT and IL-36R-KO mice. These cells participate in antigen presentation, antibody production, and lymphocyte activation, contributing to the progression of renal lesions [54,85,110]. Although the author did not detect IL-38 modifications in renal phenotypes of IL-36R deficient MRL/lpr mice, a lack of IL-36R signaling might be associated with immunological responses via IL-38. Further experiments are needed to clarify whether IL-38 signaling, and not IL-36R, has a positive or negative effect on the nephritis pathology.

Interestingly, IL-36α was localized in the nuclei and cytoplasm of parietal and distal tubular epithelial cells. Similarly, a few IL-1 family members, such as IL-33 and IL-1α, also localize to the nucleus [23,98]. At steady state, IL-33 localizes to the nuclei of fibroblasts, endothelial cells, and epithelial cells in the lungs and skin. Importantly, cell injury or necrosis triggers IL-33 secretion from nuclei, which acts as a damage-associated molecular pattern at the early stage of inflammation [23]. Moreover, IL-33 binds to histones and chromatin in nuclei, although its function remains unclear [23]. Similar to IL-33, IL-1α can be translocated from the cytoplasm to the nucleus by HS-1-associated protein X-1, which binds to pro- and truncated IL-1α [65,98]. IL-1α localizes to the nucleus and interacts with the p300, p300/CBP-associated factor, and GCN5, histone acetyltransferases, leading to the upregulation of inflammatory cytokines, such as IL-6 and IL-8, independent of IL-1R [98]. Although the IL-36α counterpart in the nuclei of renal epithelial cells was unclear, the author found that IL-36α was partially localized in nuclei with Ac-lysine. Some IL-36α$^+$ nuclei co-localized with GCN5. These findings indicate that IL-36α signaling may contribute to the development of tubular injury through the IL-36R-independent pathway.

Studies on psoriasis showing immune mediated inflammatory skin condition have revealed that IL-36α, IL-36β, IL-36γ and IL-36Ra are upregulated, and is being developed as a target for the treatment [62]. In the kidneys, IL-36α is also expressed in parietal and distal tubular epithelial cells of human patients with CKD and AKI as well as the mouse models [28,94]. Moreover, Chapter 1 reveled that IL-36R gene localized to those cells in cat kidneys consistent with the localization

of IL-36R and IL-36α in the mouse kidneys, indicating that IL-36R ligands may be novel targets for the treatment and diagnosis of renal diseases showing lesions of distal tubular or parietal epithelial cells.

In conclusion, this chapter demonstrate that deficiency of IL-36R signaling partially inhibited the progression of renal histopathological injuries in autoimmune disease-mediated nephritis model mice but did not improve renal function and immunological condition. Although the pathogenetic role of IL-36α was partially blocked, the obtained data suggests that nuclei expressing IL-36α in renal epithelial cells may play a role in the progression of renal injuries. Furthermore, IL-36R deficiency did not prevent IL-38 signaling through another receptor pathway. The findings might support the novel insight that IL-36R ligands participate in the pathogenesis of autoimmune disease-mediated nephritis with IL-36α-dominant renal epithelial cell injuries that is dependent or independent of IL-36R.

Summary

Chapter 1 demonstrated that IL-36R ligands ectopically expressed in renal epithelial cells and mesenchymal cells contribute to the glomerular and tubulointerstitial lesions with morphological alteration of renal epithelial cells in MRL/lpr mice for a spontaneous nephritis model. In this chapter, the author established and analyzed IL-36R deficient MRL/lpr mice, compared to WT mice, to examine whether IL-36R-KO mice show amelioration of renal phenotypes. In both genotypes, indices for immune abnormalities and renal functions were comparable, although female WT mice showed higher serum autoantibody levels than males. IL-36R ligand expression did not differ significantly between genotypes at the mRNA level or in IL-36α and IL-38 scores. However, glomerular lesions, especially mesangial matrix expansion, were significantly ameliorated in both sexes of IL-36R-KO mice compared to WT mice. Cell infiltration into the tubulointerstitium with the development of tertiary lymphoid structures was comparable between genotypes. However, the positive correlation with IL-36α score in WT mice was not evident in IL-36R-KO mice. Fibrosis surrounding renal tubules was less in female IL-36R-KO mice than in WT mice. Importantly, some IL-36α^{+} nuclei in renal epithelial cells co-localized with Ac-lysine and GCN5 histone acetyltransferase, in both genotypes. Therefore, IL-36R ligands, especially IL-36α in renal epithelial cells, contribute to the progression of renal pathology showing renal epithelial cell injuries in the nephritis via IL-36R dependent and independent pathways.

Tables and Figures

Table 2-1. List of primers used in this study

Gene symbol (Gene ID)	Primer sequence (5′-3′) F: Forward, R: Reverse		Product size (bp)
Ifng (15978)	F: CCTTTGGACCCTCTGACTTG	R: TTCCACATCTATGCCACTTGAG	201
Il10 (16153)	F: GCATTTGAATTCCCTGGGTGAG	R: TTGTAGACACCTTGGTCTTGGAG	147
Il6 (16193)	F: CAACGATGATGCACTTGCAGA	R: GGTACTCCAGAAGACCAGAGGA	112
Tgfb1 (21803)	F: ATGCTAAAGAGGTCACCCGC	R: TGCTTCCCGAATGTCTGACG	119
Tnf (21926)	F: TCTTCTCATTCCTGCTTGTGGC	R: CATAGAACTGATGAGAGGGAGGC	119
Primers sequence for genotyping (5′-3′) F: Forward, R: Reverse			
Il1rl2 (wild type)	F: GACAGAGACTAAGGGCAGAAGAG	R: GTCTGGTCCTGGTGAACTCTAAG	468
Il1rl2 (knockout type)	F: GCATCCTTTGTCATTCATCTCCG	R: CGGAAATGGCAGCAATCTCATT	534

Table 2-2. List of antibodies used in this study

Primary antibody	Host	Dilution	Source	Antigen retrieval	Blocking serum	
					IHC	IF
Acetylated lysine	Rabbit	1:2,000	Cell Signaling Technology, Danvers, MA, USA	None	10% NGS	5% NDS
GCN5	Rabbit	1:400	Cell Signaling Technology	Tris	10% NGS	-

Tris:20 mM Tris-HCl buffer (pH 9.0) at 110 °C for 15 min; NDS, normal donkey serum; NGS, normal goat serum

Table 2-3. Correlation between number of IL-36α$^+$ tubules and cell infiltration score

	IL-36R		$CD3^+$ T cells	$IBA1^+$ macrophages
IL-36α$^+$ tubules	WT	ρ	0.770**	0.624
		P	< 0.01	0.052
	KO	ρ	0.173	-0.036
		P	0.612	0.915

$n \geq 10$; ρ: Spearman's correlation coefficient (**$P < 0.01$). WT: wild type, KO: knockout.

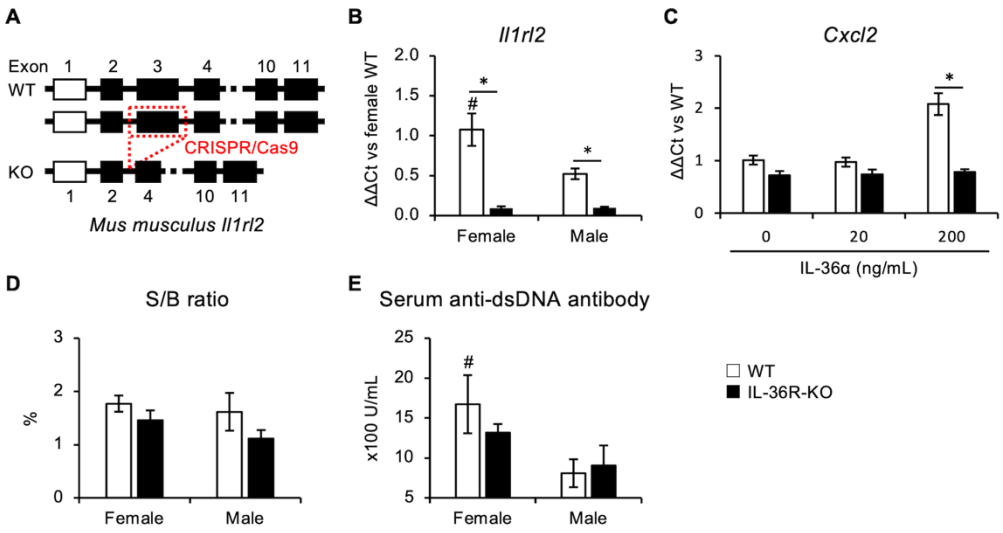

Fig. 2-1 Establishment of IL-36R-KO nephritis model mouse with systemic autoimmune condition.

(A) Genomic stricture of *Il1rl2* coding IL-36R. A part of exon 3 is deleted using the CRISPR/Cas9 system to generate IL-36R-KO mice. The deleted region in IL-36R-KO allele is indicated red dashed-line box. **(B)** Relative mRNA expression of *Il1rl2* in mouse kidneys. The expression levels are normalized to the values of *Actb* and those of female WT mice. Each bar represents mean ± SE ($n \geq 5$). * indicates a significant difference in IL-36R-KO mice compared with WT one of same sex ($*P < 0.05$). # indicates a significant difference in female mice compared with male one of same genotype ($\#P < 0.05$). Mann-Whitney *U*-test, qPCR analysis. **(C)** Relative mRNA expression of *Cxcl2* in spleen cells stimulated by IL-36α (0-200 ng/mL). The expression levels are normalized to the values of *Actb* and those of WT with IL-36α at 0 ng/mL. Each bar represents mean ± SE ($n \geq 5$). * indicates a significant difference in IL-36R-KO mice compared with WT one of same sex ($*P < 0.05$). Mann-Whitney *U*-test, qPCR analysis. **(D and E)** S/B ratio (panel d) and serum level of anti-ds DNA antibody (panel e). Each bar represents mean ± SE ($n \geq 5$). # indicates a significant difference in female mice compared with male one of same genotype ($\#P < 0.05$). Mann-Whitney *U*-test. KO: knockout, WT: wild-type, S/B ratio: the weight ratio of spleen to body.

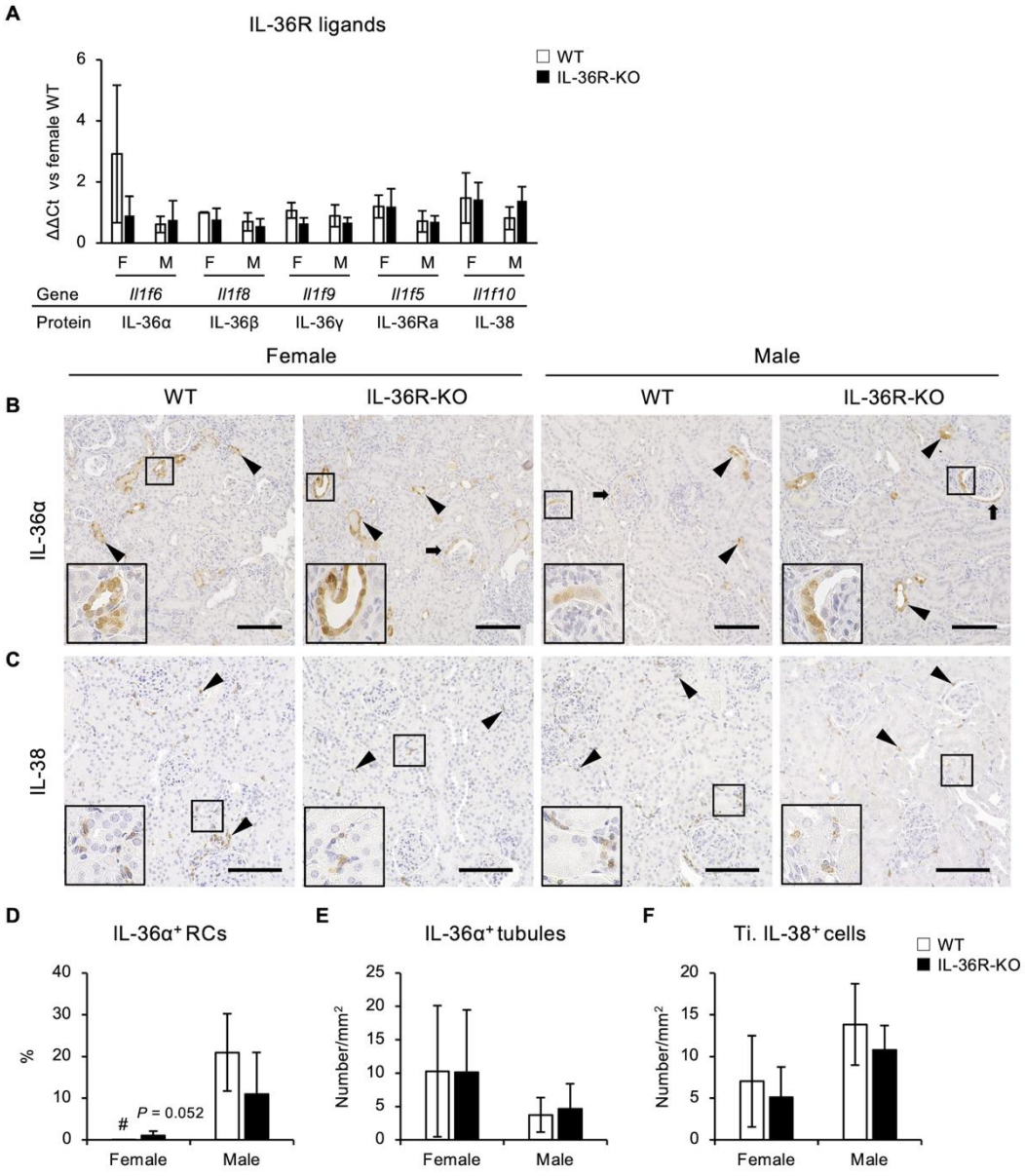
A
IL-36R ligands
WT
IL-36R-KO
ΔΔCt vs female WT
F M F M F M F M F M
Gene Il1f6 Il1f8 Il1f9 Il1f5 Il1f10
Protein IL-36α IL-36β IL-36γ IL-36Ra IL-38
Female
Male
WT
IL-36R-KO
B
IL-36α
C
IL-38
D
IL-36α+ RCs
%
P = 0.052
Female
Male
E
IL-36α+ tubules
Number/mm2
F
Ti. IL-38+ cells

Fig. 2-2 IL-36R ligand expression in kidneys of IL-36R-KO nephritis model mice.

(A) Relative mRNA expression of IL-36R ligands in mice kidneys. The expression levels are normalized to the values of *Actb* and those of female WT mice. Each bar represents mean ± SE ($n \geq 5$). qPCR analysis. **(B and C)** Localization of IL-36a and IL-38 in mouse kidneys. In both WT and IL-36R-KO mice, IL-36α is observed in cytoplasm and nuclei of distal tubular epithelial cells (arrowheads) and parietal epithelial cells (arrows). The latter cells in male mice express more IL-36α compared with female cells. However, no difference in the localization and the positive cell number is evident between them (panel B). IL-38 is found in the cells localizing to tubulointerstitium (arrowheads), although the positive cell number is comparable between WT and IL-36R-KO mice (panel C). IHC. Bars = 100 μm. **(D-F)** Percentage of the number of IL-36α^{+} renal corpuscles to that of total ones (panel D), number of IL-36α^{+} renal tubules (panel e), and number of IL-38^{+} cells in the tubulointerstitium (panel F). Each bar represents mean ± SE ($n \geq 5$). # indicates a significant difference in female mice compared with male one of same genotype ($\#P < 0.05$). Mann-Whitney *U*-test. F: female, M: male, KO: knockout, WT: wild-type, RC: renal corpuscle, Ti: tubluolinterstitium.

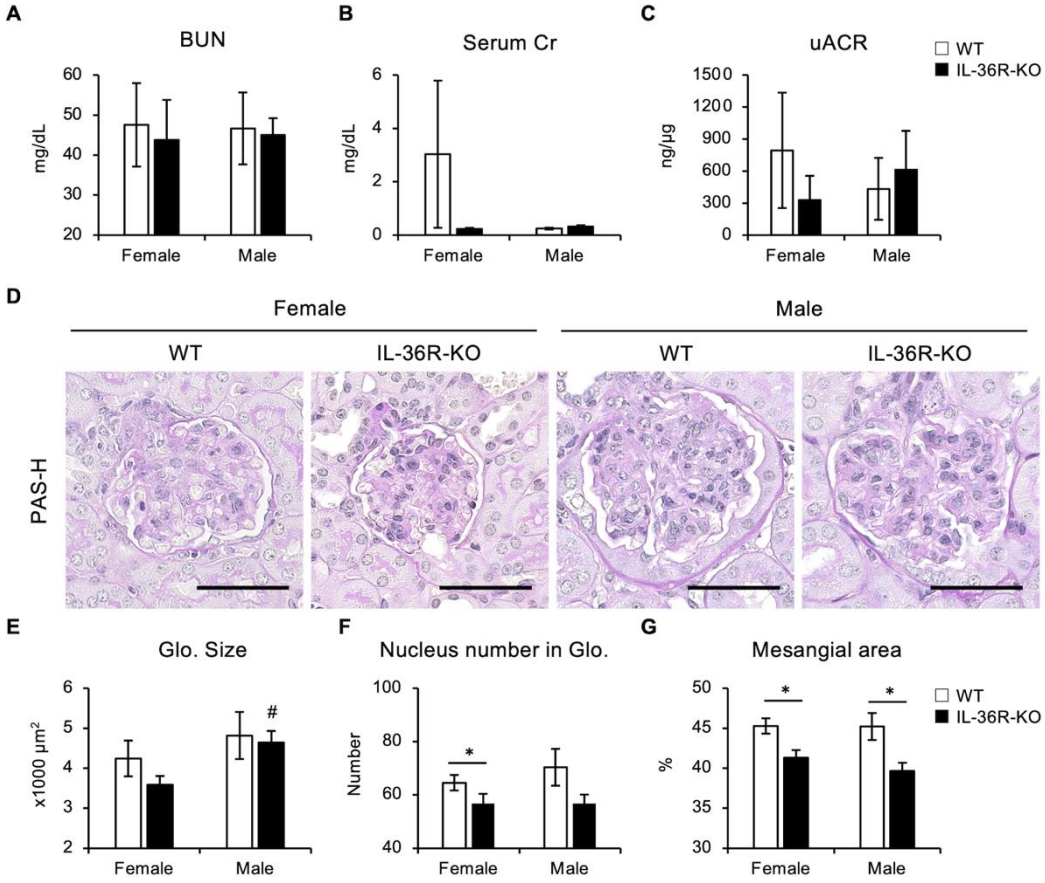

Fig. 2-3 Renal functions and glomerular lesions in IL-36R-KO nephritis model mice.

(A-C) The level of BUN (panel A), serum Cr (panel B), and uACR (panel C). Each bar represents mean ± SE (n ≥ 5). **(D)** PAS-H staining images of the glomeruli. Glomerular hypercellularity and hypertrophy as well as mesangial matrix expansion are observed in all groups, and are more severe in both sexes of WT mice than in the same sex of IL-36R-KO mice. Bars = 50 μm. **(E-G)** Glomerular size (panel E), number of nuclei in a glomerulus (panel F), and area percentage of mesangium to glomerulus (panel G). Each bar represents mean ± SE (n ≥ 5). * indicates a significant difference in IL-36R-KO mice compared with WT ones of same sex (*$P < 0.05$). # indicates a significant difference in female mice compared with male one of same genotype (#$P < 0.05$). Mann-Whitney *U*-test. KO: knockout, WT: wild-type, BUN: blood urea nitrogen, Cr: creatinine, uACR: urinary albumin to creatinine ratio, PAS-H: periodic acid Schiff-hematoxylin, Glo: glomerulus.

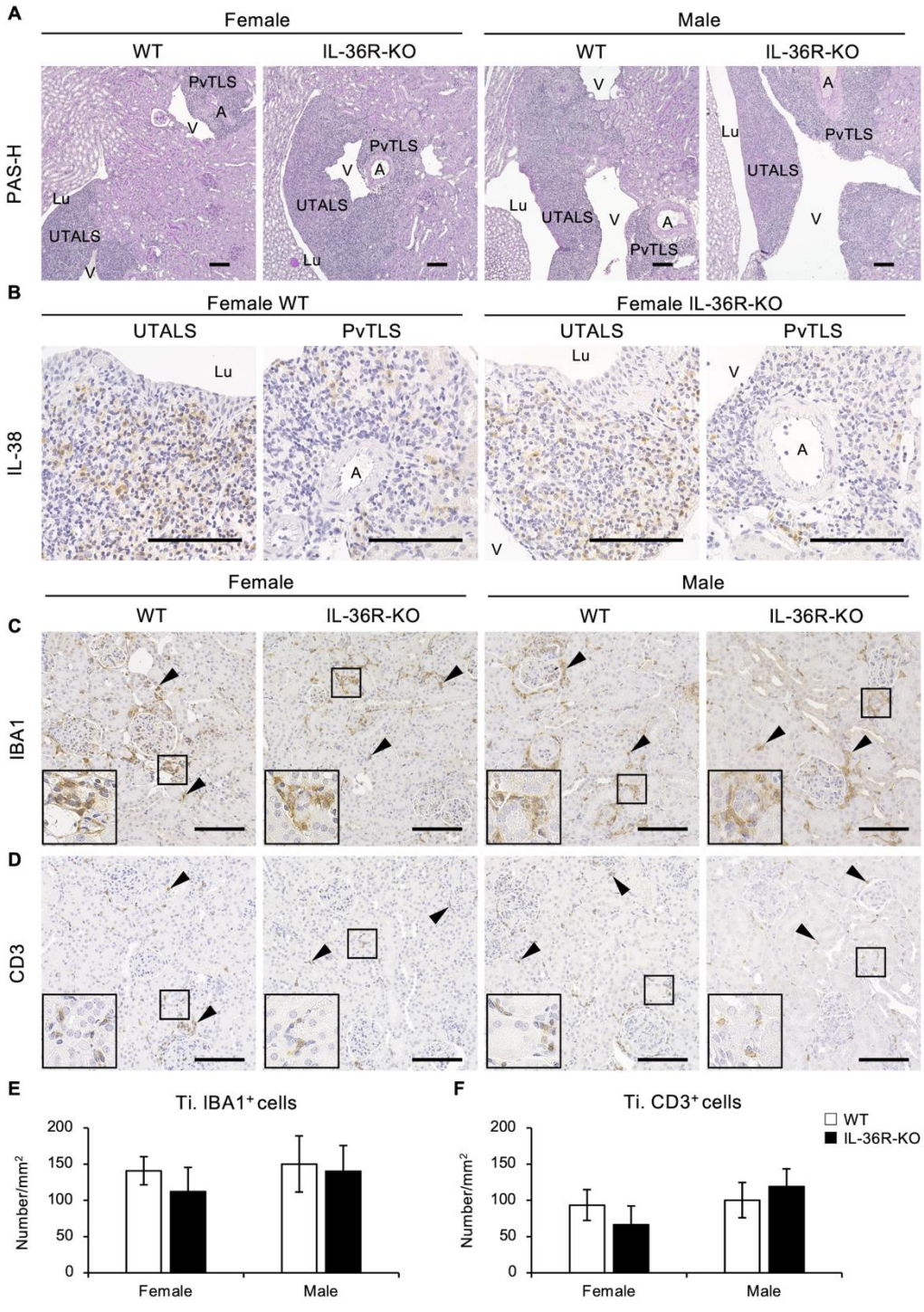
A
Female
Male
WT
IL-36R-KO
WT
IL-36R-KO
PAS-H
PvTLS
A
V
Lu
UTALS
V
PvTLS
V
A
UTALS
Lu
Lu
UTALS
V
A
PvTLS
A
Lu
PvTLS
UTALS
V
B
Female WT
Female IL-36R-KO
UTALS
PvTLS
UTALS
PvTLS
IL-38
Lu
A
Lu
V
V
A
C
Female
Male
WT
IL-36R-KO
WT
IL-36R-KO
IBA1
D
CD3
E
Ti. IBA1⁺ cells
Number/mm²
200
150
100
50
0
Female
Male
F
Ti. CD3⁺ cells
WT
IL-36R-KO
Number/mm²
200
150
100
50
0
Female
Male

Fig. 2-4 Immune cells in tubulointerstitium of IL-36R-KO nephritis model mouse.

(A) PAS-H staining images of tertiary lymphoid structures in the kidneys. In all groups, perivascular tertiary lymphoid structures and UTALSs are observed close to arteries and urothelium, respectively. Bars = 100 μm. **(B)** Representative IHC images of IL-38 in the tertiary lymphoid structures of the kidneys. In both female WT and IL-36R-KO mice, IL-38^{+} cells are observed in UTALSs and perivascular tertiary lymphoid structure. Bars = 100 μm. **(C and D)** Localization of IBA-1^{+} macrophages and $CD3^{+}$ T cells in kidneys. Both positive cells (arrowheads) are clearly observed in tubulointerstitium and glomeruli of all groups; especially, IBA-1^{+} cells are abundant. **(E and F)** The number of IBA-1^{+} (panel D) and $CD3^{+}$ (panel E) cells in the tubulointerstitium (Ti). Each bar represents mean ± SE ($n \geq 5$). KO: knockout, WT: wild-type, PAS-H: periodic acid Schiff-hematoxylin, PvTLS: perivascular tertiary lymphoid structure, UTALS: urinary tract associated lymphoid structure, Lu: lumen of renal pelvis, V: vein, A: artery.

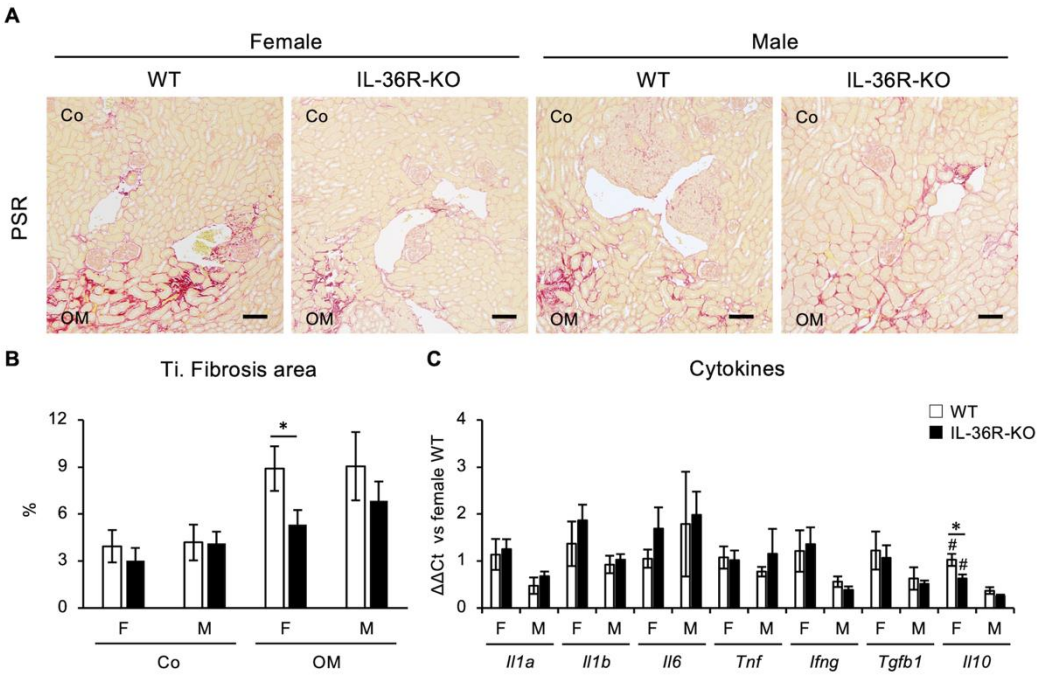

Fig. 2-5 Tubulointerstitial fibrosis and cytokine expression in kidneys of IL-36R-KO nephritis model mouse.

(A) Picrosirius red staining images of the kidneys. In all groups, picrosirius red^{+} collagen fibers are more abundant in tubuloinrterstitium of outer medulla compared with that of cortex. Especially, female WT mice show abundant fibers. Bars = 100 μm. **(B)** Percentage of picrosirius red^{+} fibrosis area in tubulointerstitium of cortex and outer medulla. Each bar represents mean ± SE (n ≥ 5). * indicates a significant difference in IL-36R-KO mice compared with WT ones of same sex (*P < 0.05). Mann-Whitney U-test. **(C)** Relative mRNA expression of representative cytokines in the mouse kidneys. The expression levels are normalized to the values of *Actb* and those of female WT. Each bar represents mean ± SE (n ≥ 5). qPCR analysis. * indicates a significant difference in IL-36R-KO mice compared with WT ones of same sex (*P < 0.05). # indicates a significant difference in female mice compared with male one of same genotype (#P < 0.05). Mann-Whitney U-test. KO: knockout, WT: wild-type, PSR: picrosirius red, OM: outer medulla, Co: cortex, Ti: tubulointerstitium, F: female, M: male.

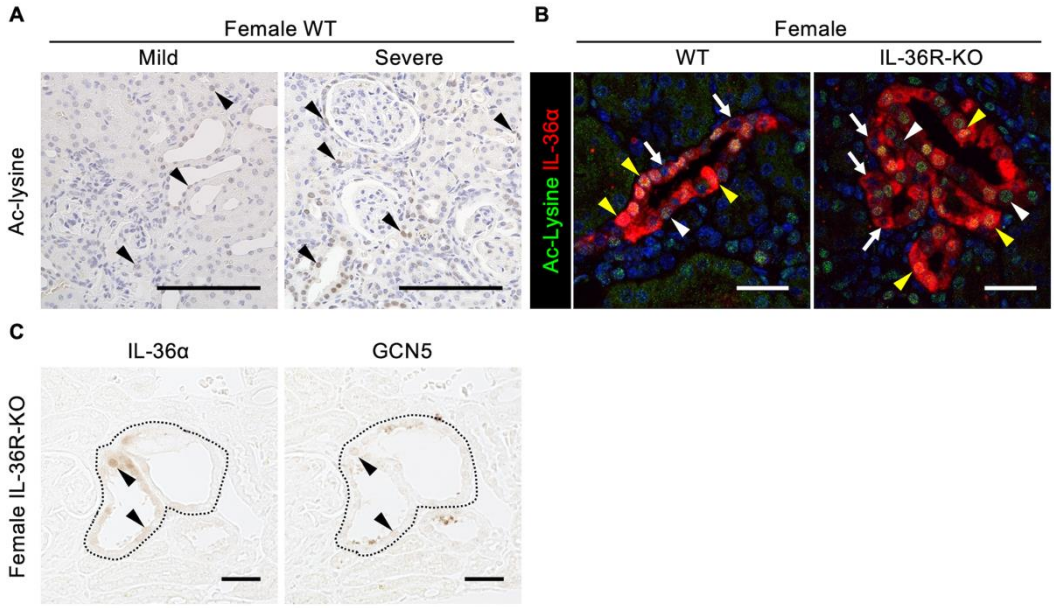

Fig. 2-6 Localization of Ac-lysine in IL-36α$^+$ nuclei in kidneys of IL-36R-KO nephritis model mice.

(A) Representative IHC images for Ac-lysine in female WT mice. Ac-lysine$^+$ nuclei (arrowheads) are observed in parietal epithelial cells, proximal and distal tubular epithelial cells, and myeloid cells. The number is abundant in the kidneys showing severe nephritis. Bars = 100 μm. **(B)** Representative IF images for Ac-lysine with IL-36α. In IL-36α$^+$ distal tubules of both WT and IL-36R-KO mice, Ac-lysine is found in IL-36α-positive and negative nuclei (yellow and white arrowhead, respectively). In the cells with IL-36α$^+$ cytoplasm, IL-36α$^-$ Ac-lysine$^-$ nuclei are observed (arrows). These expression manners are comparable between WT and IL-36R-KO mice. Bars = 25 μm. **(C)** Representative serial sections followed by IHC for IL-36α and GCN5 in female IL-36R-KO mice. GCN5 is found in some of IL-36α$^+$ nuclei (arrowheads). Dotted lines indicate same distal tubule. Bars = 25 μm. Ac-lysine: acetylated lysine, KO: knockout, WT: wild-type.

Chapter 3

Ectopically expressed collagen 17A1 regulates urothelial integrity and local immunological responses in obstructive uropathy

Introduction

Chapter 1 and 2 revealed the pathological role of IL-36R ligands in the renal epithelial cell-associated renal injuries; however, injuries of urothelial cells covering lumen of lower organs from the kidneys also induce UEB disruption, leading to the development of urinary system disorders including kidneys. The urothelium has stretchable and impermeable characteristics to accommodate a large change of urine amount, and functions as a protective barrier against urine. It is derived from intermediate mesoderm and endoderm; the former develops into renal pelvis and ureter, while the latter does into urinary bladder and urethra. Histologically, urothelium has a variable number of cell layers dependent on urine amount, and is stratified into three distinct layers; superficial-, intermediate-, and basal-cell layers. However, all urothelial cells attach to the basement membrane [33,125]. The urothelial injuries are caused by infections and urinary stasis, pathologically showing exfoliating superficial urothelial cells in addition to neutrophil and macrophage infiltration [125,131]. Importantly, multiple studies indicate that urothelial cells have rapidly regenerative response to the injury, and those at the basal layers predominantly proliferate [33,91,113,125].

Recently, it is revealed that urine is involved in the development of UTALSs under urothelium in an inducible manner by stimulating the production of cytokines and chemokines in immune and stromal cells of renal pelvis [54]. UTALS development is also affected by aging and systemic immune conditions and is positively correlated with the progression of renal lesions. The renal pelvis urothelium that covers UTALSs of mice and humans with chronic nephritis, COL17A1 (known as BP180) was ectopically expressed. In the skin, COL17A1 is known as a transmembrane structural component for hemidesmosomes and is constitutively expressed in keratinocytes to attach the epidermis to the basement membrane. While it can be an autoantigen for bullous pemphigoid [121], previous results have indicated that COL17A1 in the renal pelvis is induced via the Fos/ Jun proto-oncogene, activator protein 1 (AP-1) transcription factor subunit (FOS/JUN)-related pathway and plays a role in UTALS development by stimulating the production of IL-6, IL-22, and CXCL9 from UTALS-forming cells [54].

Previous studies focused on the UEB disruption in renal pelvis during chronic nephritis, while urothelium injuries are commonly observed in several diseases due to urinary stasis, including obstructive nephropathy [131]. The obstruction of urinary tracts is caused by anatomical defects, urolithiasis, bacterial infections, cystitis, as well as neoplasia [82]. A previous study reported UEB disruption in the renal pelvis of mice and humans with chronic nephritis and urine leakage from the renal pelvis lumen into the parenchyma of this murine model [54]. Disorders of the upper urinary tract including the renal pelvis and ureters can lead to various degrees of hydronephrosis [127]. The prevalence of urolithiasis in humans is increasing worldwide with a range from 1-13% depending on obstructive positions [115]. Moreover, urinary bladder cancer is ranked

in the top ten forms of cancer worldwide, with a higher frequency in males than in females, thus making urinary bladder cancer, the sixth most common form of cancer in males [19]. In neonates and infants, the ureteropelvic junction can be a major obstruction site in the urinary tract due to the characteristic anatomical abnormality. It has been reported that 1 in 1,500 live births exhibit the obstruction [50]. In veterinary fields, especially cats, 15-23% of the lower urinary tract diseases are caused by urolithiasis [36], and 73% of the patients with CKD show urolithiasis [52]. Thus, renal disfunctions are developed underlying several pathogeneses. A few studies have shown that injured urothelium is characterized by cell proliferation, flattening cell-shape, and broken tight junctions [48,64]. However, no report clearly indicates the characteristics of UEB disruption in urinary tracts, the subsequent pathological events, and the crucial molecules in the urinary tract obstruction-related diseases, with a special focus on the role of urine.

In this chapter, the author clarified the relationship between UEB disruption-induced leakage of urine and local immune response with the unique role of COL17A1 by analyzing the renal pelvis and ureters of UUO-injured mice. Importantly, COL17A1 ectopic expression in urothelium was also clearly demonstrated in obstructed ureters of both clinical human and feline cases, indicating its usefulness as a novel indicator for UEB disruption among various mammals.

Materials and Methods

Ethics statement

The study of human samples was approved by the Ethics Committee of the Faculty of Veterinary Medicine and International Institute for Zoonosis Control, Hokkaido University (approval No. 29-5). The collection of samples from human subjects was performed in accordance with the Declaration of Helsinki and the Declaration of Istanbul. All animal experimentation was approved by the Institutional Animal Care and Use Committee of the Faculty of Veterinary Medicine, Hokkaido University (approved by the Association for Assessment and Accreditation of Laboratory Animal Care International, approval No. 21-0008 for mice, 14-0054, 20-0081 for cats).

Human sample analysis

Ten percent NBF-fixed and paraffin-embedded normal and diseased ureters (female Caucasian, 58 and 60-year-old, respectively) were obtained from KAC Inc. (Kyoto, Japan). Sections were used for Masson's trichrome staining and IHC targeting COL17A1 and CD11b.

Cat sample analysis

Normal ureters were obtained from male healthy cats euthanized in other experiments. Diseased ureters, surgically resected from the obstructed lesion to ureter-urinary bladder junction were collected from male and female cats manifesting obstructive urolithiasis at the Matsubara Animal Hospital (Osaka, Japan). All ureters were fixed using 10% NBF (n = 5 in each group). For ISH, paraffin sections (5-μm thick) were assessed using an RNAscope 2.5 HD Reagent Kit-BROWN (Advanced Cell Diagnostics, Inc.) with custom-ordered probe-Fc-*COL17A1* (#1147271-C1).

Mouse sample preparation

Two-month-old B6 and 6-month-old MRL/+ mice were purchased from Japan SLC, Inc., and three-month-old *Col17a1*-KO mice (B6 back ground) were maintained under the conditions as described in Chapter 1 [92,93,128]. For B6 mice, the UUO group was assessed for 1, 4, 7, or 28 days (d) after UUO induction or its equivalent sham-operation group (Sham) was prepared (n = 4 or 5). UUO at 1d was performed in *Col17a1*-KO (n = 4 or 5). Bromodeoxyuridine (BrdU; 1 mg/g), a proliferation marker, was administrated into B6 mice with UUO and Sham two hours before sample collection.

Anesthesia and blood collection were performed as done in Chapter 1.

Histopathology

Kidneys and ureters were collected and fixed using 4% paraformaldehyde. Histological paraffin sections (2-μm thick) were stained using Masson's trichrome and PAS-H. IHC or IF was performed as described in Chapter 1. Information regarding immunostaining is listed in Table 1-1 and 3-1. Stained sections were examined using a BZ-X710 microscope and converted to virtual slides using NanoZoomer 2.0-RS.

The luminal area of the ureter was measured, and the average was calculated in five sections from each mouse using NDP. view2.

For the IHC sections, the relative $COL17A1^+$ area in the examined urothelium area was measured using a BZ-X Analyzer. This measurement was performed in three regions: distal and proximal renal pelvis, which was defined by the presence or absence of smooth muscle layers, and ureters. Ureter lumen area was also measured. Consecutive length of $COL17A1^+$ cells were measured from the junction between proximal and distal renal pelvis to each part. To evaluate renal pelvis histology in *Col17a1*-KO, the number of urothelial cells, cytokeratin 14 $(CK14)^+$ urothelial cells, and $CD11b^+$ cells under the urothelium were counted in the urothelium region frequently expressing COL17A1 (400 μm length from the renal pelvis junction to the distal part). For tubulointerstitial lesion indices, the number of $CD11b^+$ cells in tubulointerstitum and IL-36α^+ injured distal tubules in the cortex area were evaluated as done in Chapter 1.

Transmission electron microscopy (TEM)

Small pieces of kidney tissues including the renal pelvis 1d after UUO were pre-fixed using 4% paraformaldehyde/0.1 M cacodylate buffer containing 2.5% glutaraldehyde for 2 h at room temperature. The specimens were treated using the osmium-thiocarbohydrazide-osmium method. First, samples were washed five times using 0.1M cacodylate buffer and block-stained using 1.5% potassium ferrocyanide/2% OsO_4/0.1M cacodylate buffer for 1 h at 4 °C. After washing four times in distilled water, specimens were block-stained using 1% thiocarbohydrazide solution for 20 min at room temperature and washed again. These were post-fixed using 2% OsO_4 for 30 min at room temperature, washed again, and stained using 1% uranyl acetate overnight at 4 °C. After washing four times in distilled water, the specimens were block-stained using 0.4% L-aspartic acid/0.66% lead nitrate solution for 30 min at 60 °C followed by four washes with distilled water. Next, specimens were dehydrated using a series of ethanol concentrations (30-95%) for 10 min at 4 °C. After being dehydrated three times in 100% ethanol at 4 °C, the specimens were soaked in an equal volume mixture of 100% ethanol and QY-1 for 10 min at room temperature, and subsequently substituted twice in QY1 for 30 min at room temperature. Next, specimens were soaked in an equal volume mixture of QY-1 and Epon 812 (#R1078; TAAB, Berkshire, England) for 1 h at room temperature followed by Epon 812 only overnight at room temperature. After exchanging resin and keeping the specimens at room temperature for 1 h, specimens were

embedded and polymerized in fresh Epon 812 for 48 h at 60 °C. Ultrathin sections (60-nm thick) were observed using a JEOL TEM (JEM-1400plus; LEOL, Tokyo, Japan).

Urothelium integrity analysis

The author used previously reported method with modifications [54]. Firstly, UUO was generated using a vascular clip (#KN-353-AS-1-40 g; Natsume Seisakusho, Tokyo, Japan) and released after 1d. Evans blue (5 mg/mL; #E2129; Merck, Kenilworth, NJ, USA) was mixed with bovine serum albumin (BSA, 40 mg/mL; #013-27054; FUJIFILM Wako Pure Chemical Corporation), incubated for 30 min, and filtered using a 0.22 μm syringe filter to produce Evans blue-conjugated BSA solution. The urethra of mice were ligated under combined anesthesia (0.3 mg/kg medetomidine, 4.0 mg/kg midazolam, and 5.0 mg/kg butorphanol), and a 21 G butterfly needle was inserted from the apex of the urinary bladder and fixed via ligation. After clamping one ureter with vascular clips, 50 μL of Evans blue-conjugated BSA was injected into the urinary bladder through the inserted needle. Evans blue-conjugated BSA injection into the renal pelvis was confirmed via a color change in the other ureter. After 5 min of contact time, kidneys were immediately collected and embedded in optimal cutting temperature compound (#4583; Sakura Finetek Japan, Tokyo, Japan) using liquid nitrogen. Frozen sections (4-μm thick) were prepared and air dried. Lastly, the Evans blue-conjugated BSA fluorescence was observed using a BZ-X710 microscope and the Cy5 filter (Keyence).

Cell culture

Mimic lymphoid structures were prepared as previously described[54]. The spleen of a 6-month-old male MRL/+ mouse was collected and minced in a culture dish. Next, 10 mL of 1× PBS (#164-25511; FUJIFILM Wako Pure Chemical Corporation, Osaka, Japan) was added, after which the sample was filtered using 100 μm cell strainers (#352360; Corning Inc.) and centrifuged at 210 g for 5 min. After supernatant aspiration, cells were resuspended, incubated with 10 mL of 0.017 M tris buffer containing 0.75% ammonium chloride (pH 7.65) for 5 min, and washed with 10 mL PBS. This solution was filtered using 40 μm cell strainers (#352340; Corning Inc.) and centrifuged at 1,000 rpm for 5 min. After washing twice with PBS, the collected cells were resuspended in RPMI1640 with L-glutamine (#189-02025; FUJIFILM Wako Pure Chemical Corporation) without antibiotics and harvested in 24-well culture plates (#92424; Techno Plastic Products).

Cells were defined as mimic lymphoid structures containing immune and stromal cells. Furthermore, some spleen cells were similarly collected without ammonium chloride treatment, and then T, B, and $CD11b^+$ cells were separately isolated using magnetic-activated cell sorting-based commercial kits (EasySep, #ST-19851RF, #ST-19854RF, #ST-18970RF; VERITAS, Santa

Clara, CA, USA). The mimic lymphoid structures or separated cells were stimulated using recombinant human COL17A1 (rhCOL17A1; #MBS1265558; MyBioSource, San Diego, CA, USA) or BSA. Endotoxin levels in rhCOL17A1 were <1.0 endotoxin unit per 1.0 μg protein as determined using a limulus amebocyte lysate test (MyBioSource). Urine was collected from six male MRL/+ mice at 6 months of age via compressive urination, after which, samples from each strain were pooled and centrifuged at 1,500 rpm for 5 min. The urine supernatant was filtered using a 0.22 μm syringe filter (#SLPES2522S; Hawach Scientific, Shaanxi, China) and used for mimic lymphoid structure stimulation. The mimic lymphoid structure or isolated cell experiments were performed using 2.5×10^7 cells/mL and 500 μL medium/well or 1.25×10^6 cells/mL and 500 μL medium/well, respectively. The mimic lymphoid structures or separated cells were stimulated using urine, rhCOL17A1, BSA, or PBS, and they were collected for RNA analysis.

Microarray analysis

Total RNA of mimic lymphoid structures was prepared from the PBS- or MRL/+ urine-treated group (n = 3) using the RNeasy Mini Kit (Qiagen, Hilden, Germany) to evaluate chemokine expression in the mimic lymphoid structures. RNA integrity validation, complementary DNA synthesis, gene expression analysis, raw data normalization were performed as done in Chapter 1.The data was deposited in the NCBI Gene Expression Omnibus (GEO Series accession numbers GSE207999).

qPCR

Kidneys and ureters 1d after UUO and non-treated collateral ones were preserved using an RNAlater solution (#R0901; Merck KGaA). The renal pelvis was manually isolated from kidneys through microdissection under a stereo-microscope, as reported previously [54]. Purification of total RNA from those specimens and mimic lymphoid structures as well as qPCR analysis were performed as done in Chapter 1 by using gene-specific primers (Table 1-2 and 3-2). The data was normalized according to the values of *Actb*.

Serological analysis and urinalysis

Serum concentration of Cr and BUN were measured as performed in Chapter 1.

Statistical analysis

The results are expressed as mean ± SE and statistically analyzed in a non-parametric manner. The significance between two groups was analyzed using the Mann-Whitney *U*-test. The significance among over three groups was analyzed using the Kruskal-Wallis test followed by the Scheffé's method. Correlation between two parameters was analyzed using the Spearman's

correlation test. $P < 0.05$ was considered statistically significant.

Results

COL17A1 expression in the ureters of humans and cats with urinary tract obstruction

A previous study demonstrated that COL17A1 was expressed in human renal pelvis urothelium with infectious pyelonephritis and non-infectious chronic nephritis [54]. Thus, the author examined the COL17A1 expression in human ureters with urolithiasis. Cats, which also show a high susceptibility to urinary tract obstruction (incidence, 7-8%), were also analyzed [36,57]. Compared with healthy ureters, diseased (urolithiasis) ureters of both humans and cats presented a dilated lumen, abundant collagen fibers and immune cell infiltration in the lamina propria and submucosa. Cell aggregation was clearly observed in the human ureter (Fig. 3-1A). In a human ureter showing normal histology, COL17A1 was partially detected in the basal portion of the urothelium, whereas in a diseased ureter with urolithiasis, COL17A1$^+$ reactions were more prevalent, with immune cell aggregation (Fig. 3-1B). In both healthy and diseased ureters of cats, *COL17A1*$^+$ reactions were observed in the basal portion of the urothelium, while being highly abundant in each cell of the diseased ureter (Fig. 3-1C), indicating that COL17A1 expression dynamics are common among different species.

COL17A1 ectopically expressed in the ureter urothelium of UUO mice

COL17A1 expression was also examined in the ureter of UUO-injured B6 mice, in which, hydroureteronephrosis with the ureter luminal expansion, smooth muscle layer degradation, and an increase in collagen fibers was remarkable from 4d onward (Fig. 3-2A and B). Furthermore, luminal size of the ureter as well as the renal histopathological scores, including CD11b$^+$ myeloid cells in tubulointerstitium and IL-36α$^+$ injured distal tubules, significantly increased in a time-dependent manner following UUO induction (Fig. 3-2C-G). Although COL17A1 localized in the basal portion of UUO-injured ureter urothelium from 1d but not in the Sham, COL17A1$^+$ urothelium and its histological score following IHC significantly increased from 4d onward (Fig. 3-3A and B). Moreover, urothelium COL17A1$^+$ scores were positively correlated with injury indices for the ureters and kidneys including, ureter luminal size, CD11b$^+$ cell number in tubulointerstitium, and IL-36α$^+$ tubule number, (Fig. 3-3C).

Next, ureter UEB integrity was evaluated in the ureter after UUO. Histologically, urothelium disruption in the ureter was apparent from 4d onward, consistent with COL17A1 overexpression (Fig. 3-3D). The mRNA expression of epithelium-associated genes, uroplakin 2 (*Upk2*) and *Tjp1*, but not Occludin (*Ocln*), was significantly lower in the isolated ureter at 7d after UUO than that of collateral control (Fig. 3-3E). TJP1 (also known as zonula occludens 1, ZO-1), which was observed in the apical portion of the Sham ureter, was partially defective in the UUO urothelium. The OCLN$^+$ reaction was temporarily increased in ureter urothelium 4d after UUO, and both OCLN-faint and -overexpressing cells were observed on 7d (Fig. 3-3F). Moreover, COL17A1

was partially expressed in BrdU-incorporated cells (Fig. 3-3G), indicating urothelium reconstruction after UUO.

Migration and activation of CD11b$^+$ cells stimulated by urine and COL17A1

Urine can stimulate the production of cytokines and chemokines from fibroblasts and immune cells [54]. Based on the histopathological results, the author hypothesized that UEB disruption and subsequent urine leakage due to UUO led to an immune response in the ureter parenchyma.

Figure 3-4A summarizes the microarray data analyzing the urine-stimulated mimic lymphoid structures, focusing on chemokine genes. The *Cxcl2*, *Cxcl11*, *Cxcl12*, *Cxcl10*, *Ccl6*, *Cxcl13*, *Ccl1*, and *Ccl25* expression in mimic lymphoid structure stimulated by urine was twice more than that stimulated by PBS. qPCR analysis of the ureter with UUO indicated that *Cxcl2* expression is significantly higher in UUO samples on 7d than those of collateral controls among examined chemokine genes (Fig. 3-4B).

Furthermore, in the diseased renal pelvis, urine as well as COL17A1 can be an immune stimulator [54], thus separately isolated murine B, T, and CD11b$^+$ cells were stimulated using rhCOL17A1, and *Cxcl2* expression was analyzed. Following rhCOL17A1 stimulation, the *Cxcl2* expression level was significantly upregulated in T cells and CD11b$^+$ cells compared to the expression observed following BSA stimulation. The CD11b$^+$ cells showed the highest values among the examined cell types (Fig. 3-4C, note logarithmic form). Histologically, CXCL2$^+$ cells aggregated beneath disrupted ZO-1$^+$ epithelial cells, and COL17A1$^+$ urothelium was also observed near these regions (Fig. 3-4D). Importantly, CXCL2$^+$ reactions were co-localized with CD11b$^+$ cells (Fig. 3-4D), and most CD11b$^+$ cells were Gr-1$^+$ neutrophils and IBA-1$^+$ macrophages (Fig. 3-4E). Representative inflammatory and fibrotic gene expression (*Il1b*, *Il6*, and *Tgfb*) was significantly higher in the ureter of 7d UUO samples compared to that of collateral controls (Fig. 3-4F). Additionally, CD11b$^+$ cells also infiltrated the lamina propria and submucosa in the diseased ureter of humans and cats with urolithiasis (Fig. 3-4G). These findings indicate that urine and COL17A1 can stimulate CXCL2 expression in CD11b$^+$ cells infiltrating the UUO ureter.

COL17A1 overexpressed in the renal pelvis urothelium of mice from 1d after UUO

To identify the initiation site of COL17A1 expression in the upper urinary tract after UUO, the author also examined the renal pelvis. Firstly, UUO-injured renal pelvis showed an increase in collagen fibers from 4d (Fig. 3-5A). Next, mouse proximal and distal renal pelvis were separately analyzed; the former lacked smooth muscle layer and was localized in the deep portion of the renal parenchyma, while the latter, close to ureters, exhibited α-SMA$^+$ smooth muscle layer (Fig. 3-5B-E). Characteristically, at the junction between the proximal and distal renal pelvis, few

COL17A1$^+$ urothelial cells were observed in the Sham. From 1d after UUO, COL17A1 clearly localized in the basal portion of the renal pelvis urothelium (Fig. 3-6A), and COL17A1$^+$ urothelial cells increased in the proximal and distal renal pelvis from 4d onward (Fig. 3-6A and B). The UUO 1d group also showed urothelium disruption with decreasing platelet-derived growth factor receptor alpha (PDGFRα)$^+$ fibroblasts (Fig. 3-6B). In renal pelvis isolated at 1d, *Col17a1* expression was significantly higher than that of the collateral control, indicating that *Col17a1* mRNA was induced earlier than that in the ureter, as no significance in *Col17a1* expression of the ureter was observed on 1d (Fig. 3-6C). At 1d after UUO, the consecutive length of COL17A1$^+$ urothelial cells from renal pelvis junction was longer than the length to the distal part compared with that to the proximal (Fig. 3-6D). Urothelium COL17A1$^+$ scores were significantly higher in the distal renal pelvis at 1d compared with those of the Sham and increased in a time-dependent manner following UUO-induction in both distal and proximal renal pelvis. Furthermore, COL17A1$^+$ scores in both renal pelvis urothelia at 7d UUO were significantly higher than those in the Sham (Fig. 3-6E). Importantly, COL17A1 expression in the renal pelvis urothelium, especially the distal part, was positively correlated with the renal histopathological scores (Fig. 3-6F).

Based on previous findings that the FOS/JUN-related pathway induced COL17A1 expression in the renal pelvis urothelium [54], both molecules localized in the urothelial cell nuclei at the beginning of the distal renal pelvis (Fig. 3-6G), indicating a crucial site for the initiation of COL17A1 expression after obstructive uropathy.

At 28d UUO, the renal pelvis urothelium kept expressing COL17A1; however, it was diminished in the urothelium of the ureter with progression of fibrosis (Fig. 3-6H).

Altered UEB integrity of the renal pelvis urothelium post UUO

Next, UEB integrity was evaluated in the renal pelvis at 1d UUO, which presented urothelial cells deciduation at the junction between proximal and distal renal pelvis (Fig. 3-7A). Consistent with the ureter 7d UUO, mRNA levels of *Upk2* and *Tjp1* were significantly decreased in the ureter of UUO on 1d compared to that of collateral controls, while *Ocln* showed a decreasing tendency in the UUO renal pelvis ($P = 0.063$; Fig. 3-7B). For IF in the Sham, ZO-1 localized at the apical portion of the renal pelvis urothelium, whereas OCLN localized at the apical and basal portion (Fig. 3-7C). On day 1, ZO-1$^+$ reactions were partially faint and OCLN localized mainly at the basal portion. Furthermore, these reactions clarified the partial disruption of urothelium at the renal pelvis junction. Although OCLN$^+$ intensity partially increased on 4d, both TJPs decreased on 7d (Fig. 3-7C).

Next, the author performed COL17A1 co-localization with CK14 and CD44; the former was a marker for urothelial stem cells, and the latter, which was a receptor for hyaluronic acid, laminin,

collagen or fibronectin, was a marker for urothelial cell proliferation in addition to immune cell activation [35,51,67]. In the Sham renal pelvis, $CK14^+$ urothelial cells were found and partially co-expressed with COL17A1, whereas the renal pelvis urothelium on 1d UUO showed an increase in $COL17^+$ $CD44^+$ $CK14^-$ urothelial cells as well as few $CK14^+$ urothelial cells co-expressing COL17A1 and CD44. From 4d onward, $COL17A1^+$ $CD44^+$ $CK14^+$ and $COL17A1^-$ $CD44^+$ $CK14^-$ urothelial cells were predominantly observed (Fig. 3-7D).

For TEM observation of the renal pelvis urothelium on 1d, folded apical membrane, abundant lysosomes, and ectopic red blood cells beneath the basement membrane were noted in comparison to the collateral controls (Fig. 3-7E). Characteristically, urothelial cells increased the intracellular spaces and their cell processes extended to the lamina propria to interact with cells in the smooth muscle layer. Furthermore, a cell migrated from the lamina propria to the partially effaced basement membrane (Fig. 3-7E).

To examine UEB integrity in renal pelvis, Evans blue-conjugated BSA from the urinary bladder was administered into the renal pelvis as previously reported [54]. Although the urothelium of collateral kidneys retained Evans blue-conjugated BSA in the lumen of the renal pelvis, it leaked into the renal pelvis parenchyma of UUO after 1d; thus, suggesting a UEB dysfunction (Fig. 3-7F).

$CXCL2^+$ $CD11b^+$ cells induced in the UUO-injured renal pelvis

Similar to the ureter, the expression of *Cxcl2* was significantly higher in the 1d renal pelvis than that of collateral controls (Fig. 3-8A). Histologically, $CXCL2^+$ cells aggregated beneath the renal pelvis urothelium-leaking area induced by UUO (Fig. 3-8B). In the renal pelvis, 1d after UUO, expression of integrin alpha M (*Itgam*, encoding CD11b) was significantly higher compared to that of collateral controls although *Cd3e* expression was lower (Fig. 3-8C). $CD11b^+$ cells were observed to migrate to the lamina propria in the renal pelvis at 1d, especially near the beginning of the distal renal pelvis, which later decreased by 4d, and fibrosis progressed (Fig. 3-8D). In line with the ureter results, $CXCL2^+$ reactions were co-localized with $CD11b^+$ cells beneath the $COL17A1^+$ urothelium in 1d UUO samples (Fig. 3-8E). Furthermore, mRNA levels of *Il1b*, *Il6*, and *Tgfb* were significantly higher in the renal pelvis of 1d UUO samples compared to that of collateral controls (Fig. 3-8F).

Abnormal urothelium morphology and inhibition of immune cell infiltration in the renal pelvis of Col17a1-KO mice 1d after UUO

Fig. 3-9 and 10 show the urothelium histopathology of *Col17a1*-KO mice. In the renal pelvis histology of the collateral kidneys, superficial urothelial cells partially presented a pale cytoplasm in *Col17a1*-KO mice, and absent mucosal folds and urothelial cell hypertrophy, especially

umbrella cells, were found in the ureter of *Col17a1*-KO mice compared to the WT mice (Fig. 3-9A). Regarding epithelium-associated molecules, $OCLN^+$ urothelial cells were ectopically observed at the basal side in the renal pelvis and ureter urothelial cells of *Col17a1*-KO mice with or without UUO (Fig. 3-9B and C). WT mice showed partially faint $ZO\text{-}1^+$ and $OCLN^+$ reactions in the renal pelvis urothelium after UUO; however, those reactions in *Col17a1*-KO mice were relatively abundant at the apical portion compared to those observed in the WT mice (Fig. 3-9C). At the renal pelvis junctions 1d after UUO, urothelium disruption and proliferation were observed; however, infiltrating cell numbers were less in *Col17a1*-KO mice than that of the WT mice (Fig. 3-9D). To evaluate the renal pelvis urothelium, a region from the renal pelvis junction to the distal part was examined. The WT mice 1d after UUO possessed the increased urothelial cell numbers, although *Col17a1*-KO mice did not (Fig. 3-9E).

In both WT and *Col17a1*-KO mice, $CK14^+$ urothelial cells predominantly localized from around the proximal renal pelvis to the junction in collateral kidneys, whereas the number was decreased in the kidneys after UUO (Fig. 3-10A). Moreover, the number of $CK14^+$ urothelial cells with or without UUO was significantly less in the *Col17a1*-KO renal pelvis than that of the WT mice (Fig. 3-10A and B). In the proximal renal pelvis, collateral control kidneys of WT mice showed $COL17A1^+$ $CK14^+$ urothelial cells; however, $CK14^+$ reaction was diminished in the kidneys 1d after UUO (Fig. 3-10C). Further, in the renal pelvis junction to distal part of the WT mice after UUO, $COL17A1^+$ urothelial cells were co-expressed with CD44 and partially localized in $CK14^+$ urothelial cells, although $CD44^+$ urothelial cells were mainly found in that of *Col17a1*-KO mice (Fig. 3-10D).

Importantly, following UUO, numerous $CD11b^+$ cells aggregated beneath the renal pelvis urothelium at the junction between proximal and distal renal pelvis in the WT mice; however, the $CD11b^+$ cells were scattered in *Col17a1*-KO mice and had few $CXCL2^+$ reactions (Fig. 3-10E and F).

Deterioration of renal histopathology in the kidneys of Col17a1-KO mice 1d after UUO

The author also evaluated renal injuries in *Col17a1*-KO mice after UUO. In the indices for renal function, including BUN and serum Cr levels, the former tended to be higher in *Col17a1*-KO mice than that in WT mice, while the latter values were comparable between genotypes (Fig. 3-11A and B). Histopathologically, the IL-$36\alpha^+$ renal tubular injury score, not $CD11b^+$ infiltration cell number in tubulointerstitium, was deteriorated in *Col17a1*-KO mice compared with those in WT mice (Fig. 3-11C-F). Moreover, the kidneys of *Col17a1*-KO 1d UUO presented urothelial cell deciduation covering renal papilla (Fig. 3-11G), suggesting that renal pathology after UUO was exhausted in *Col17a1*-KO mice compared with that in WT.

Discussion

This chapter demonstrated that obstructive uropathy disrupted UEB in both renal pelvis and ureters with ectopic urothelial expression of COL17A1, which was involved in urothelial cell proliferation and local immunoreactivity (Fig. 3-12). In contrast to the urothelium, the stratified epithelial cells in the epidermis or cornea are attached to the basement membrane constitutively through COL17A1 as a hemidesmosome component [128]. The author discovered that following UUO, the beginning of the distal renal pelvis urothelium expressed COL17A1 as well as FOS/JUN, which are upstream signaling molecules of COL17A1 in urothelial cells [54]. Both transcriptional factors composing AP-1 respond to mechanical stress, bacterial infection, or inflammatory cytokines such as IL-1β, IL-6, and TNF-α [54,86,136]. Other studies analyzing murine renal pelvis urothelium after UUO or IRI reported that fibroblast growth factor receptor 2 (FGFR2) is activated by FGF7 [48,124], which is produced in smooth muscle cells and fibroblasts [2,27,100], leading to urothelial cell proliferation. Further, there are several reports that FGFR2 signaling triggers JUN activation in human hepatocytes and gastric cancer [108,140]. Hence, UUO stimulation including internal pressure of the renal pelvis cavity and cytokines from urine might activate the FOS/JUN-related pathway and subsequently promote COL17A1 expression in urothelial cells.

The present study showed that COL17A1$^+$ urothelial cells forms multiple urothelial layers co-expressing CD44, which was a glycoprotein involved in cell-cell interactions, cell adhesion, migrations, and proliferation in a normal urothelium, its cancer, or regeneration of injured renal epithelium [35,38,51,73]. Further, COL17A1 was partially localized in urothelial cells incorporating BrdU, a proliferation marker. Importantly, *Col17a1*-KO urothelium 1d following UUO presented CD44$^+$ mono- or bi-layers. Studies on normal epidermis, wound healing, and epithelial cancers have revealed that COL17A1, an epidermal stem cell marker, plays a role in regulating epithelial cell proliferation [67,78,121,128]. The present study also demonstrated that CK14, one of the stem cell markers for urothelial cells, were mainly localized in the urothelium from the proximal renal pelvis to the beginning of the distal part, and some were co-expressed COL17A1 [51]. CK14 expression was diminished 1d after UUO instead of COL17A1 upregulation, whereas COL17A1$^+$ CD44$^+$ CK14$^+$ urothelial cells were increasing at the basal side of the urothelium from 4d onward. In *Col17a1*-KO mice, CK14$^+$ urothelial cell numbers decreased in the renal pelvis urothelium of both control and UUO kidneys compared with the WT mice. Consistently, epidermal studies have reported that COL17A1 functions as an epidermal stem cell marker and a loss of the stem cells in *Col17a1*-KO mice [78,119]. As shown in Fig. 3-12D, COL17A1 overexpression was followed by CD44 and CK14 induction, indicating that COL17A1 has an important role in urothelial cell proliferation as the stem cell marker.

UUO also altered TJP expression in the urothelium. OCLN was localized at both the apical

and basal portions of the urinary tract urothelium, whereas ZO-1 mainly localized at the apical portion, which is partially consistent with other reports addressing murine urinary bladder [1]. After UUO, both TJPs were partially absent in urothelial cells at the apical portion of the renal pelvis, as TJPs are decreased in urinary bladders with interstitial cystitis [70]. However, *Col17a1*-KO 1d after UUO maintained TJP expression at the apical portion of the renal pelvis urothelium. Moreover, the control renal pelvis and ureters of *Col17a1*-KO mice showed predominant expression of OCLN at the basal portion, indicating that COL17A1 deficiency caused abnormal TJP expression. Furthermore, superficial cells exhibited a pale cytoplasm and hypertrophy in the renal pelvis and ureter of *Col17a1*-KO mice, respectively, which is consistent with transient hyperproliferation of intrafollicular epidermal cells during prematuration [128]. Therefore, COL17A1 may regulate the balance between cell proliferation and differentiation with alteration of cell adhesion in urothelial cells.

Notably, in the renal pelvis 1d after UUO, UEB disruption at the junction between the proximal and distal renal pelvis urothelium promoted COL17A1 induction. A junction between two organs, such as the ureteropelvic junction and the gastroesophageal junction, represents an origin of pathological development [20,50]. In ureteropelvic junction obstruction, a crucial pathological mechanism is the presence of abnormalities in synaptic vesicles and the smooth muscle cell structure, which induce alterations of the synaptophysin and epidermal growth factor [50]. Interestingly, smooth muscle cells in murine renal pelvis are both typical and atypical; they function as peristaltic contractors and peacemakers, respectively [49]. Thus, atypical and fiber-structural smooth muscle cells that comprise the junction urothelium might lose toughness upon UUO-induced renal pelvis cavity pressure, leading to UEB disruption and COL17A1 expression.

COL17A1 expressed in mesenchymal stem cells of bone marrow influences regulation of granulocyte production [76]. The present findings supported a COL17A1 function in immunoreactivity; thus, suggesting that COL17A1 was associated with an initial stage of inflammation in the urinary tract mucosa through migration of $CD11b^+$ cells secreting CXCL2. CXCL2 is synthesized in macrophages, neutrophils, and mast cells. It is involved in neutrophil recruitment and vascularization in addition to skin, intestine, and lung tissue reconstruction [5,39,42]. This study demonstrated that CXCL2 derived from $CD11b^+$ cells was stimulated by COL17A1 and urine. It is possible that ecto- or intra-domains composing COL17A1 derived from intact or deciduate urothelial cells as well as the former domain in the lamina propria via ectodomain shedding may bind to and activate $CD11b^+$ cells [121]; however, this mechanism of action remains unclear. Another immuno-activator was represented by urine leakage from the lumen to the parenchyma, which was one of the factors promoting UTALS development [54]. In interstitial cystitis, symptoms such as pelvic pain, urgency, and urination frequency are caused by depolarization of sensory nerves and muscles following urinary potassium diffusion into the

bladder wall due to the UEB disruption [70]. Thus, the author propose that both COL17A1 expression and urine leakage into the parenchyma of the urinary tract might recruit $CD11b^+$ cells followed by CXCL2 production and contribute to early inflammation and the UEB reconstruction via fibrosis in order to localize the reactions.

The limitation of this study is that the findings using *Col17a1*-KO mice did not show obvious COL17A1 contribution to the progression of hydronephrosis pathology. The IL-36α$^+$ renal tubular injury score, not $CD11b^+$ infiltration cell number in tubulointerstitium, was deteriorated in *Col17a1*-KO mice, while $CD11b^+$ cell infiltration into the renal pelvis was inhibited. The kidneys of *Col17a1*-KO mice 1d UUO presented urothelial cell deciduation covering renal papilla, suggesting necrosis followed by renal pathology exacerbation, although further investigations are needed to elucidate the COL17A1 function in renal injury induced by UUO. Of note, $COL17A1^+$ $CK14^+$ urothelial cells, which might be the progenitor cells, were found in the beginning of the proximal renal pelvis in collateral kidneys of the WT. Reportedly, IRI model mice have shown that Ki-67^+ proliferating urothelial cells, which express CK14, are abundant in this part (called the fornix area), but not in renal papilla [124]. These findings suggest that the urothelial cells localizing in the beginning of the proximal renal pelvis are a potential cell source for the renal pelvis and papillary urothelium.

The author discovered that ureter urothelium of humans and cats with urolithiasis also overexpressed COL17A1. Previous studies only showed upregulation of COL17A1 mRNA in human patients with urinary incontinence and canine bladder cancer [37,60]; furthermore, these findings indicate that COL17A1 is a common therapeutic target and potential marker for urothelial disorders in several mammals. This study also demonstrated that COL17A1 expression in the renal pelvis and ureter after UUO correlated with urothelial and renal lesions, suggesting that UEB disruption in renal pelvis leads to renal injury. Importantly, renal pelvis tissue must not be collected by renal biopsy because of its location. Therefore, urinary COL17A1 can represent a diagnostic marker for urinary system disorders. Nevertheless, additional research is needed to support our findings.

In conclusion, this chapter clarified a novel pathological pathway involving COL17A1 in the urothelium of mice, humans, and cats with obstructive uropathy. The present data provided a description of a new pathological mechanism through which COL17A1 and urine leakage in the urothelium leads to local inflammation. These findings may contribute to the development of therapeutic and diagnostic strategies for urinary organ diseases.

Summary

Chapters 1 and 2 revealed that the pathological role of IL-36R ligands in the renal epithelial cell-associated renal injuries. In this chapter, COL17A1, urothelial cell-associated pathological molecule, was examined. This epidermal hemidesmosome component is ectopically induced in the urothelial cells of mouse and human renal pelvis and involved in UTALS development. Here, the author found that COL17A1 was induced in the obstructive uropathy-prone ureters of humans and cats. To ascertain its function, the urinary organs of UUO-injured mice were analyzed for 1 week after surgery. From 1d, COL17A1 expression increased in urothelial cells of renal pelvis and ureters and positively correlated with tubulointerstitial lesions. A part of the renal pelvis where smooth muscle layer from the ureter was interrupted was sensitive to urothelial deciduation and COL17A1 induction with the expression of FOS/JUN, COL17A1 upstream-signal molecules. In this area, urothelial cell adhesions were changed, and urine leaked from the renal pelvis lumen into the parenchyma. After urine stimulation, cultured immune cells induced CXCL2, which was also produced by $CD11b^+$ cells following COL17A1 stimulation. On 1d, $CXCL2^+$ $CD11b^+$ cells infiltrated the urothelium-disrupted area; however, the number was significantly diminished in *Col17a1*-KO mice. Moreover, $COL17A1^+$ urothelial cells partially expressed CK14 and CD44, while *Col17a1*-KO mice exhibited decreased $CK14^+$ urothelial cells. Thus, COL17A1 maintains urothelium integrity by regulating urothelial cell adhesion and proliferation, and activates local immune response during obstructive uropathy in mammals.

Tables and Figures

Table 3-1. List of antibodies used in this chapter

Primary antibody	Host	Dilution	Source	Antigen retrieval	Blocking serum	
					IHC	IF
α-SMA	Mouse	1:8000	Proteintech, Rosemont, IL, USA	Tris	-	5% NDS
CD11b	Rabbit	1:5000	Abcam, Cambridge, UK	Tris	10% NGS	5% NDS
CK14	Mouse	1:500	Proteintech, Rosemont, IL, USA	Tris	Mouse kit	5% NDS
COL17A1	Rabbit	1:100	Abcam, Cambridge, UK	Tris	10% NGS	5% NDS
CXCL2	Goat	1:400	R and D system, Minneapolis, MN, USA	Tris	-	5% NDS
c-FOS	Rabbit	1:400	Abcam, Cambridge, UK	Tris	10% NGS	-
c-JUN	Rabbit	1:400	Abcam, Cambridge, UK	Tris	10% NGS	-
IBA-1	Goat	1:600	Abcam, Cambridge, UK	Tris	-	5% NDS
OCLN	Mouse	1:1000	Proteintech, Rosemont, IL, USA	Pepsin	-	5% NDS
PDGFRα	Goat	1:300	R and D system, Minneapolis, MN, USA	Tris	-	5% NDS
ZO-1	Rabbit	1:1000	Abcam, Cambridge, UK	Pepsin	-	5% NDS

Tris: 20 mM Tris-HCl buffer (pH 9.0) at 110 °C for 15 min, Pepsin: 0.1% pepsin at 37 °C for 5 min, NDS: normal donkey serum, NGS: normal goat serum.

Table 3-2. List of primers used in this chapter

Gene symbol (Gene ID)	Primer sequence (5′-3′) F: Forward, R: Reverse		Product size (bp)
Cd3e (12501)	F: TGCCTCAGAAGCATGATAAGC	R: TTGGCCTTCCTATTCTTGCTC	244
Col17a1 (12821)	F: ACTTGCGGTCATCAGGCTAC	R: AGACAGGAGGGACCCATCTC	170
Ccl1 (20290)	F: GCAAGAGCATGCTTACGGTC	R: TTTGTTAGTTGAGGCGAGC	170
Ccl6 (20305)	F: CAGGAGGATGAGAAACTCCAA	R: TTGGAGGGTTATAGCGACGA	119
Ccl25 (20300)	F: AGTGGAAGCTGCAACCTACG	R: CCTCACGCTTGTACTGTTGG	216
Cxcl2 (20310)	F: TGTCAATGCCTGAAGACCCTG	R: CAGTTAGCCTTGCCTTTGTTCAG	197
Cxcl10 (15945)	F: ATGACGGGCCAGTGAGAATG	R: CGGATTCAGACATCTCTGCTCAT	125
Cxcl11 (56066)	F: AGTAACGGCTGCGACAAAG	R: AGACGTTCCCAGGATGTCAC	160
Cxcl12 (20315)	F: CTTCGAGAGCCACATCGCC	R: GTTGTTGTTCTTCAGCCGTGC	100
Cxcl13 (55985)	F: ATCCTCGTGCAAATGGTTACA	R: AGATGATAGTGGCTTCAGGCAG	115
Itgam (16409)	F: CATGACCTTCCAAGAGAATGC	R: GCTTGTGCTGTAGTCACACTGG	142
Ms4a1 (12482)	F: ATCATGAATGGCCTCTTCCA	R: TGCCAGGAGTGATCCTGAA	138
Ocln (18260)	F: TCCACCTCCTTACAGACCTGA	R: AGAGTACGCTGGCTGAGAGA	112
Tjp1 (21872)	F: AATTATCCCACAAGGAGCCATTCC	R: TTTAGGGTCACAGTGTGGCAA	196
Upk2 (22269)	F: AAGCCTGTTAATTGCCTTGCC	R: CATGGAGGCACCACAAAGTC	114
Primers sequence for genotyping (5′-3′) F: Forward, R: Reverse			
Col17a1 (wild type)	F: ACCTTCCAGTGAAGAGCCAT	R: GTGGATTCCCAAAGCCATAC	533
Col17a1 (knockout type)	F: TGGATGTGGAATGTGTGCGA	R: GTGGATTCCCAAAGCCATAC	590

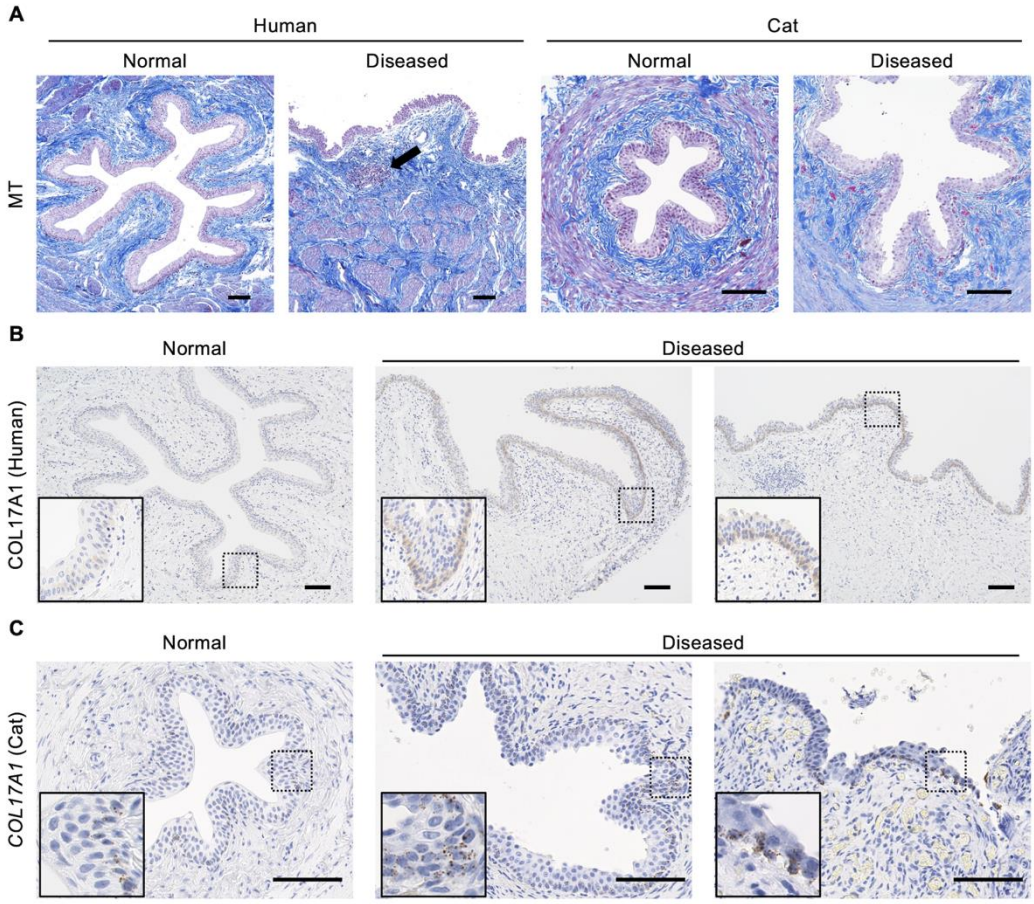

Fig. 3-1. COL17A1 expression in human and cat ureters with urolithiasis

(A) Representative images of human and cat ureters. More collagen fibers are observed in diseased human and feline ureters than those observed in the healthy ureter. Infiltrated cells localize in the lamina propria and submucosa of humans and cats with urolithiasis. In the former specimen, immune cell aggregation is observed (arrow). Masson's trichrome staining. Bars = 100 μm. **(B)** Localization of COL17A1 in human ureters. Few $COL17A1^+$ cells are observed at the basal portion of normal ureter urothelia. There are numerous $COL17A1^+$ cells in the diseased ureters with cell aggregation. Insets indicate high magnification images of areas marked by the black squares. IHC. Bars = 100 μm. **(C)** Localization of *COL17A1* in cat ureters. $COL17A1^+$ reactions are observed at the basal portion of both the normal and diseased ureters. The positive dots in each cell are abundant in the diseased ureters. Insets indicate high magnification images of areas marked by the black squares. ISH. Bars = 100 μm. MT: Masson's trichrome staining.

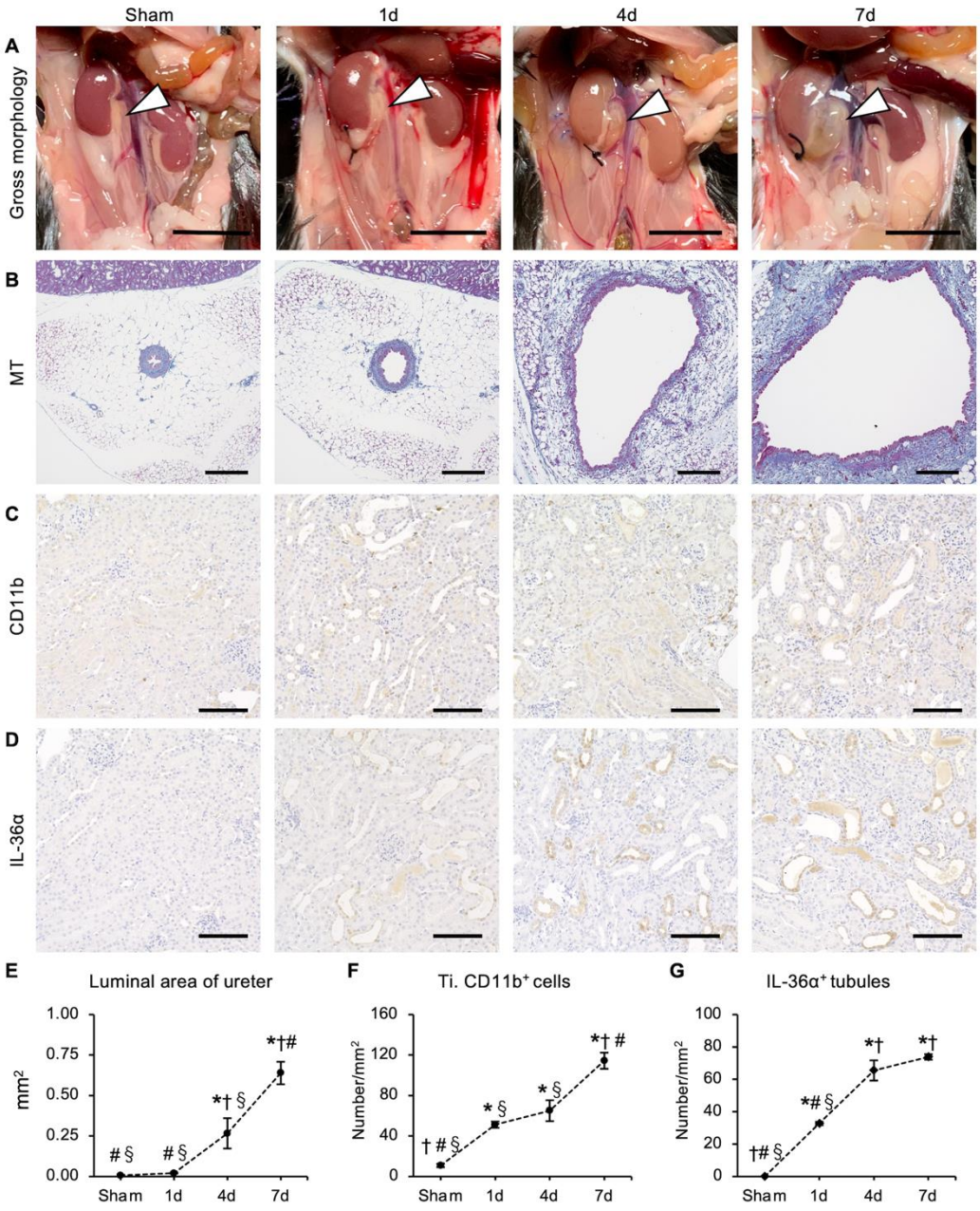
Sham
1d
4d
7d
A
Gross morphology
B
MT
C
CD11b
D
IL-36α
E
Luminal area of ureter
mm²
1.00
0.75
0.50
0.25
0.00
*†#
*† §
# §
# §
Sham
1d
4d
7d
F
Ti. CD11b⁺ cells
Number/mm²
160
120
80
40
0
*† #
* §
* §
† # §
Sham
1d
4d
7d
G
IL-36α⁺ tubules
Number/mm²
100
80
60
40
20
0
*†
*†
*# §
†# §
Sham
1d
4d
7d

Fig. 3-2. Pathology of ureters and kidneys after UUO

(A) Gross morphological images of kidneys and ureters at 1, 4, and 7d after UUO compared to the Sham. Hydronephrosis and hydroureter are observed from 4d after UUO onwards. Arrowheads indicate proximal ureters from ligation. Bars = 10 mm. **(B)** Representative images of ureter 1, 4, and 7d after UUO compared to that of the Sham. Dilation of the ureter lumen with fibrosis and degeneration of smooth muscle cells is clearly observed from 4d after UUO onwards. Masson's trichrome staining. Bars = 100 μm. **(C and D)** Localization of CD11b (panel C) and IL-36α (panel D) in kidneys at 1, 4, and 7d after UUO compared to those in the Sham. $CD11b^+$ myeloid cells and IL-$36\alpha^+$ injured distal tubules are increasing in a time-dependent manner after UUO. IHC. Bars = 100 μm. **(E-G)** Luminal area of ureters (panel E), and the number of $CD11b^+$ cells in tubulointerstitium (panel F) and IL-$36\alpha^+$ renal tubules (panel G). Each dot represents the mean ± SE (n = 5). *, †, #, and § indicate a significant difference with Sham 1, 4, and 7d after UUO, respectively ($P < 0.05$). Kruskal-Wallis test followed by Scheffé's method. MT: Masson's trichrome staining, Ti: tubulointerstitium.

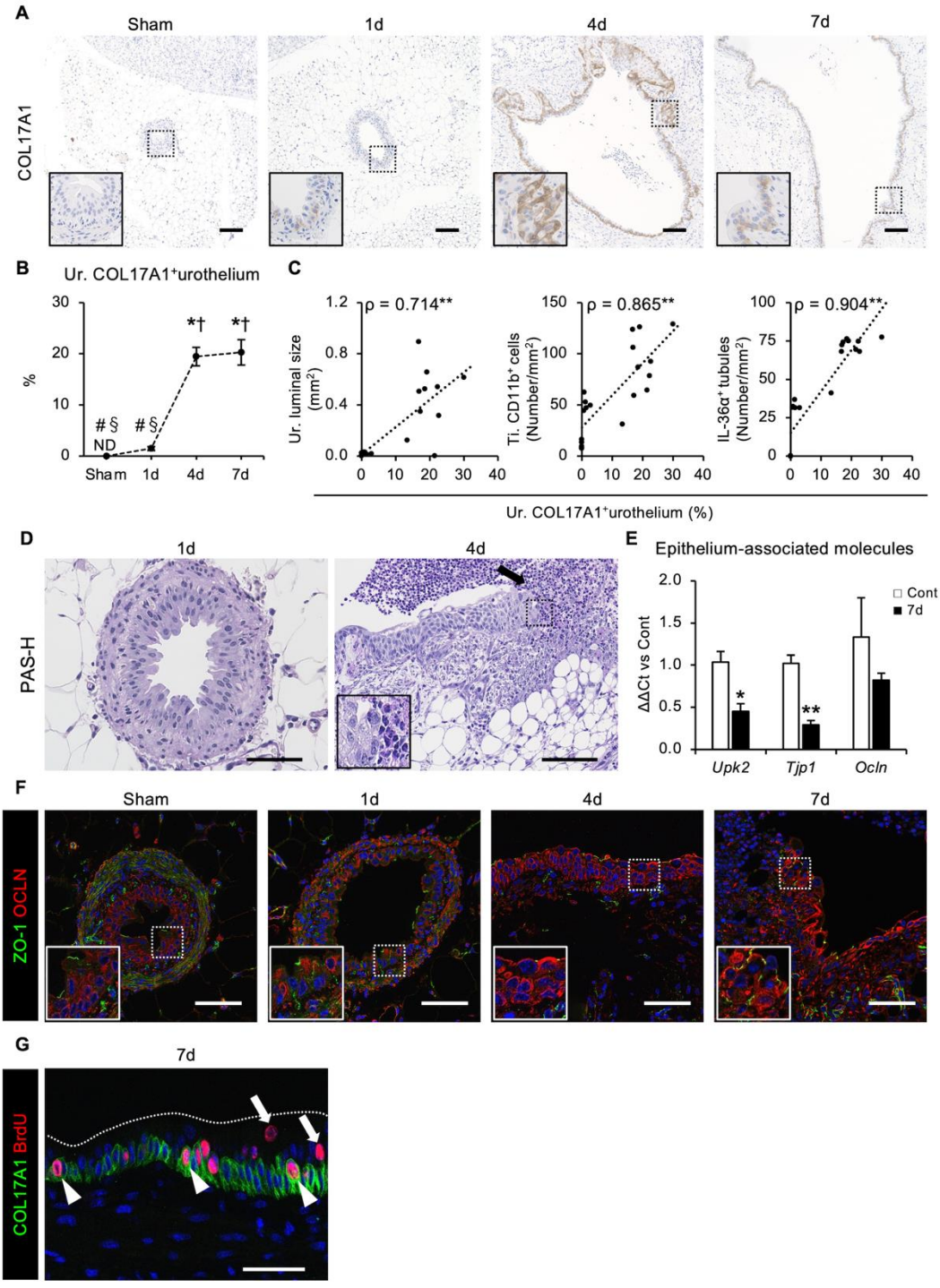
A
Sham
1d
4d
7d
COL17A1
B
Ur. COL17A1+urothelium
%
ND
Sham
1d
4d
7d
C
ρ = 0.714**
Ur. luminal size (mm²)
ρ = 0.865**
Ti. CD11b+ cells (Number/mm²)
ρ = 0.904**
IL-36α+ tubules (Number/mm²)
Ur. COL17A1+urothelium (%)
D
1d
4d
PAS-H
E
Epithelium-associated molecules
Cont
7d
ΔΔCt vs Cont
Upk2
Tjp1
Ocln
F
Sham
1d
4d
7d
ZO-1 OCLN
G
7d
COL17A1 BrdU

Fig. 3-3. COL17A1 expression in the urothelium of murine ureters induced by UUO

(A) Localization of COL17A1 in ureters at 1, 4, and 7d after UUO compared with those in the Sham. $COL17A1^+$ urothelial cells were not detected in the Sham ureters. The positive urothelial cells are observed in the ureter basal portion 1d after UUO and are drastically increasing from day 4 onwards. Insets indicate high magnification images of areas marked by the black squares. IHC. Bars = 500 μm. **(B)** $COL17A1^+$ area in ureter urothelium. Each dot represents mean ± SE (n = 5). *, †, #, and § indicate a significant difference with Sham, 1, 4, and 7d after UUO, respectively ($P < 0.01$). Kruskal-Wallis test followed by Scheffé's method. **(C)** Correlation of $COL17A1^+$ area in the ureter urothelium with luminal size of ureter and the indices for renal lesions including $CD11b^+$ cells in tubulointerstitium as well as IL-$36\alpha^+$ injured renal tubules. ρ indicates the Spearman's correlation coefficient (n = 20, ** $P < 0.01$). **(D)** Representative images of ureter 1 and 4d after UUO. Deciduation of urothelial cells (arrow) observed with mono-nuclear cells at 4d, but not 1d after UUO. Inset indicates high magnification images of areas marked by the black square. PAS-H. Bars = 100 μm. **(E)** Relative mRNA expression of epithelium-associated genes in ureters at 7d after UUO. The expression levels are normalized to the values of *Actb* and those of the collateral control. Each bar represents mean ± SE (n = 4–5). * indicates a significant difference compared to the collateral control (*$P < 0.05$, ** $P < 0.01$). Mann-Whitney *U*-test, qPCR analysis. **(F)** Localization of ZO-1 (green) and OCLN (red) in ureter at 1, 4, and 7d after UUO compared with those in the Sham. $ZO\text{-}1^+$ or $OCLN^+$ staining in the Sham urothelium is observed at the apical and apical/basal portion, respectively. $ZO\text{-}1^+$ staining is faint after UUO. Although $OCLN^+$ staining is also faint in the apical portion 1d after UUO, it increases temporarily 4d after UUO, and subsequently OCLN-overexpressing and -faint urothelial cells are observed 7d after UUO. The nucleus is stained using Hoechst (blue). Insets indicate high magnification images of areas marked by the white squares. IF. Bars = 100 μm. **(G)** Localization of COL17A1 (green) using BrdU (red) in ureters at 7d after UUO. Some BrdU-incorporated cells express COL17A1 (arrowheads), whereas $COL17A1^-$ urothelial cells incorporating BrdU (arrows) are also found at the apical side of urothelium. White dotted lines represent the apical side of the urothelium. The nucleus is stained using Hoechst (blue). IF. Bars = 50 μm. Ur: ureter, ND: not detected, Ti: tubulointerstitium, PAS-H: periodic acid Schiff-hematoxylin staining, Cont: collateral control, BrdU: bromodeoxyuridine.

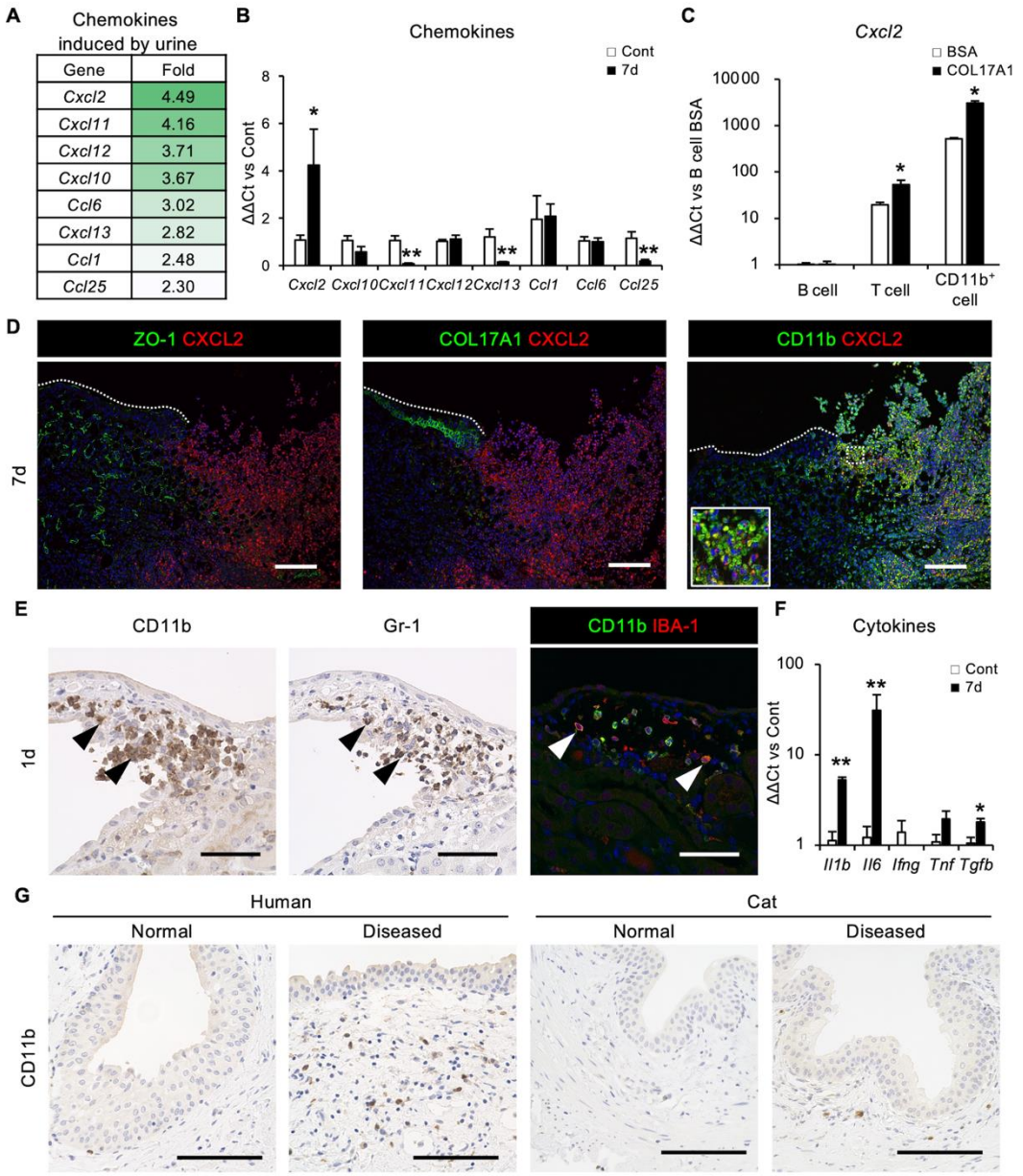
A
Chemokines induced by urine
Gene
Fold
Cxcl2
4.49
Cxcl11
4.16
Cxcl12
3.71
Cxcl10
3.67
Ccl6
3.02
Cxcl13
2.82
Ccl1
2.48
Ccl25
2.30
B
Chemokines
Cont
7d
ΔΔCt vs Cont
Cxcl2 Cxcl10 Cxcl11 Cxcl12 Cxcl13 Ccl1 Ccl6 Ccl25
C
Cxcl2
BSA
COL17A1
ΔΔCt vs B cell BSA
B cell
T cell
CD11b+ cell
D
ZO-1 CXCL2
COL17A1 CXCL2
CD11b CXCL2
7d
E
CD11b
Gr-1
CD11b IBA-1
1d
F
Cytokines
Cont
7d
ΔΔCt vs Cont
Il1b Il6 Ifng Tnf Tgfb
G
Human
Cat
Normal
Diseased
Normal
Diseased
CD11b

Fig. 3-4. Activation of CD11b$^+$ cells by COL17A1 and urine leakage in mice with UUO

(A) Relative mRNA expression of chemokines in mouse lymphoid structures stimulated by urine. Expression levels are normalized to the values of the PBS control. Microarray. **(B)** Relative mRNA expression of chemokines measured from ureters 7d after UUO. The expression levels are normalized to the values of *Actb* and those of the collateral control. Each bar represents mean ± SE (n = 5). * indicates a significant difference compared to collateral control (*P < 0.05, **P < 0.01). Mann-Whitney U-test, qPCR analysis. **(C)** Relative mRNA expression of *Cxcl2* in B, T, and CD11b$^+$ cells stimulated using BSA or recombinant human COL17A1. The expression levels are normalized to the values of *Actb* and those of B cell stimulated with BSA. Each bar represents the mean ± SE (n = 4). * indicates a significant difference compared with the BSA-stimulated group (*P < 0.05). Mann-Whitney U-test, qPCR analysis. **(D)** Localization of CXCL2 (red) with ZO-1, COL17A1, or CD11b (green) in ureters at 7d after UUO. CXCL2$^+$ staining is observed beneath the ZO-1 faint urothelium as well as close to the COL17A1$^+$ urothelium and localizes in CD11b$^+$ cells. White dotted lines represent the apical side of the urothelium. The nucleus is stained using Hoechst (blue). IF. Bars = 100 μm. **(E)** Localization of CD11b with Gr-1 or IBA-1 in renal pelvis 1d after UUO. CD11b$^+$ staining co-localizes in Gr-1$^+$ neutrophils (observed using serial sections of subsequent IHC analyses) and in IBA-1$^+$ macrophages (observed using IF). Arrowheads indicate the positive cells. Bars = 50 μm. **(F)** Relative mRNA expression of inflammatory cytokines measured in ureters 7d after UUO. The expression levels are normalized to the values of *Actb* and those of the collateral control. Each bar represents the mean ± SE (n = 4–5). * indicates a significant difference compared with collateral control (*P < 0.05, **P < 0.01). Mann-Whitney U-test, qPCR analysis. **(G)** Localization of CD11b in human and cat ureters. Infiltrated CD11b$^+$ cells are observed in the lamina propria and submucosa of humans and cats with urolithiasis. IHC. Bars = 100 μm. Cont: collateral control, BSA: bovine serum albumin.

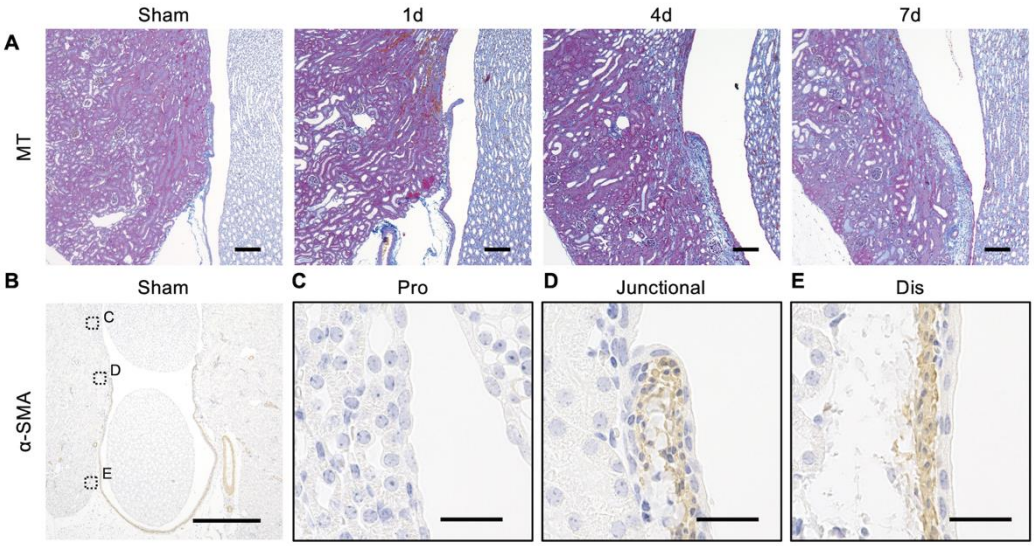

Fig. 3-5. Histopathology of the mouse renal pelvis after UUO

(A) Representative images of kidneys at 1, 4, and 7d after UUO. Dilation of renal tubules is observed from 1d after UUO, and fibrosis in the renal pelvis parenchyma is progressing from 4d after UUO onwards. Masson's trichrome staining. Bars = 100 μm. **(B-E)** Localization of α-SMA in the Sham renal pelvis. There is no α-SMA$^+$ smooth muscle layer in the proximal renal pelvis urothelium (panel C). At the junction between the proximal and distal renal pelvis urothelium, α-SMA$^+$ cells exhibit a fiber structure, not smooth muscle layer (panel D). smooth muscle layer is observed in the distal renal pelvis urothelium (panel E). IHC. Bars = 500 μm (B) and 25 μm (C-E). MT: Masson's trichrome staining, Pro: proximal renal pelvis urothelium, Dis: distal renal pelvis urothelium.

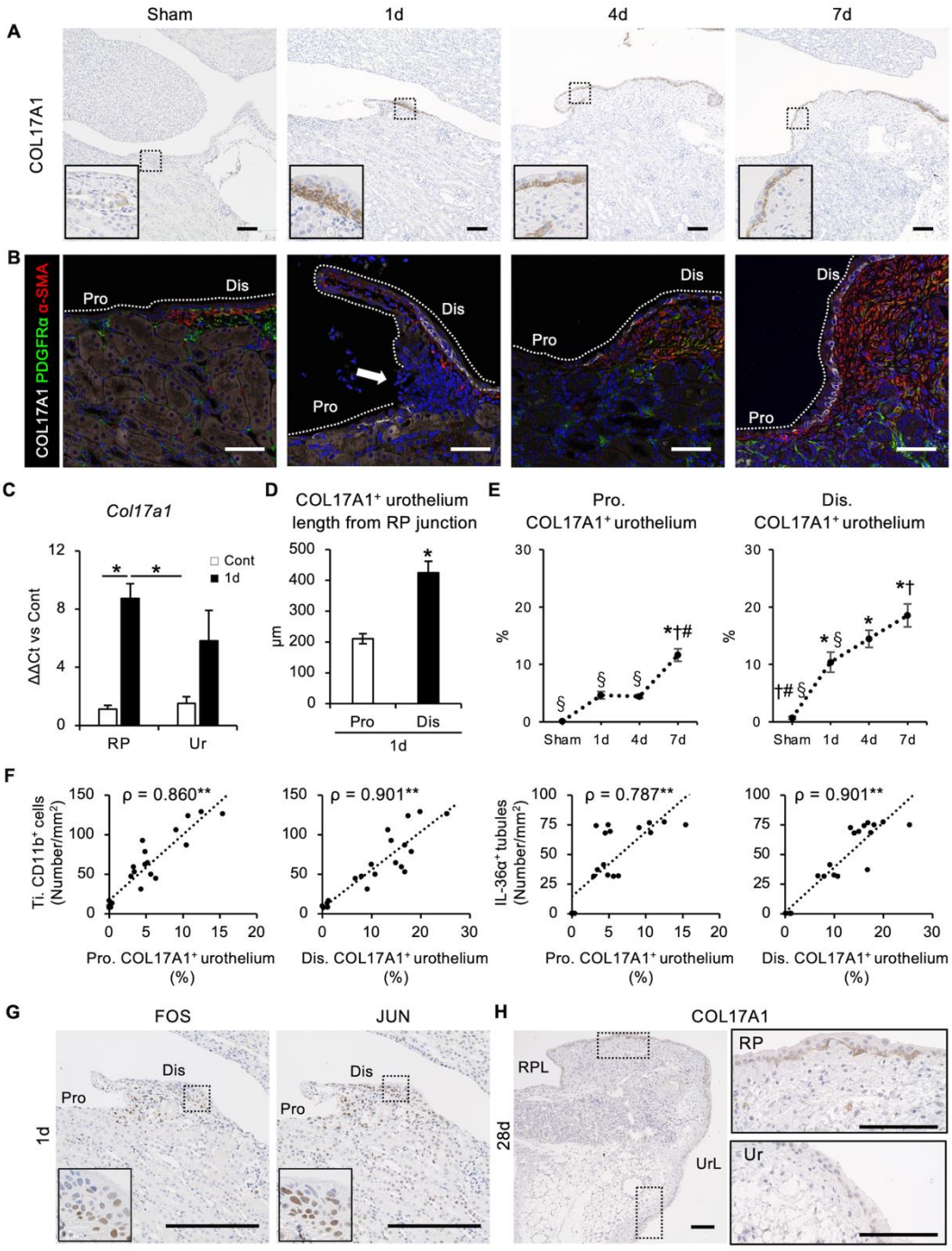
A
Sham
1d
4d
7d
COL17A1
B
COL17A1 PDGFRα α-SMA
Pro
Dis
C
Col17a1
ΔΔCt vs Cont
Cont
1d
RP
Ur
D
COL17A1+ urothelium length from RP junction
μm
Pro
Dis
1d
E
Pro. COL17A1+ urothelium
Dis. COL17A1+ urothelium
%
Sham
1d
4d
7d
F
Ti. CD11b+ cells (Number/mm2)
IL-36α+ tubules (Number/mm2)
ρ = 0.860**
ρ = 0.901**
ρ = 0.787**
ρ = 0.901**
Pro. COL17A1+ urothelium (%)
Dis. COL17A1+ urothelium (%)
G
FOS
JUN
1d
H
COL17A1
28d
RPL
UrL
RP
Ur

Fig. 3-6. COL17A1 dynamics in mouse renal pelvis after UUO

(A) Localization of COL17A1 in renal pelvis 1, 4, and 7d after UUO compared to that in the Sham. COL17A1$^+$ urothelial cells localize at the basal portion of the renal pelvis urothelium and drastically increase in a time-dependent manner after UUO. Insets indicate high magnification images of areas marked by black squares. IHC. Bars = 100 μm. **(B)** Co-localization of COL17A1 (white) with PDGFRα (green, fibroblast marker) and α-SMA (red, smooth muscle fiber and myofibroblast marker) in the renal pelvis at 1, 4, and 7d after UUO compared with that in the Sham. The renal pelvis urothelium in the Sham is divided into the proximal renal pelvis urothelium without the α-SMA$^+$ smooth muscle layer and the distal one with the smooth muscle layer, and the latter urothelium obviously possesses COL17A1$^+$ cells at 1d UUO. COL17A1$^+$ cells are increasing in both types of urothelia with αSMA$^+$ myofibroblasts increasing from 4d after UUO onward. The nucleus is stained using Hoechst (blue). Arrow indicates deciduation of urothelial cells. White dotted lines represent the apical side of urothelium. IF. Bars = 100 μm. **(C)** Relative mRNA expression of *Col17a1* in isolated renal pelvis and ureter 1d after UUO. The expression levels are normalized to the values of *Actb* and those of the collateral control. Each bar represents the mean ± SE (n = 4–5). * indicates a significant difference between groups (*$P < 0.05$). Mann-Whitney *U*-test, qPCR analysis. **(D)** Consecutive length of CO17A1$^+$ urothelial cells from the renal pelvis junction to the proximal and distal parts 1d after UUO. Each bar represents the mean ± SE (n = 5). * indicates a significant difference between groups (*$P < 0.05$). Mann-Whitney *U*-test. **(E)** COL17A1$^+$ area in the proximal and distal renal pelvis urothelium. Each bar represents mean ± SE (n = 5). *, †, #, and § indicate a significant difference compared to that in Sham 1, 4, and 7d, respectively ($P < 0.01$). Kruskal-Wallis test followed by Scheffé's method. **(F)** Correlation of COL17A1$^+$ area in proximal or distal renal pelvis urothelium with the examined indices for renal lesions, CD11b$^+$ cells in tubulointerstitium and IL-36α$^+$ renal tubules. ρ indicates the Spearman's correlation coefficient (n = 20, ** $P < 0.01$). **(G)** Localization of FOS and JUN in renal pelvis. Both FOS and JUN-positive reactions are observed in urothelial nuclei at the beginning of the distal urothelium 1d after UUO. Insets indicate high magnification images of areas marked by black squares. IHC. Bars = 100 μm. **(H)** Localization of COL17A1 in the renal pelvis and ureter 28d after UUO. COL17A1 is observed in the urothelium of both the renal pelvis and ureter, whereas the former highly expresses COL17A1 than that in the latter. Bars = 100 μm. Pro: proximal renal pelvis urothelium, Dis: distal renal pelvis urothelium, Cont: collateral control, renal pelvis: renal pelvis, Ur: ureter, Ti: tubulointerstitium, RPL: lumen of renal pelvis, UrL: lumen of ureter.

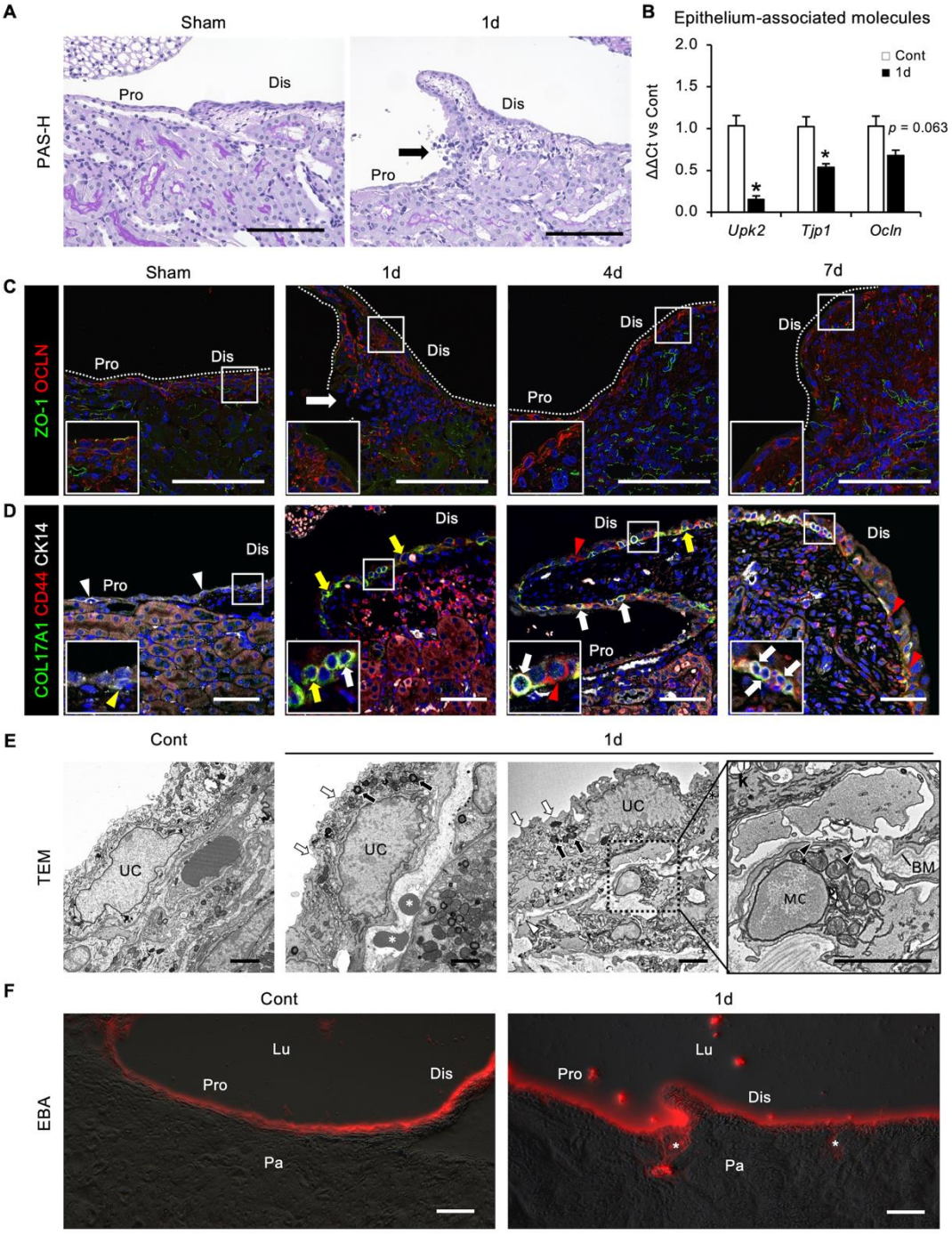
A
Sham
1d
PAS-H
Pro
Dis
B
Epithelium-associated molecules
ΔΔCt vs Cont
Cont
1d
p = 0.063
Upk2
Tjp1
Ocln
C
Sham
1d
4d
7d
ZO-1 OCLN
D
COL17A1 CD44 CK14
E
Cont
1d
TEM
UC
BM
MC
K
F
EBA
Lu
Pa

Fig. 3-7. Disruption of the UEB in the murine renal pelvis with UUO

(A) Representative images of renal pelvis 1d after UUO. Although intact urothelium of the renal pelvis is observed in the Sham, deciduation of urothelial cells is observed at the junction between the proximal and distal renal pelvis urothelium 1d after UUO (arrow). PAS-H. Bars = 100 μm. **(B)** Relative mRNA expression of epithelium-associated genes in isolated renal pelvis at 1d after UUO. The expression levels are normalized to the values of *Actb* and those of collateral control. Each bar represents mean ± SE (n = 4–5). * indicates a significant difference compared with collateral control (*P< 0.05). Mann-Whitney U-test, qPCR analysis. **(C)** Localization of ZO-1 (green) and OCLN (red), as markers for tight junctions in the renal pelvis at 1, 4, and 7d after UUO compared with those in the Sham. ZO-1^{+} or OCLN^{+} staining is observed at the apical or apical/basal portion of the renal pelvis urothelium in the Sham, respectively. Both positive reactions are partially faint at the apical portion on day 1 after UUO with urothelial deciduation (arrow). OCLN-faint and -overexpressing urothelial cells are observed 4d after UUO. The former cells increase 7d after UUO. The nucleus is stained using Hoechst (blue). White dotted lines represent the apical side of the urothelium. Insets indicate high magnification images of areas marked by the white squares. IF. Bars = 100 μm. **(D)** Localization of COL17A1 (green) with CD44 (red) and CK14 (white) in the renal pelvis at 1, 4, and 7d after UUO compared with those in the Sham. In the Sham, COL17A1^{-} CD44^{-} CK14^{+} cells (whiter arrowheads) are found and partially co-expressed with COL17A1 (yellow arrowheads). At 1d, COL17A1^{+} CD44^{+} CK14^{-} cells (yellow arrows) are dominant, and few COL17A1^{+} CD44^{+} CK14^{+} cells (whiter arrowheads) are observed. From 4d onward, triple positive cells are dominant, and some COL17A1^{-} CD44^{+} CK14^{-} cells are found. The nucleus is stained using Hoechst (blue). White dotted lines represent the apical side of urothelium. IF. Bars = 50 μm. **(E)** Representative TEM images of the renal pelvis. In urothelial cells 1d after UUO, folded apical membrane (white arrows), numerous lysosomes (black arrows), ectopic red blood cells beneath basement membrane (white asterisks), and intracellular spaces (black asterisks) are observed compared with those in the collateral control. Urothelial cell processes extending to the lamina propria interact with smooth muscle cells (white arrowheads). A migrating cell from lamina propria is observed in the partially effaced basement membrane (BM; black arrowheads). Bars = 2 μm. **(F)** Localization of Evans blue-conjugated BSA in renal pelvis. Evans blue-conjugated BSA injected from the urinary bladder is observed along the urothelium in the Sham, while it leaked into the renal pelvis parenchyma from the lumen 1d after UUO (asterisks). Bars = 100 μm. Pro: proximal renal pelvis urothelium, Dis: distal renal pelvis urothelium, PAS-H: Periodic acid Schiff-hematoxylin staining, Cont: collateral control, TEM: transmission electron microscopy, UC: urothelial cell, MC: migrating cell, EBA: Evans-blue conjugated with bovine serum albumin, Pa: parenchyma, Lu: renal pelvis lumen.

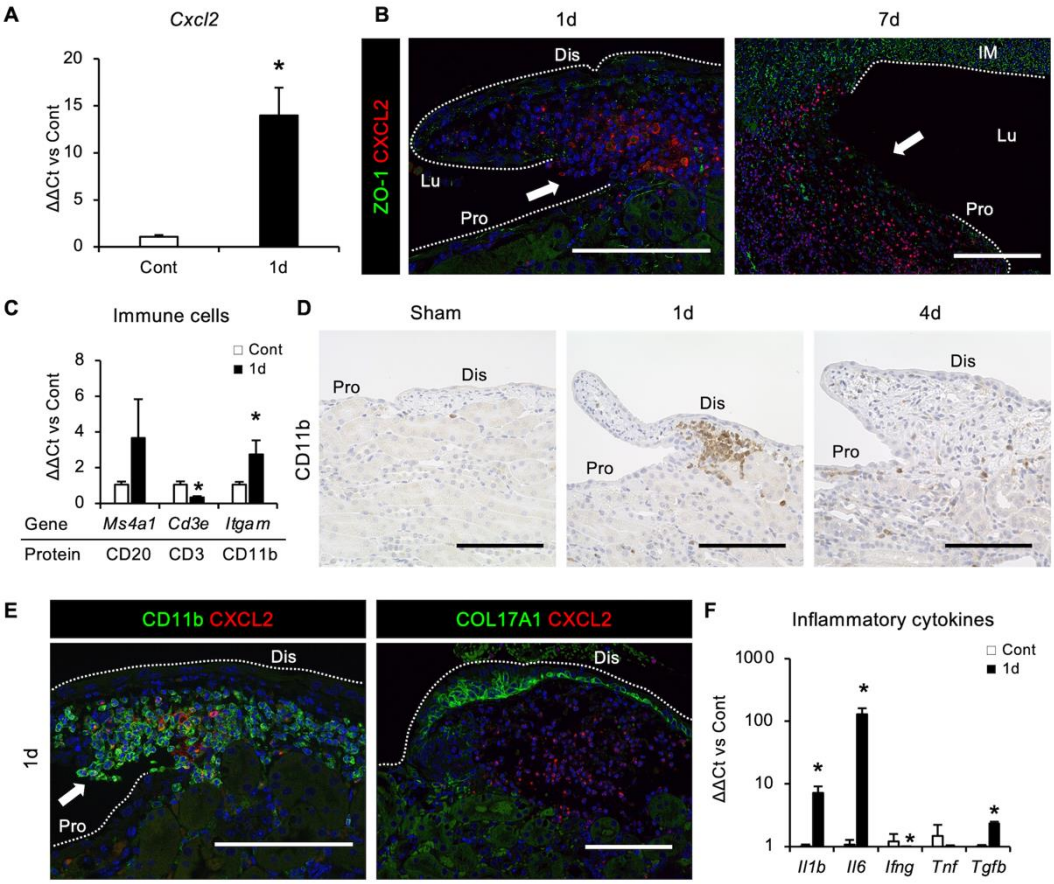
A
Cxcl2
ΔΔCt vs Cont
20
15
10
5
0
*
Cont
1d
B
1d
7d
ZO-1 CXCL2
Dis
Lu
Pro
IM
C
Immune cells
Cont
1d
ΔΔCt vs Cont
8
6
4
2
0
*
*
Gene
Ms4a1
Cd3e
Itgam
Protein
CD20
CD3
CD11b
D
Sham
1d
4d
CD11b
Pro
Dis
E
CD11b CXCL2
COL17A1 CXCL2
1d
Dis
Pro
F
Inflammatory cytokines
Cont
1d
ΔΔCt vs Cont
1000
100
10
1
*
*
*
*
Il1b
Il6
Ifng
Tnf
Tgfb

Fig. 3-8. Activation of CXCL2$^+$ CD11b$^+$ cells in the murine renal pelvis 1d after UUO

(A) Relative mRNA expression of *Cxcl2* in isolated renal pelvis 1d after UUO. The expression levels are normalized to the values of *Actb* and those of collateral control. Each bar represents mean ± SE (n = 4–5). * indicates a significant difference compared with collateral control (*P < 0.05). Mann-Whitney *U*-test, qPCR analysis. **(B)** Localization of ZO-1 (green) and CXCL2 (red) in renal pelvis. CXCL2$^+$ staining is observed beneath ZO-1 deficient urothelium (arrows) at the junction between proximal and the distal renal pelvis urothelium 1d after UUO or proximal urothelium at 7d after UUO. The nucleus is stained using Hoechst (blue). White dotted lines represent the apical side of urothelium. IF. Bars = 100 μm. **(C)** Relative mRNA expression of immune cell genes in renal pelvis 1d after UUO. The expression levels are normalized to the values of *Actb* and those of the collateral control. Each bar represents mean ± SE (n = 4–5). * indicates a significant difference compared to the collateral control (*P < 0.05). Mann-Whitney *U*-test, qPCR analysis. **(D)** Localization of CD11b$^+$ cells in renal pelvis. There are few CD11b$^+$ cells in the Sham, and the number is increasing from 1d after UUO, and decreasing 4d after UUO. IF. Bars = 100 μm. **(E)** Localization of CXCL2 (red) with CD11b or COL17A1 (green) in the renal pelvis. CXCL2$^+$ staining is observed in CD11b$^+$ cells beneath the COL17A1$^+$ urothelium 1d after UUO. The nucleus is stained using Hoechst (blue). White dotted lines indicate the apical side of urothelium. The arrow indicates deciduation of urothelial cells. IF. Bars = 100 μm. **(F)** Relative mRNA expression of inflammatory cytokines measured in isolated renal pelvis 1d after UUO. The expression levels are normalized to the values of *Actb* and those of collateral control. Each bar represents the mean ± SE (n = 4–5). * indicates a significant difference compared with collateral control (*P < 0.05). Mann-Whitney *U*-test, qPCR analysis. Cont: collateral control, Pro: proximal renal pelvis urothelium, Dis: distal renal pelvis urothelium, Lu: renal pelvis lumen, IM: inner medulla.

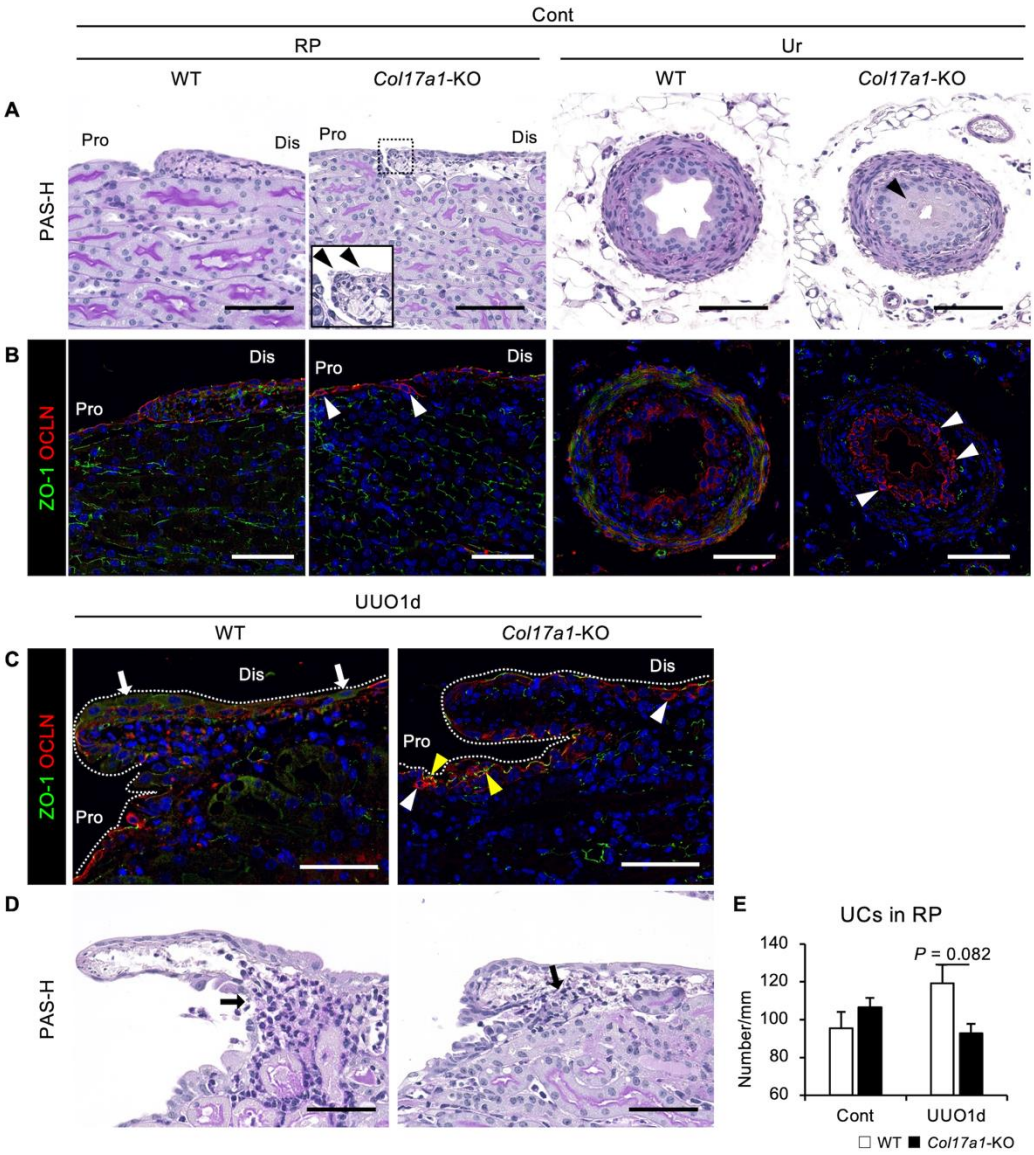
Cont
RP
Ur
WT
Col17a1-KO
WT
Col17a1-KO
A
PAS-H
Pro
Dis
Pro
Dis
B
ZO-1 OCLN
Pro
Dis
Pro
Dis
UUO1d
WT
Col17a1-KO
C
ZO-1 OCLN
Dis
Pro
Dis
Pro
D
PAS-H
E
UCs in RP
P = 0.082
Number/mm
140
120
100
80
60
Cont
UUO1d
WT
Col17a1-KO

Fig. 3-9. Urothelium morphology in *Col17a1*-KO mice with or without UUO

(A) Representative images of the renal pelvis and ureter from the *Col17a1-KO* collateral control compared to those of the WT mice. In the renal pelvis of *Col17a1*-KO mice, superficial cells with pale cytoplasm are found. In the ureter, mucosal folds are observed in the WT mice, whereas these are not clear in the *Col17a1*-KO ureter, in which swelling umbrella cells are observed (arrowhead). PAS-H. Bars = 50 μm. **(B)** Localization of ZO-1 (green) with OCLN (red) in the renal pelvis and ureter of the *Col17a1*-KO collateral control. In *Col17a1*-KO mice, $OCLN^+$ staining is observed in urothelial cells localizing at the basal side of the urothelium, especially in the ureter (arrows). The nucleus is stained using Hoechst (blue). White dotted lines represent the apical side of urothelium. IF. Bars = 50 μm. **(C)** Localization of ZO-1 (green) with OCLN (red) in renal pelvis 1d after UUO. $ZO\text{-}1^+$ and $OCLN^+$ staining is observed at the apical portion of renal pelvis urothelium in *Col17a1*-KO mice, while the reaction is defect in WT mice (arrows). In *Col17a1*-KO mice, $ZO\text{-}1^+$ staining shows irregularly upregulation pattern (yellow arrowheads), and $OCLN^+$ reaction is found in basal urothelial cells as well (white arrowheads). The nucleus is stained using Hoechst (blue). White dotted lines represent the apical side of urothelium. IF. Bars = 50 μm. **(D)** Representative images of renal pelvis from *Col17a1*-KO and the WT mice at 1d after UUO. Deciduation of urothelial cells is equally observed in the WT and *Col17a1*-KO kidneys. Cell infiltration is more frequently observed in *Col17a1*-KO mice, compared to the WT renal pelvis. PAS-H. Bars = 50 μm. **(E)** The number of urothelial cells in the distal renal pelvis. Each bar represents mean ± SE (n = 5–6). Mann-Whitney *U*-test. Cont: collateral control, RP: renal pelvis, Ur: ureter, WT: wild-type, KO: knockout, PAS-H: Periodic acid Schiff-hematoxylin staining, Pro: proximal renal pelvis urothelium, Dis: distal renal pelvis urothelium, UUO: unilateral ureteral obstruction, UC: urothelial cell.

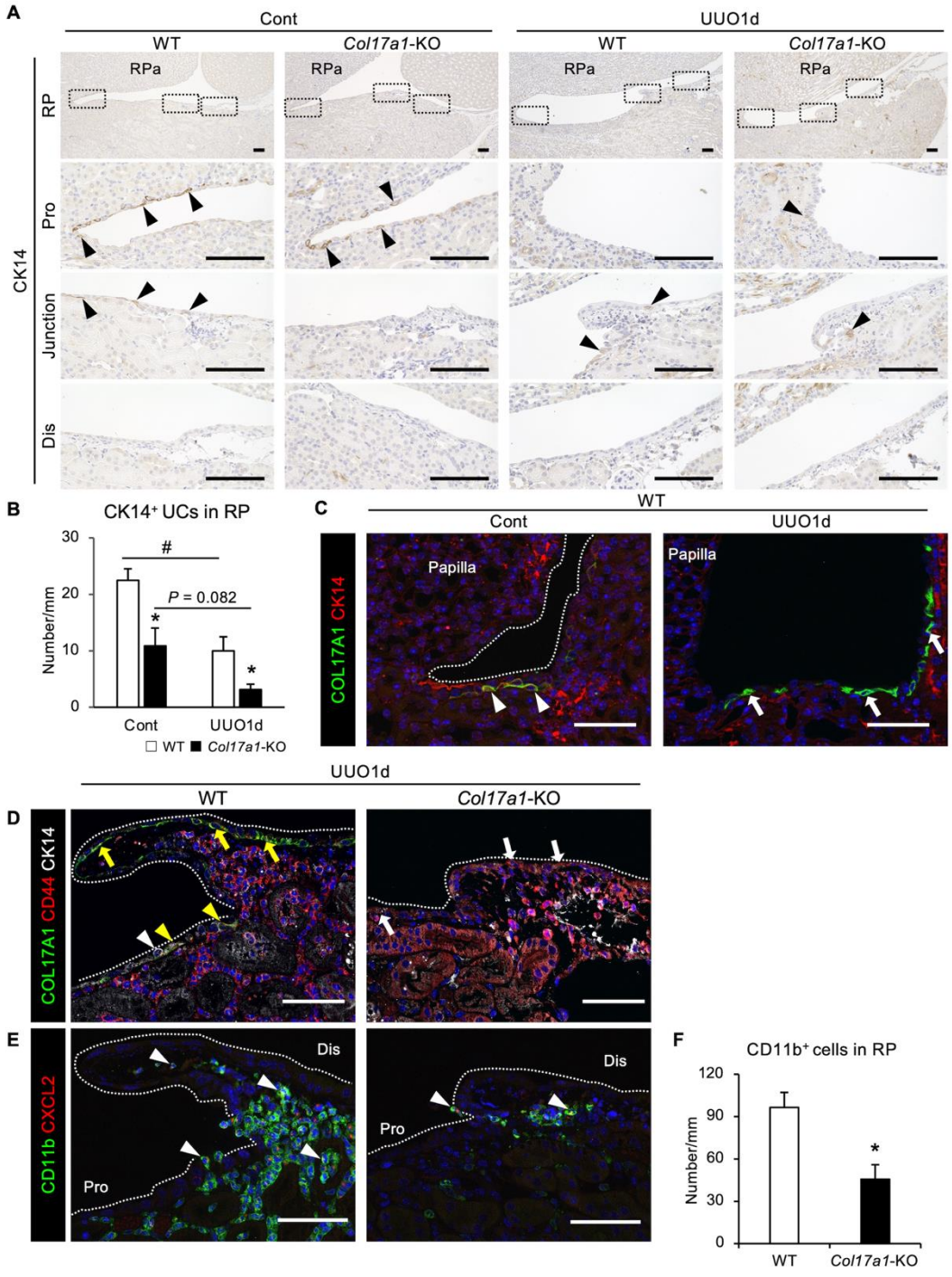
A
Cont
UUO1d
WT
Col17a1-KO
WT
Col17a1-KO
RPa
RPa
RPa
RPa
CK14
RP
Pro
Junction
Dis
B
CK14⁺ UCs in RP
Number/mm
30
20
10
0
#
P = 0.082
*
*
Cont
UUO1d
WT
Col17a1-KO
C
WT
Cont
UUO1d
COL17A1 CK14
Papilla
Papilla
UUO1d
D
WT
Col17a1-KO
COL17A1 CD44 CK14
E
CD11b CXCL2
Dis
Pro
Dis
Pro
F
CD11b⁺ cells in RP
Number/mm
120
90
60
30
0
*
WT
Col17a1-KO

Fig. 3-10. Altered pathology of the renal pelvis urothelium in *Col17a1*-KO mice 1d after UUO

(A) Localization of CK14 in the renal pelvis from *Col17a1*-KO mice 1d after UUO compared with the WT mice and collateral control. In the collateral control renal pelvis, the number of $CK14^+$ urothelial cells (arrowheads) is comparable in the proximal part between the WT and *Col17a1*-KO mice, whereas the positive cell number is few in the junction and distal parts of *Col17a1*-KO mice compared to the WT mice. However, in both the WT and *Col17a1*-KO renal pelvis 1d after UUO, $CK14^+$ cell number is decreasing compared to that of the collateral control. Bars = 100 μm. **(B)** The number of $CK14^+$ urothelial cells in the distal renal pelvis. Each bar represents mean ± SE (n = 5–6). * indicates a significant difference compared with collateral control (*$P < 0.05$). # indicates a significant difference between the collateral control and UUO1d. IHC. Mann-Whitney *U*-test. **(C)** Localization of COL17A1 (green) with CK14 (red) in the WT renal pelvis 1d after UUO compared with the collateral control. $COL17A1^+$ $CK14^+$ urothelial cells (arrowheads) are observed in the proximal renal pelvis of the collateral control kidney, whereas $COL17A1^+$ $CK14^-$ urothelial cells (arrows) are dominant in that 1d after UUO. IF. Bars = 50 μm. **(D)** Localization of COL17A1 (green) with CD44 (red) and CK14 (white) in renal pelvis 1d after UUO. $COL17A1^+$ urothelium co-localizing with CD44 (yellow arrows) partially forms multiple layers and co-expresses with CK14 (yellow arrowheads) in the WT mice, whereas $COL17A1^-$ $CD44^-$ $CK14^+$ urothelial cells are observed to be less (white arrowhead). $CD44^+$ mono- or bi-layer of urothelium are observed in *Col17a1*-KO mice. The nucleus is stained using Hoechst (blue). White dotted lines represent the apical side of urothelium. IF. Bars = 100 μm. **(E)** Localization of CD11b (green) with CXCL2 (red) in renal pelvis 1d after UUO. $CD11b^+$ $CXCL2^+$ cells (arrowheads) are abundantly observed at the junction between the proximal and distal renal pelvis urothelium in the WT mice, whereas $CD11b^+$ cells are scattered under the renal pelvis urothelium in *Col17a1*-KO mice and few co-express CXCL2. The nucleus is stained using Hoechst (blue). White dotted lines represent the apical side of urothelium. IF. Bars = 50 μm. **(F)** The number of $CD11b^+$ cells under distal renal pelvis urothelium 1d after UUO. Each bar represents mean ± SE (n = 5–6). * indicates a significant difference compared with collateral control (*$P < 0.05$). # indicates a significant difference between collateral control and UUO1d. Mann-Whitney *U*-test. Cont: collateral control, WT: wild-type, KO: knockout, UUO: unilateral ureteral obstruction, RP: renal pelvis, Pro: proximal renal pelvis urothelium, Dis: distal renal pelvis urothelium, RPa: renal papilla, UC: urothelial cell.

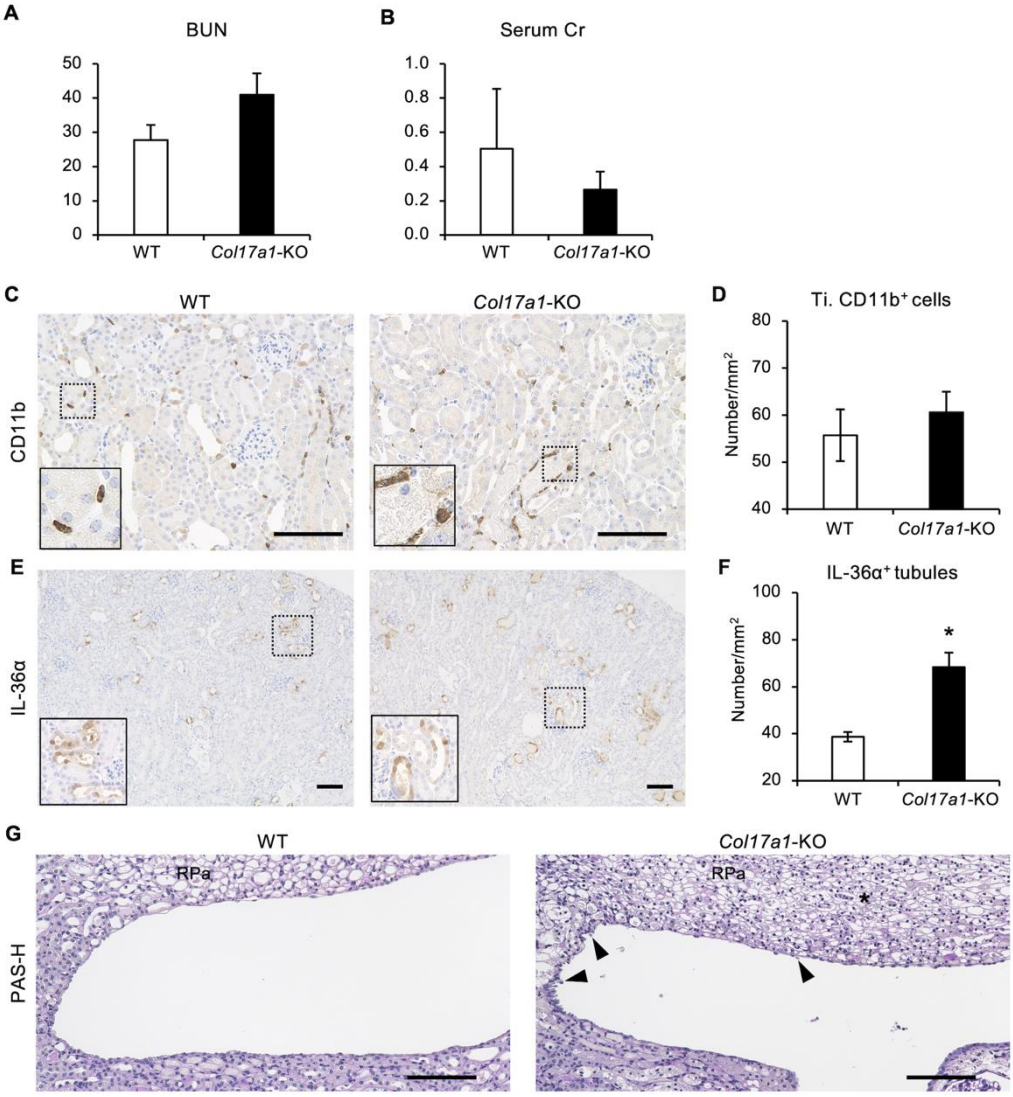

Fig. 3-11. Deteriorated renal histopathology in *Col17a1*-KO mice 1d after UUO

(A and B) The level of BUN (panel A) and serum Cr (panel B). Each bar represents mean ± SE (n = 5, 6). **(C)** Localization of CD11b in kidneys. The number of $CD11b^+$ cells are comparable between the WT and *Col17a1*-KO mice. IHC. Bars = 100 μm. **(D)** The number of $CD11b^+$ cells in tubulointerstitium. Each bar represents mean ± SE (n = 4 –5). **(E)** Localization of IL-36α in kidneys. $IL\text{-}36\alpha^+$ injured renal tubules are more abundant in the *Col17a1*-KO mice compared to those observed in the WT mice. IHC. Bars = 100 μm. **(F)** The number of $IL\text{-}36\alpha^+$ renal tubules in the cortex. Each bar represents mean ± SE (n = 4–5). * indicates a significant difference compared to the WT (*$P < 0.05$). Mann-Whitney *U*-test. **(G)** Representative images of kidneys from the *Col17a1*-KO and WT mice at 1d after UUO. Necrosis of renal papilla (asterisk) with urothelial deciduation (arrowheads) is more frequently observed in the *Col17a1*-KO mice compared to the WT kidneys. PAS-H. Bars = 100 μm. BUN: blood urea nitrogen, Cr: creatinine, WT: wild-type, KO: knockout, Ti: tubulointerstitium, PAS-H: Periodic acid Schiff-hematoxylin staining, RPa: renal papilla.

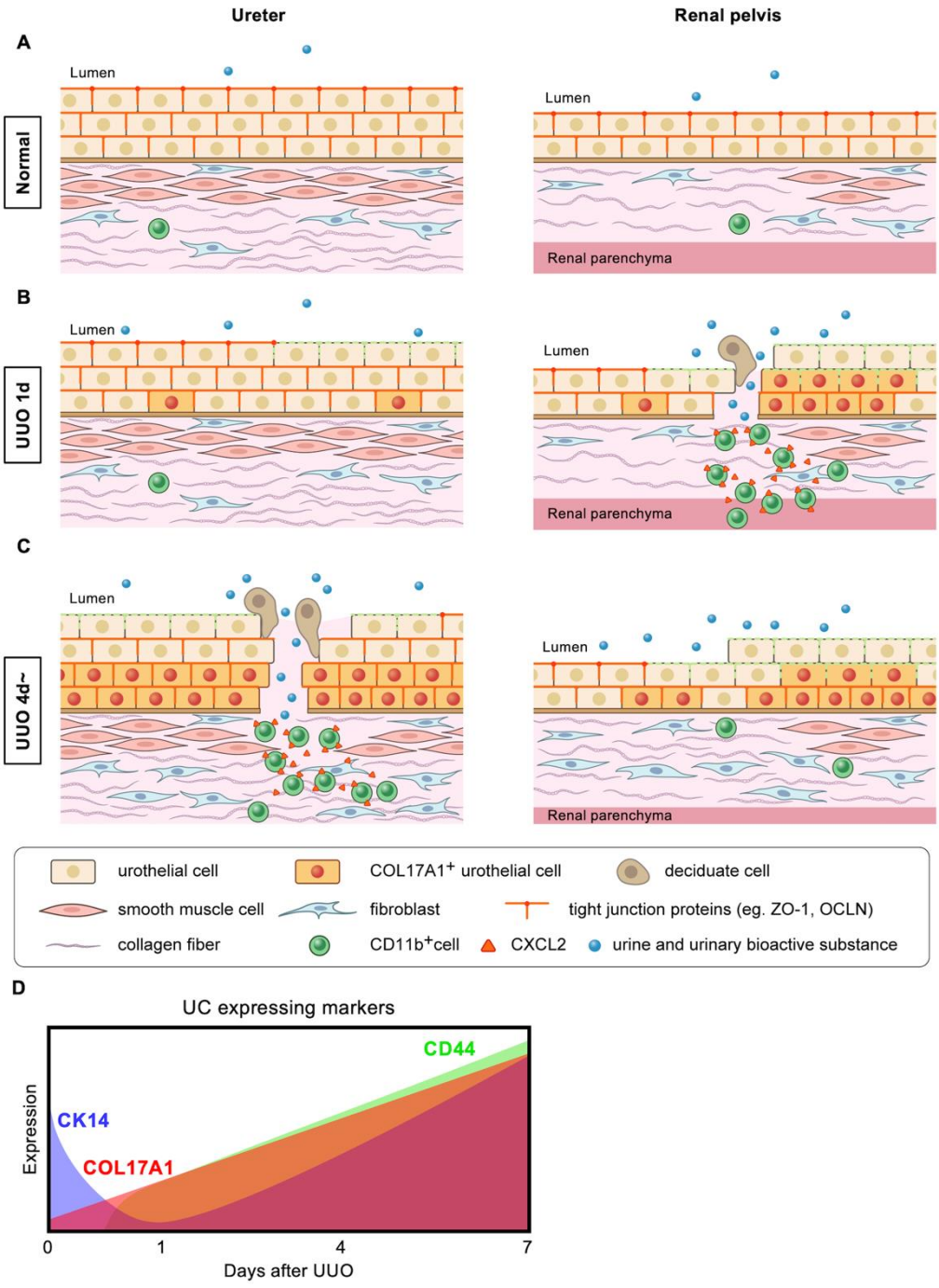
Ureter
Renal pelvis
A
Normal
Lumen
Renal parenchyma
B
UUO 1d
C
UUO 4d~
urothelial cell
COL17A1+ urothelial cell
deciduate cell
smooth muscle cell
fibroblast
tight junction proteins (eg. ZO-1, OCLN)
collagen fiber
CD11b+cell
CXCL2
urine and urinary bioactive substance
D
UC expressing markers
CD44
CK14
COL17A1
Expression
0
1
4
7
Days after UUO

Fig. 3-12. Schematic illustration of the hypothetic mechanism through which obstructive uropathy induces urothelium disruption and COL17A1 expression

(A) Normal ureters and renal pelvis consist of urothelial cells, fibroblasts, and smooth muscle cells. Renal pelvis are divided into the distal renal pelvis connecting the ureter to the smooth muscle layer and proximal renal pelvis connecting kidneys without smooth muscle layer. Under the urothelium, there are few $CD11b^+$ immune cells. **(B)** In the ureters on day 1 after UUO, there are some $COL17A1^+$ urothelial cells but no urothelial cell deciduation. In the renal pelvis, urothelial cell deciduation and a subsequent urine leakage occurred with partial defects in the TJPs at the junction between the distal and proximal renal pelvis urothelium. urothelial cells from the junction to the distal urothelium express COL17A1, and $CD11b^+$ cells migrate to connective tissue covered by $COL17A1^+$ proliferating urothelial cells and beneath UEB disruption, which also express CXCL2. **(C)** Collagen fibers increase in renal pelvis from 4d after UUO onwards instead of urothelial cell deciduation and $CD11b^+$ cell migration, even though there are abundant $COL17A1^+$ urothelial cells. The ureter presents similar histopathology to the renal pelvis 1d after UUO. **(D)** Expression manner of urothelial cell markers at the basal side of the renal pelvis urothelium. CK14 (blue) is expressed in the normal renal pelvis, and partially co-expressed with COL17A1 (red). At 1d after UUO, COL17A1 upregulation followed by CD44 (green) induction occurred, instead of a decrease in CK14. From 4d onward, $CK14^+$ $COL17A1^+$ $CD44^+$ urothelial cells are increasing and $CK14^-$ $COL17A1^-$ $CD44^+$ urothelial cells appear.

Conclusion

The clinical cases of kidney disease, in particular CKD, are increasing in dogs, cats, and human. Pathophysiology of kidney diseases are divided into pre-, intrinsic-, and post-renal injuries, such as hypertension, ischemia, immune abnormality, and urinary obstruction, according to their causes. The urinary organs are lined by epithelial cells to maintain the UEB bordering urine and tissue at healthy status. Importantly, recent studies emphasizes the pathological contribution of UEB disruption; the injuries of renal epithelial cells and urothelial cells in CKD are associated with overexpression of the novel pathological molecules, IL-36α and COL17A1, respectively. Because of the characteristic of the urinary system, the epithelial cell-expressing molecules can be targets to develop the diagnosis method using urine and the therapeutic strategy. Hence, the author analyzed the pathological significance of these candidate molecules in the kidney and urinary tract disorders by using mouse models and clinical specimens.

In Chapter 1, IL-36R and its ligands belonging to IL-1 family were focused on as renal epithelial cell-injury mediated molecules, and autoimmune disease prone-MRL/lpr mice were pathologically analyzed as spontaneous nephritis model. IL-36R ligands composed of agonists (IL-36α, IL-36β, IL-36γ) and antagonists (IL-36Ra, IL-38), and those expression manners were divided into constitutive and induced. Constitutively, IL-36Ra and IL-36γ were expressed in smooth muscle cells and sympathetic axons of kidneys, respectively. However, at the late stage of nephritis, IL-36α was induced in injured distal tubular epithelial cells and $CD44^{+}$-activated parietal epithelial cells. Further, kidneys with nephritis showed IL-36Ra localization in tubular epithelial cells and parietal epithelial cells, in addition to that of IL-36β and IL-38 in interstitial plasma cells. Of note, IL-36α and IL-38 expression level was positively correlated with the nephritis severity. IL-36R gene was ubiquitously expressed in the murine kidneys, and was induced in the injured epithelium with the disease progression, leading to upregulated IL-36R downstream candidates, including NF-κB- or MAPK-pathway organizing molecules. Importantly, IL-36R gene in cat kidneys was expressed in distal tubular and parietal epithelial cells, in accordance with IL-36R and IL-36α localization in the murine kidneys.

In Chapter 2, to further investigate IL-36R signaling in the nephritis, the author analyzed MRL/lpr with IL-36R-KO, compared to WT mice. In both genotypes, immune abnormalities and renal functions as well as IL-36R expression in kidneys were comparable. However, glomerular lesions were significantly ameliorated in both sexes of IL-36R-KO mice compared to WT mice, and tubulointerstitial fibrosis was less in female IL-36R-KO mice than in WT mice. Both genotypes presented IL-36α^{+} nuclei in renal epithelial cells co-localized with Ac-lysine and GCN5 histone acetyltransferase, suggesting IL-36α signaling in the nuclei via IL-36R independent pathway. Thus, a balance of IL-36R agonists and antagonists is maintained in the healthy kidneys, whereas renal inflammation induce an IL-36α-dominant imbalance, contributing to the

progression of renal pathology with UEB disruption in both glomeruli and renal tubules, in IL-36R dependent and independent pathways.

In Chapter 3, the author focused on COL17A1 as an urothelial cell-injury mediated molecule. COL17A1 is known as an epidermal hemidesmosome component but ectopically induced in the ureters of obstructive uropathy-prone mammals as humans and cats, underlining as a potential of novel pathological molecule. The murine obstructive uropathy model also induced COL17A1 in urothelial cells of renal pelvis and ureters. Pathological analysis revealed that COL17A1 induction associated with the urothelium integrity as cell adhesion, differentiation, and proliferation and positively correlated with tubulointerstitial lesion severities. The renal pelvis, especially where smooth muscle layer from the ureter was interrupted, was sensitive to urothelial deciduation and COL17A1 induction, indicating the UEB disruption; urine leaked into the renal pelvis parenchyma at this area. Cultured immune cells stimulated by urine induced CXCL2, which was also produced by $CD11b^+$ cells following COL17A1 stimulation. Importantly, $CXCL2^+$ $CD11b^+$ cells infiltrated the urothelium-disrupted area, whereas it was suppressed in *Col17a1*-KO mice. Thus, COL17A1 maintains urothelium integrity and activates local immune response during obstructive uropathy.

The present study by using each model mouse demonstrated that IL-36α-dominant expression in injured renal epithelial cells are associated with glomerular lesions as well as tubulointerstitial lesions in spontaneous nephritis, and that COL17A1 expression in urothelial cells contributes to urothelium regeneration with local inflammation in obstructive uropathy. The injured epithelial cell-associated molecules in the urinary system induce UEB disruption, while they are potential for the treatment and urinalysis-dependent diagnosis. Particularly, both localization of IL-36R gene in renal epithelial cells and COL17A1 in urothelial cells of mice were coincide with those in cats and/or humans. These findings suggest that molecular pathology in renal epithelium and urothelium dependent on IL-36R ligands and COL17A1is common among several animals, leading to the development of veterinary medicine concurrently with human medicine. Therefore, this study provides novel candidates for the targets of zoobiquity, an approach to devise a strategy for common diseases among all animals including humans, in urinary system disorders.

Conclusion in Japanese

動物の泌尿器異常を導く上皮障害関連分子の研究

北海道大学大学院獣医学院
基礎獣医科学講座　解剖学教室
難波貴志

慢性腎臓病（CKD）はヒトの主要な泌尿器疾患であり、イヌやネコにおいてもその症例数が増加している。腎臓の病態はその要因から腎前性、腎性、腎後性に区分され、高血圧や虚血、免疫異常、尿路障害等が各病態を導く。腎臓から尿道に至る尿路では、各管状臓器構造を内張する上皮が尿とその実質組織を画し、尿―上皮バリア（UEB）を形成する。これまでの研究において、泌尿器の病態形成機序の一つとして、UEB の崩壊とそれに付随する上皮病態関連分子の発現異常が報告されている。その中でも、IL-36α および 17 型コラーゲン A1（COL17A1）の発現は、それぞれ障害された腎上皮細胞および尿路上皮細胞で増加する。これら泌尿器に発現する上皮病態関連分子は、治療標的や尿中の病態診断マーカーの候補として重要である。そこで本研究では、疾患モデルマウスと臨床検体を用いて、両分子を介した腎臓および尿路の病態形成機構について精査し、泌尿器疾患領域における獣医療および医療の発展に貢献することを目的とした。

第一章では、腎上皮細胞障害関連分子として IL-36 受容体（IL-36R）およびそのリガンド群（IL-36 群）に着目した。IL-36 群は IL-1 ファミリーに属し、3 つの作動分子（IL-36α, IL-36β, IL-36γ）と 2 つの拮抗分子（IL-36Ra, IL-38）から成る。自己免疫性腎炎モデルマウス MRL/MpJ-*Fas*$^{lpr/lpr}$（MRL/lpr）を用いた解析によって、IL-36 群はその腎臓内発現様式から、恒常型と誘導型に区別された。IL-36Ra は平滑筋、IL-36γ は交感神経において恒常的に発現していた一方、腎炎の進行に伴い、IL-36α の発現は障害された遠位尿細管上皮細胞や CD44^{+}活性化型の糸球体包外壁の上皮細胞に誘導された。さらに腎炎マウスでは、IL-36Ra は腎上皮細胞で、IL-36β と IL-38 は形質細胞で発現した。本分子群において、特に IL-36α および IL-38 の腎臓内発現定量値が腎炎スコアと正に相関した。また、IL-36R は腎臓内で遍在性に局在する一方、腎炎進行に伴い障害された腎上皮細胞で発現誘導され、その下流にあたる NF-κB や MAPK 経路関連分子群の腎臓内遺伝子発現が増加した。加えて、ネコ腎組織を用いた解析において、IL-36R の mRNA が遠位尿細管や糸球体包外壁の上皮細胞に検出され、これはマウス IL-36α および IL-36R の局在と一致していたため、IL-36R シグナルを介した腎病態形成機構は動物種に共通する可能性が示唆された。

第二章では、IL-36R シグナルを介した腎病態形成機構のさらなる解析のため、IL-36R を欠損した MRL/lpr マウス（IL-36R-KO）を用いて、その腎表現型を野生型マウスと比較した。両群間において、自己免疫異常や腎機能指標、IL-36 群の腎内発現量は同等だった。一方、腎病理解析において、雌雄 IL-36R-KO の糸球体病理の重篤度および雌の尿細管間質の線維化は、野生型と比べ軽度だった。また IL-36R の有無に関わらず、IL-36α は腎上皮細胞の細胞質と核に局在し、

その一部はアセチル化リジンやヒストンアセチル化酵素 GCN5 と共局在を示した。これにより、IL-36R を介さない核内 IL-36α シグナルの存在が示唆された。以上、腎臓に発現する IL-36 群は、その脈管神経系で機能する恒常発現型と、障害を受けた腎上皮細胞や浸潤細胞に発現する誘導型に大別され、その局在から前者は腎恒常性の調節に、後者は炎症性病態の形成に関与すると考えられた。特に、腎臓における IL-36α の過剰発現は、IL-36R 依存的および非依存的な経路を介して、糸球体および尿細管における UEB 崩壊に寄与すると考えられた。

第三章では、尿路上皮細胞障害関連分子として COL17A1 に着目した。COL17A1 は表皮のヘミデスモソーム構成分子として生理的な機能を担う。一方、本研究では、COL17A1 が閉塞性尿路疾患を呈したヒトやネコの尿管尿路上皮細胞で異所性に発現することを見出した。閉塞性尿路疾患モデルマウスにおいても、腎盤および尿管の尿路上皮細胞で COL17A1 発現が検出された。さらに、尿路上皮細胞関連分子群との共局在解析により、COL17A1 は尿路上皮細胞の細胞接着、分化や増殖に関与することが明らかとなり、COL17A1 発現の定量値は尿細管間質の病理指標と正に相関した。本モデルマウスの腎盤を組織学的に精査したところ、特に尿管から連続する平滑筋層が消失する部位において、尿路上皮細胞の脱落と COL17A1 の発現誘導が顕著だった。さらに、UEB 崩壊によってその下層の腎盤実質に尿が浸潤した。また、免疫細胞培養系を尿で刺激すると、ケモカイン群、特に *Cxcl2* 遺伝子の発現が増加し、COL17A1 で刺激した $CD11b^+$細胞においてもその発現は上昇した。また、UEB 崩壊部位では $CXCL2^+CD11b^+$細胞が観察された一方、*Col17a1*-KO マウスではその浸潤が軽度だった。以上、尿路閉塞病態において、COL17A1 は尿路上皮細胞の増殖等の病態応答に関与する一方、炎症細胞の局所誘導にも寄与すると考えられた。

結論として、各泌尿器疾患モデルマウスを用いた解析により、本研究は 1）腎炎の進行に伴い障害された腎上皮細胞では、IL-36α 優位な発現変化が糸球体および尿細管間質病変の形成に関与すること、2）閉塞性尿路疾患において、COL17A1 が尿路上皮細胞で異所性に発現し、尿路上皮の再構築と局所の炎症に関与することを示した。これら泌尿器における上皮障害関連分子は UEB 崩壊を導く一方、新たな治療標的および尿中診断マーカーになり得る。近年、ヒトを含む複数の生物種に共通する疾患に着目し、生物種横断的にその病態解明や治療法・診断法を考察する学問は “汎動物学” と称される。マウス、ネコ、ヒトにおける IL-36R と COL17A1 の泌尿器内発現動態には共通性がみられるため、これらの結果を汎動物学的視点から考察することは、獣医療さらにはヒト医療への応用に向けて意義深い。以上、本研究は動物ならびにヒトの泌尿器疾患に対する診断および治療戦略の発展に向けて、新たな知見を提供した。

Acknowledgments

I would like to thank and my appreciation to those who have encouraged me during years of graduate studies. First and foremost, I would like to express my sincere gratitude towards my supervisor, Professor Yasuhiro Kon for his support, advice, and guidance during this project. I am extremely grateful to my supervisors, Associate Professor Osamu Ichii for his patient guidance, invaluable advice and technical support. I sincerely appreciate Professor Mitsuyoshi Takiguchi and Professor Takashi Kimura for time taken to provide advice, critical comments and assistance in completing the thesis. I would like to thank Associate Professor Teppei Nakamura and Dr. Yuki Otani for their great support and advice throughout my university days. I deeply appreciate Professor Tadashi Okamura, Department of Laboratory Animal Medicine, Research Institute, National Center for Global Health and Medicine for establishing IL-36R-KO mice, and Associate Professor Ken Natsuga, Department of Dermatology, Faculty of Medicine and Graduate School of Medicine, Hokkaido University for providing *Col17a1*-KO mice. I am also grateful to thank all members in Laboratory of Anatomy and my friends in our faculty for their encouragement, support, and great times. Finally, I would like to express my sincere gratitude to all animals supporting this research.

References

1) Acharya P, Beckel J, Ruiz WG, Wang E, Rojas R, Birder L, Apodaca G. Distribution of the tight junction proteins ZO-1, occludin, and claudin-4, -8, and -12 in bladder epithelium. Am J Physiol Renal Physiol 287, F305-F318, 2004.
2) Agha EE, Schwind F, Ruppert C, Günther A, Bellusci S, Schermuly RT, Kosanovic D. Is the fibroblast growth factor signaling pathway a victim of receptor tyrosine kinase inhibition in pulmonary parenchymal and vascular remodeling? Am J Physiol Lung Cell Mol Physiol 315, L248-L252, 2018.
3) Ahmadizadeh M, Echt R, Chao-Hen K, Hook JB. Sex and strain differences in mouse kidney: Bowman's capsule morphology and susceptibility to chloroform. Toxicol Lett 20, 161-171, 1984.
4) Ahsan F, Maertzdorf J, Guhlich-Bornhof U, Kaufmann SHE, Moura-Alves P. IL-36/LXR axis modulates cholesterol metabolism and immune defense to Mycobacterium tuberculosis. Sci Rep 8, 1520, 2018.
5) Al-Alwan LA, Chang Y, Mogas A, Halayko AJ, Baglole CJ, Martin JG, Rousseau S, Eidelman DH, Hamid Q. Differential roles of CXCL2 and CXCL3 and their receptors in regulating normal and asthmatic airway smooth muscle cell migration. J Immunol 191, 2731-2741, 2013.
6) Almaani S, Meara A, Rovin BH. Update on lupus nephritis. Clin J Am Soc Nephrol 12, 825-835, 2017.
7) Amdur RL, Chawla LS, Amodeo S, Kimmel PL, Palant CE. Outcomes following diagnosis of acute renal failure in U.S. veterans: focus on acute tubular necrosis. Kidney Int 76, 1089-1097, 2009.
8) Andrews BS, Eisenberg RA, Theofilopoulos AN, Izui S, Wilson CB, Meconahey PJ, Murphy ED, Roths JB, Dixon FJ. Spontaneous murine lupus-like syndromes. Clinical and immunopathological manifestations in several strains. J Exp Med 148, 1198-1215, 1978.
9) Bartfai T, Schultzberg M. Cytokines in neuronal cell types. Neurochem Int 22, 435-444, 1993.
10) Bensen JT, Dawson PA, Mychaleckyj JC, Bowden DW. Identification of a novel human cytokine gene in the interleukin gene cluster on chromosome 2q12-14. J Interferon Cytokine Res 21, 899-904, 2001.
11) Berger K, Moeller MJ. Mechanisms of epithelial repair and regeneration after acute kidney injury. Semin Nephrol 34, 394-403, 2014.
12) Bhat HK, Hacker HJ, Bannasch P, Thompson EA, Liehr JG. Localization of estrogen receptors in interstitial cells of hamster kidney and in estradiol-induced renal tumors as

evidence of the mesenchymal origin of this neoplasm. Cancer Res 53, 5447-5451, 1993.

13) Bikbov B, Bikbov B, Purcell CA, Levey AS, Smith M, Abdoli A, Abebe M, Adebayo OM, Afarideh M, Agarwal SK, Agudelo-Botero M, Ahmadian E, Al-Aly Z, Alipour V, Almasi-Hashiani A, Al-Raddadi RM, Alvis-Guzman N, Amini S, Andrei T, Andrei CL, Andualem Z, Anjomshoa M, Arabloo J, Ashagre AF, Asmelash D, Ataro Z, Atout MMW, Ayanore MA, Badawi A, Bakhtiari A, Ballew SH, Balouchi A, Banach M, Barquera S, Basu S, Bayih MT, Bedi N, Bello AK, Bensenor IM, Bijani A, Boloor A, Borzì AM, Cámera LA, Carrero JJ, Carvalho F, Castro F, Catalá-López F, Chang AR, Chin KL, Chung SC, Cirillo M, Cousin E, Dandona L, Dandona R, Daryani A, Das Gupta R, Demeke FM, Demoz GT, Desta DM, Do HP, Duncan BB, Eftekhari A, Esteghamati A, Fatima SS, Fernandes JC, Fernandes E, Fischer F, Freitas M, Gad MM, Gebremeskel GG, Gebresillassie BM, Geta B, Ghafourifard M, Ghajar A, Ghith N, Gill PS, Ginawi IA, Gupta R, Hafezi-Nejad N, Haj-Mirzaian A, Haj-Mirzaian A, Hariyani N, Hasan M, Hasankhani M, Hasanzadeh A, Hassen HY, Hay SI, Heidari B, Herteliu C, Hoang CL, Hosseini M, Hostiuc M, Irvani SSN, Islam SMS, Jafari Balalami N, James SL, Jassal SK, Jha V, Jonas JB, Joukar F, Jozwiak JJ, Kabir A, Kahsay A, Kasaeian A, Kassa TD, Kassaye HG, Khader YS, Khalilov R, Khan EA, Khan MS, Khang YH, Kisa A, Kovesdy CP, Kuate Defo B, Kumar GA, Larsson AO, Lim LL, Lopez AD, Lotufo PA, Majeed A, Malekzadeh R, März W, Masaka A, Meheretu HAA, Miazgowski T, Mirica A, Mirrakhimov EM, Mithra P, Moazen B, Mohammad DK, Mohammadpourhodki R, Mohammed S, Mokdad AH, Morales L, Moreno Velasquez I, Mousavi SM, Mukhopadhyay S, Nachega JB, Nadkarni GN, Nansseu JR, Natarajan G, Nazari J, Neal B, Negoi RI, Nguyen CT, Nikbakhsh R, Noubiap JJ, Nowak C, Olagunju AT, Ortiz A, Owolabi MO, Palladino R, Pathak M, Poustchi H, Prakash S, Prasad N, Rafiei A, Raju SB, Ramezanzadeh K, Rawaf S, Rawaf DL, Rawal L, Reiner RC, Rezapour A, Ribeiro DC, Roever L, Rothenbacher D, Rwegerera GM, Saadatagah S, Safari S, Sahle BW, Salem H, Sanabria J, Santos IS, Sarveazad A, Sawhney M, Schaeffner E, Schmidt MI, Schutte AE, Sepanlou SG, Shaikh MA, Sharafi Z, Sharif M, Sharifi A, Silva DAS, Singh JA, Singh NP, Sisay MMM, Soheili A, Sutradhar I, Teklehaimanot BF, Tesfay B, Teshome GF, Thakur JS, Tonelli M, Tran KB, Tran BX, Tran Ngoc C, Ullah I, Valdez PR, Varughese S, Vos T, Vu LG, Waheed Y, Werdecker A, Wolde HF, Wondmieneh AB, Wulf Hanson S, Yamada T, Yeshaw Y, Yonemoto N, Yusefzadeh H, Zaidi Z, Zaki L, Zaman SB, Zamora N, Zarghi A, Zewdie KA, Ärnlöv J, Coresh J, Perico N, Remuzzi G, Murray CJL. Global, regional, and national burden of chronic kidney disease, 1990–2017: a systematic analysis for the global burden of disease study 2017. Lancet 395, 709-733, 2020.

14) Blumberg H, Dinh H, Dean C, Trueblood ES, Bailey K, Shows D, Bhagavathula N, Aslam MN, Varani J, Towne JE, Sims JE. IL-1RL2 and its ligands contribute to the cytokine network in psoriasis. J Immunol 185, 4354-4362, 2010.
15) Blumberg H, Dinh H, Trueblood ES, Pretorius J, Kugler D, Weng N, Kanaly ST, Towne JE, Willis CR, Kuechle MK, Sims JE, Peschon JJ. Opposing activities of two novel members of the IL-1 ligand family regulate skin inflammation. J Exp Med 204, 2603-2614, 2007.
16) Bohle A, Christ H, Grund KE, Mackensen S. The role of the interstitium of the renal cortex in renal disease. Contrib Nephrol 16, 109-114, 1979.
17) Born TL, Smith DE, Garka KE, Renshaw BR, Bertles JS, Sims JE. Identification and characterization of two members of a novel class of the interleukin-1 receptor (IL-1R) family: Delineation of a new class of IL-1R-related proteins based on signaling. J Biol Chem 275, 29946-29954, 2000.
18) Boutet MA, Bart G, Penhoat M, Amiaud J, Brulin B, Charrier C, Morel F, Lecron JC, Rolli-Derkinderen M, Bourreille A, Vigne S, Gabay C, Palmer G, Le Goff B, Blanchard F. Distinct expression of interleukin (IL)-36α, β and γ, their antagonist IL-36Ra and IL-38 in psoriasis, rheumatoid arthritis and Crohn's disease. Clin Exp Immunol 184, 159-173, 2016.
19) Bray F, Ferlay J, Soerjomataram I, Siegel RL, Torre LA, Jemal A. Global cancer statistics 2018: GLOBOCAN estimates of incidence and mortality worldwide for 36 cancers in 185 countries. CA Cancer J Clin 68, 394-424, 2018.
20) Buas MF, Vaughan TL. Epidemiology and risk factors for gastroesophageal junction tumors: understanding the rising incidence of this disease. Semin Radiat Oncol 23, 3-9, 2013.
21) Caielli S, Veiga DT, Balasubramanian P, Athale S, Domic B, Murat E, Banchereau R, Xu Z, Chandra M, Chung C-H, Walters L, Baisch J, Wright T, Punaro M, Nassi L, Stewart K, Fuller J, Ucar D, Ueno H, Zhou J, Banchereau J, Pascual V. A $CD4^+$ T cell population expanded in lupus blood provides B cell help through interleukin-10 and succinate. Nat Med 25, 75-81, 2018.
22) Cash H, Relle M, Menke J, Brochhausen C, Jones SA, Topley N, Galle PR, Schwarting A. Interleukin 6 (IL-6) deficiency delays lupus nephritis in mrl-faslpr mice: the IL-6 pathway as a new therapeutic target in treatment of autoimmune kidney disease in systemic lupus erythematosus. J Rheumatol 37, 60-70, 2010.
23) Cayrol C, Girard JP. Interleukin-33 (IL-33): A nuclear cytokine from the IL-1 family. Immunol Rev 281, 154-168, 2018.
24) Chang A, Henderson SG, Brandt D, Liu N, Guttikonda R, Hsieh C, Kaverina N, Utset

TO, Meehan SM, Quigg RJ, Meffre E, Clark MR. In situ B cell-mediated immune responses and tubulointerstitial inflammation in human lupus nephritis. J Immunol 186, 1849-1860, 2011.

25) Chen TK, Knicely DH, Grams ME. Chronic kidney disease diagnosis and management: A review. JAMA 322, 1294-1304, 2019.

26) Chen WJ, Yu X, Yuan XR, Chen BJ, Cai N, Zeng S, Sun YS, Li HW. The Role of IL-36 in the pathophysiological processes of autoimmune diseases. Front Pharmacol 12, 2643, 2021.

27) Cheng X, Lai H, Luo W, Zhang M, Miao J, Song W, Xing S, Wang J, Gao WQ. Single-cell analysis reveals urothelial cell heterogeneity and regenerative cues following cyclophosphamide-induced bladder injury. Cell Death Dis 12, 446, 2021.

28) Chi H-H, Hua K-F, Lin Y-C, Chu C-L, Hsieh C-Y, Hsu Y-J, Ka S-M, Tsai Y-L, Liu F-C, Chen A. IL-36 signaling facilitates activation of the NLRP3 inflammasome and IL-23/IL-17 axis in renal inflammation and fibrosis. J Am Soc Nephrol 28, 2022-2037, 2017.

29) Chu M, Tam LS, Zhu J, Jiao D, Liu DH, Cai Z, Dong J, Kai Lam CW, Wong CK. In vivo anti-inflammatory activities of novel cytokine IL-38 in Murphy Roths Large (MRL)/lpr mice. Immunobiology 222, 483-493, 2017.

30) Chu M, Wong CK, Cai Z, Dong J, Jiao D, Kam NW, Lam CWK, Tam LS. Elevated expression and pro-inflammatory activity of IL-36 in patients with systemic lupus erythematosus. Molecules 20, 19588-19604, 2015.

31) Clancy DM, Henry CM, Sullivan GP, Martin SJ. Neutrophil extracellular traps can serve as platforms for processing and activation of IL-1 family cytokines. FEBS J 284, 1712-1725, 2017.

32) Cohen PL, Eisenberg RA. *Lpr* and *gld* : Single gene models of systemic autoimmunity and lymphoproliferative disease. Annu Rev Immunol 9, 243-269, 1991.

33) Dalghi MG, Montalbetti N, Carattino MD, Apodaca G. The urothelium: Life in a liquid environment. Physiol Rev 100, 1621-1705, 2020.

34) Dang VD, Hilgenberg E, Ries S, Shen P, Fillatreau S. From the regulatory functions of B cells to the identification of cytokine-producing plasma cell subsets. Curr Opin Immunol 28, 77-83, 2014.

35) Denning SM, Le PT, Singer KH, Haynes BF. Antibodies against the CD44 p80, lymphocyte homing receptor molecule augment human peripheral blood T cell activation. J Immunol 144, 7-15, 1990.

36) Dru Forrester S, Roudebush P. Evidence-based management of feline lower urinary tract disease. Vet Clin North Am Small Anim Pract 37, 533-558, 2007.

37) Elbadawy M, Usui T, Mori T, Tsunedomi R, Hazama S, Nabeta R, Uchide T, Fukushima R, Yoshida T, Shibutani M, Tanaka T, Masuda S, Okada R, Ichikawa R, Omatsu T, Mizutani T, Katayama Y, Noguchi S, Iwai S, Nakagawa T, Shinohara Y, Kaneda M, Yamawaki H, Sasaki K. Establishment of a novel experimental model for muscle-invasive bladder cancer using a dog bladder cancer organoid culture. Cancer Sci 110, 2806-2821, 2019.

38) Eng DG, Sunseri MW, Kaverina N V., Roeder SS, Pippin JW, Shankland SJ. Glomerular parietal epithelial cells contribute to adult podocyte regeneration in experimental focal segmental glomerulosclerosis. Kidney Int 88, 999-1012, 2015.

39) Esser-von Bieren J, Volpe B, Sutherland DB, Bürgi J, Verbeek JS, Marsland BJ, Urban JF, Harris NL. Immune antibodies and helminth products drive CXCR2-dependent macrophage-myofibroblast crosstalk to promote intestinal repair. PLoS Pathog 11, 1-23, 2015.

40) Eymael J, Sharma S, Loeven MA, Wetzels JF, Mooren F, Florquin S, Deegens JK, Willemsen BK, Sharma V, van Kuppevelt TH, Bakker MA, Ostendorf T, Moeller MJ, Dijkman HB, Smeets B, van der Vlag J. CD44 is required for the pathogenesis of experimental crescentic glomerulonephritis and collapsing focal segmental glomerulosclerosis. Kidney Int 93, 626-642, 2018.

41) Fan X, Wüthrich RP. Upregulation of lymphoid and renal interferon-gamma mRNA in autoimmune MRL-Fas(lpr) mice with lupus nephritis. Inflammation 21, 105-112, 1997.

42) De Filippo K, Dudeck A, Hasenberg M, Nye E, Van Rooijen N, Hartmann K, Gunzer M, Roers A, Hogg N. Mast cell and macrophage chemokines CXCL1/CXCL2 control the early stage of neutrophil recruitment during tissue inflammation. Blood 121, 4930-4937, 2013.

43) Fournel C, Chabanne L, Caux C, Faure JR, Rigal D, Magnol JP, Monier JC. Canine systemic lupus erythematosus. I: A study of 75 cases. Lupus 1, 133-139, 1992.

44) Fragiadaki M, Mason RM. Epithelial-mesenchymal transition in renal fibrosis – evidence for and against. Int J Exp Pathol 92, 143-150, 2011.

45) Garlanda C, Dinarello CA, Mantovani A. The interleukin-1 family: Back to the future. Immunity 39, 1003-1018, 2013.

46) Garraud T, Harel M, Boutet MA, Le Goff B, Blanchard F. The enigmatic role of IL-38 in inflammatory diseases. Cytokine Growth Factor Rev 39, 26-35, 2018.

47) Gillette-Ferguson I, Sidman CL. A specific intercellular pathway of apoptotic cell death is defective in the mature peripheral T cells of autoimmunelpr andgld mice. Eur J Immunol 24, 1181-1185, 1994.

48) Girshovich A, Vinsonneau C, Perez J, Vandermeersch S, Verpont MC, Placier S,

Jouanneau C, Letavernier E, Baud L, Haymann JP. Ureteral obstruction promotes proliferation and differentiation of the renal urothelium into a bladder-like phenotype. Kidney Int 82, 428-435, 2012.

49) Grainger N, Freeman RS, Shonnard CC, Drumm BT, Koh SD, Ward SM, Sanders KM. Identification and classification of interstitial cells in the mouse renal pelvis. J Physiol 598, 3283-3307, 2020.

50) Hashim H, Woodhouse CRJ. Ureteropelvic junction obstruction. Eur Urol Suppl 11, 25-32, 2012.

51) Ho PL, Kurtova A, Chan KS. Normal and neoplastic urothelial stem cells: getting to the root of the problem. Nat Rev Urol 9, 583-594, 2012.

52) Hsu HH, Ueno S, Miyakawa H, Ogawa M, Miyagawa Y, Takemura N. Upper urolithiasis in cats with chronic kidney disease: prevalence and investigation of serum and urinary calcium concentrations. J Feline Med Surg 24, e70-e75, 2022.

53) Huvé R, Fontaine P, Blais MC, Conversy B. New findings associated with presumptive systemic lupus erythematosusin a kitten. JFMS Open Rep 6, 2055116920979271, 2020.

54) Ichii O, Hosotani M, Masum A, Horino T, Otani Y, Namba T, Nakamura T, Elewa YHA, Kon Y. Close association between altered urine–urothelium barrier and tertiary lymphoid structure formation in the renal pelvis during nephritis. J Am Soc Nephrol 33, 88-107, 2022.

55) Ichii O, Kimura J, Okamura T, Horino T, Nakamura T, Sasaki H, Elewa YHA, Kon Y. IL-36α regulates tubulointerstitial inflammation in the mouse kidney. Front Immunol 8, 1346, 2017.

56) Ichii O, Otsuka S, Sasaki N, Yabuki A, Ohta H, Takiguchi M, Hashimoto Y, Endoh D, Kon Y. Local overexpression of interleukin-1 family, member 6 relates to the development of tubulointerstitial lesions. Lab Investig 90, 459-475, 2010.

57) Ichii O, Oyamada K, Mizukawa H, Yokoyama N, Namba T, Otani Y, Elewa YHA, Sasaki N, Nakamura T, Kon Y. Ureteral morphology and pathology during urolithiasis in cats. Res Vet Sci 151, 10-20, 2022.

58) Ichii O, Yabuki A, Sasaki N, Otsuka S, Ohta H, Yamasaki M, Takiguchi M, Namiki Y, Hashimoto Y, Endoh D, Kon Y. Pathological correlations between podocyte injuries and renal functions in canine and feline chronic kidney diseases. Histol Histopathol 26, 1243-1255, 2011.

59) Irsik DL, Carmines PK, Lane PH. Classical estrogen receptors and erα splice variants in the mouse. PLoS One 8, e70926, 2013.

60) Isali I, Mahran A, Khalifa AO, Sheyn D, Neudecker M, Qureshi A, Conroy B, Schumacher FR, Hijaz AK, El-Nashar SA. Gene expression in stress urinary

incontinence: a systematic review. Int Urogynecol J 31, 1-14, 2020.

61) Iwata Y, Furuichi K, Kaneko S, Wada T. The role of cytokine in the lupus nephritis. J Biomed Biotechnol 2011, 594809, 2011.

62) Johnston A, Xing X, Guzman AM, Riblett M, Loyd CM, Ward NL, Wohn C, Prens EP, Wang F, Maier LE, Kang S, Voorhees JJ, Elder JT, Gudjonsson JE. IL-1F5, -F6, -F8, and -F9: A novel IL-1 family signaling system that is active in psoriasis and promotes keratinocyte antimicrobial peptide expression. J Immunol 186, 2613-2622, 2011.

63) Joo YH, Kim HK, Hak Choi I, Han HM, Lee KJ, Kim TH, Lee SH. Increased expression of interleukin 36 in chronic rhinosinusitis and its contribution to chemokine secretion and increased epithelial permeability. Cytokine 125, 154798, 2020.

64) Kawaguchi S. The ultrastructural changes of experimental hydroureter in rats. Japanese J Urol 72, 1399-1412, 1981.

65) Kawaguchi Y, Nishimagi E, Tochimoto A, Kawamoto M, Katsumata Y, Soejima M, Kanno T, Kamatani N, Hara M. Intracellular IL-1α-binding proteins contribute to biological functions of endogenous IL-1α in systemic sclerosis fibroblasts. Proc Natl Acad Sci U S A 103, 14501-14506, 2006.

66) Kimura N, Mizokami A, Oonuma T, Sasano H, Nagura H. Immunocytochemical localization of androgen receptor with polyclonal antibody in paraffin-embedded human tissues. J Histochem Cytochem 41, 671-678, 2017.

67) Kozawa K, Sekai M, Ohba K, Ito S, Sako H, Maruyama T, Kakeno M, Shirai T, Kuromiya K, Kamasaki T, Kohashi K, Tanaka S, Ishikawa S, Sato N, Asano S, Suzuki H, Tanimura N, Mukai Y, Gotoh N, Tanino M, Tanaka S, Natsuga K, Soga T, Nakamura T, Yabuta Y, Saitou M, Ito T, Matsuura K, Tsunoda M, Kikumori T, Iida T, Mizutani Y, Miyai Y, Kaibuchi K, Enomoto A, Fujita Y. The CD44/COL17A1 pathway promotes the formation of multilayered, transformed epithelia. Curr Biol 31, 3086-3097.e7, 2021.

68) Kreft ME, Hudoklin S, Jezernik K, Romih R. Formation and maintenance of blood–urine barrier in urothelium. Protoplasma 246, 3-14, 2010.

69) Kuppe C, Leuchtle K, Wagner A, Kabgani N, Saritas T, Puelles VG, Smeets B, Hakroush S, van der Vlag J, Boor P, Schiffer M, Gröne HJ, Fogo A, Floege J, Moeller MJ. Novel parietal epithelial cell subpopulations contribute to focal segmental glomerulosclerosis and glomerular tip lesions. Kidney Int 96, 80-93, 2019.

70) Lee JD, Lee MH. Decreased expression of zonula occludens-1 and occludin in the bladder urothelium of patients with interstitial cystitis/painful bladder syndrome. J Formos Med Assoc 113, 17-22, 2014.

71) Lee YH, Sato Y, Saito M, Fukuma S, Saito M, Yamamoto S, Komatsuda A, Fujiyama N, Satoh S, Lee SH, Boor P, Habuchi T, Floege J, Yanagita M. Advanced tertiary lymphoid

tissues in protocol biopsies are associated with progressive graft dysfunction in kidney transplant recipients. J Am Soc Nephrol 33, 186-200, 2022.

72) Lemay S, Mao C, Singh AK. Cytokine gene expression in the MRL/lpr model of lupus nephritis. Kidney Int 50, 85-93, 1996.

73) Lewington AJP, Padanilam BJ, Martin DR, Hammerman MR. Expression of CD44 in kidney after acute ischemic injury in rats. Am J Physiol Regul Integr Comp Physiol 278, R247-R254, 2000.

74) Lewis TW, Wiles BM, Llewellyn-Zaidi AM, Evans KM, O'Neill DG. Longevity and mortality in Kennel Club registered dog breeds in the UK in 2014. Canine Genet Epidemiol 5, 1-17, 2018.

75) Li Q, Liu S, Li L, Ji X, Wang M, Zhou J. Spinal IL-36γ/IL-36R participates in the maintenance of chronic inflammatory pain through astroglial JNK pathway. Glia 67, 438-451, 2019.

76) Lin L, Hwang B-J, Li N, Googe P, Diaz LA, Miao E, Vilen B, Thomas NE, Ting J, Liu Z. Non-cell-autonomous activity of the hemidesmosomal protein BP180/collagen XVII in granulopoiesis in humanized NC16A mice. J Immunol 205, 2786, 2020.

77) Liu BC, Tang TT, Lv LL, Lan HY. Renal tubule injury: a driving force toward chronic kidney disease. Kidney Int 93, 568-579, 2018.

78) Liu N, Matsumura H, Kato T, Ichinose S, Takada A, Namiki T, Asakawa K, Morinaga H, Mohri Y, De Arcangelis A, Geroges-Labouesse E, Nanba D, Nishimura EK. Stem cell competition orchestrates skin homeostasis and ageing. Nat 568, 344-350, 2019.

79) Lu LJ, Wallace DJ, Ishimori ML, Scofield RH, Weisman MH. Male SLE: A review of sex disparities in this disease. Lupus 19, 119-129, 2010.

80) Mackensen-Haen S, Bader R, Grund KE, Bohle A. Correlations between renal cortical interstitial fibrosis, atrophy of the proximal tubules and impairment of the glomerular filtration rate. Clin Nephrol 15, 167-171, 1981.

81) Mai S zhen, Li C jun, Xie X ying, Xiong H, Xu M, Zeng F qin, Guo Q, Han Y fang. Increased serum IL-36α and IL-36γ levels in patients with systemic lupus erythematosus: Association with disease activity and arthritis. Int Immunopharmacol 58, 103-108, 2018.

82) Makris K, Spanou L. Acute kidney injury: definition, pathophysiology and clinical phenotypes. Clin Biochem Rev 37, 85-98, 2016.

83) Mantovani A, Dinarello CA, Molgora M, Garlanda C. Interleukin-1 and related cytokines in the regulation of inflammation and immunity. Immunity 50, 778-795, 2019.

84) Marino CL, Lascelles BDX, Vaden SL, Gruen ME, Marks SL. Prevalence and classification of chronic kidney disease in cats randomly selected from four age groups and in cats recruited for degenerative joint disease studies. J Feline Med Surg 16, 465-

472, 2014.

85) Masum MA, Ichii O, Elewa YHA, Otani Y, Namba T, Kon Y. Vasculature-associated lymphoid tissue: a unique tertiary lymphoid tissue correlates with renal lesions in lupus nephritis mouse model. Front Immunol 11, 595672, 2020.

86) McKay S, Bromhaar MMG, de Jongste JC, Hoogsteden HC, Saxena PR, Sharma HS. Pro-inflammatory cytokines induce c-fos expression followed by IL-6 release in human airway smooth muscle cells. Mediators Inflamm 10, 135-142, 2001.

87) Menon MC, Chuang PY, He CJ. The glomerular filtration barrier: components and crosstalk. Int J Nephrol 2012, 749010, 2012.

88) Milora KA, Fu H, Dubaz O, Jensen LE. Unprocessed interleukin-36α regulates psoriasis-like skin inflammation in cooperation with interleukin-1. J Invest Dermatol 135, 2992-3000, 2015.

89) Misu N, Zhang M, Mori S, Miyazaki T, Furukawa H, Sasaki T, Nose M, Ono M. Autosomal loci associated with a sex-related difference in the development of autoimmune phenotypes in a lupus model. Eur J Immunol 37, 2787-2796, 2007.

90) Mora J, Schlemmer A, Wittig I, Richter F, Putyrski M, Frank AC, Han Y, Jung M, Ernst A, Weigert A, Brüne B. Interleukin-38 is released from apoptotic cells to limit inflammatory macrophage responses. J Mol Cell Biol 8, 426-438, 2016.

91) Mysorekar IU, Mulvey MA, Hultgren SJ, Gordon JI. Molecular regulation of urothelial renewal and host defenses during infection with uropathogenic Escherichia coli. J Biol Chem 277, 7412-7419, 2002.

92) Nishie W, Sawamura D, Goto M, Ito K, Shibaki A, McMillan JR, Sakai K, Nakamura H, Olasz E, Yancey KB, Akiyama M, Shimizu H. Humanization of autoantigen. Nat Med 13, 378-383, 2007.

93) Nishie W, Sawamura D, Natsuga K, Shinkuma S, Goto M, Shibaki A, Ujiie H, Olasz E, Yancey KB, Shimizu H. A novel humanized neonatal autoimmune blistering skin disease model induced by maternally transferred antibodies. J Immunol 183, 4088-4093, 2009.

94) Nishikawa H, Taniguchi Y, Matsumoto T, Arima N, Masaki M, Shimamura Y, Inoue K, Horino T, Fujimoto S, Ohko K, Komatsu T, Udaka K, Sano S, Terada Y. Knockout of the interleukin-36 receptor protects against renal ischemia-reperfusion injury by reduction of proinflammatory cytokines. Kidney Int 93, 599-614, 2018.

95) Nitta T, Muro R, Shimizu Y, Nitta S, Oda H, Ohte Y, Goto M, Yanobu-Takanashi R, Narita T, Takayanagi H, Yasuda H, Okamura T, Murata S, Suzuki H. The thymic cortical epithelium determines the TCR repertoire of IL-17-producing γδT cells. EMBO Rep 16, 638-653, 2015.

96) O'Neill DG, Church DB, McGreevy PD, Thomson PC, Brodbelt DC. Longevity and mortality of cats attending primary care veterinary practices in England. J Feline Med Surg 17, 125-133, 2014.
97) Otani Y, Ichii O, Masum MA, Namba T, Nakamura T, Kon Y. Castrated autoimmune glomerulonephritis mouse model shows attenuated glomerular sclerosis with altered parietal epithelial cell phenotype. Exp Biol Med 246, 1318-1329, 2021.
98) Di Paolo NC, Shayakhmetov DM. Interleukin 1α and the inflammatory process. Nat Immunol 17, 906-913, 2016.
99) Park KM, Bowers WJ. Tumor necrosis factor-alpha mediated signaling in neuronal homeostasis and dysfunction. Cell Signal 22, 977-983, 2010.
100) Peng Y, Wu S, Tang Q, Li S, Peng C. KGF-1 accelerates wound contraction through the TGF-β1/Smad signaling pathway in a double-paracrine manner. J Biol Chem 294, 8361-8370, 2019.
101) Ponte B, Felipe C, Muriel A, Tenorio MT, Liaño F. Long-term functional evolution after an acute kidney injury: a 10-year study. Nephrol Dial Transplant 23, 3859-3866, 2008.
102) Queen D, Ediriweera C, Liu L. Function and regulation of IL-36 signaling in inflammatory diseases and cancer development. Front Cell Dev Biol 7, 317, 2019.
103) Ramesh G, Reeves WB. Inflammatory cytokines in acute renal failure. Kidney Int Suppl 66, S56-S61, 2004.
104) Randles MJ, Lausecker F, Kong Q, Suleiman H, Reid G, Kolatsi-Joannou M, Davenport B, Tian P, Falcone S, Potter P, van Agtmael T, Norman JT, Long DA, Humphries MJ, Miner JH, Lennon R. Identification of an altered matrix signature in kidney aging and disease. J Am Soc Nephrol 32, 1713-1732, 2021.
105) Rudloff I, Godsell J, Nold-Petry CA, Harris J, Hoi A, Morand EF, Nold MF. Brief report: Interleukin-38 exerts antiinflammatory functions and is associated with disease activity in systemic lupus erythematosus. Arthritis Rheumatol 67, 3219-3225, 2015.
106) Rudofsky UH, Dilwith RL, Roths JB, Lawrence DA, Kelley VE, Magro AM. Differences in the occurrence of hypertension among (NZB X NZW)F1, MRL-lpr, and BXSB mice with lupus nephritis. Am J Pathol 116, 107-114, 1984.
107) Saraiva M, Vieira P, O'Garra A. Biology and therapeutic potential of interleukin-10. J Exp Med 217, e20190418, 2020.
108) Sato-Matsubara M, Matsubara T, Daikoku A, Okina Y, Longato L, Rombouts K, Thuy LTT, Adachi J, Tomonaga T, Ikeda K, Yoshizato K, Pinzani M, Kawada N. Fibroblast growth factor 2 (FGF2) regulates cytoglobin expression andactivation of human hepatic stellate cells via JNK signaling. J Biol Chem 292, 18961-18972, 2017.
109) Sato Y, Boor P, Fukuma S, Klinkhammer BM, Haga H, Ogawa O, Floege J, Yanagita

M. Developmental stages of tertiary lymphoid tissue reflect local injury and inflammation in mouse and human kidneys. Kidney Int 98, 448-463, 2020.

110) Sato Y, Mii A, Hamazaki Y et al. Heterogeneous fibroblasts underlie age-dependent tertiary lymphoid tissues in the kidney. JCI Insight 1, e87680, 2016.

111) Schiller AM, Pellegrino PR, Zucker IH. Eppur Si Muove: The dynamic nature of physiological control of renal blood flow by the renal sympathetic nerves. Auton Neurosci Basic Clin 204, 17-24, 2017.

112) Schwartzman-Morris J, Putterman C. Gender differences in the pathogenesis and outcome of lupus and of lupus nephritis. Clin Dev Immunol 2012, 604892, 2012.

113) Shin K, Lee J, Guo N, Kim J, Lim A, Qu L, Mysorekar IU, Beachy PA. Hedgehog/Wnt feedback supports regenerative proliferation of epithelial stem cells in bladder. Nature 472, 110-116, 2011.

114) Smeets B, Uhlig S, Fuss A, Mooren F, Wetzels JFM, Floege J, Moeller MJ. Tracing the origin of glomerular extracapillary lesions from parietal epithelial cells. J Am Soc Nephrol 20, 2604-2615, 2009.

115) Sorokin I, Mamoulakis C, Miyazawa K, Rodgers A, Talati J, Lotan Y. Epidemiology of stone disease across the world. World J Urol 35, 1301-1320, 2017.

116) Southcombe JH, Redman CWG, Sargent IL, Granne I. Interleukin-1 family cytokines and their regulatory proteins in normal pregnancy and pre-eclampsia. Clin Exp Immunol 181, 480-490, 2015.

117) Steinmetz OM, Velden J, Kneissler U, Marx M, Klein A, Helmchen U, Stahl RAK, Panzer U. Analysis and classification of B-cell infiltrates in lupus and ANCA-associated nephritis. Kidney Int 74, 448-457, 2008.

118) Stetler DA, Sipes DE, Jacob ST. Anti-RNA polymerase I antibodies in sera of MRL lpr/lpr and MRL +/+ autoimmune mice. Correlation of antibody production with delayed onset of lupus-like disease in MRL +/+ mice. J Exp Med 162, 1760-1770, 1985.

119) Tanimura S, Tadokoro Y, Inomata K, Binh NT, Nishie W, Yamazaki S, Nakauchi H, Tanaka Y, McMillan JR, Sawamura D, Yancey K, Shimizu H, Nishimura EK. Hair follicle stem cells provide a functional niche for melanocyte stem cells. Cell Stem Cell 8, 177-187, 2011.

120) Towne JE, Garka KE, Renshaw BR, Virca GD, Sims JE. Interleukin (IL)-1F6, IL-1F8, and IL-1F9 signal through IL-1Rrp2 and IL-1RAcP to activate the pathway leading to NF-κB and MAPKs. J Biol Chem 279, 13677-13688, 2004.

121) Tuusa J, Kokkonen N, Tasanen K. BP180/Collagen XVII: A molecular view. Int J Mol Sci 22, 12233, 2021.

122) Van De Veerdonk FL, Stoeckman AK, Wu G, Boeckermann AN, Azam T, Netea MG,

Joosten LAB, Van Der Meer JWM, Hao R, Kalabokis V, Dinarello CA. IL-38 binds to the IL-36 receptor and has biological effects on immune cells similar to IL-36 receptor antagonist. Proc Natl Acad Sci U S A 109, 3001-3005, 2012.

123) Vigne S, Palmer G, Lamacchia C, Martin P, Talabot-Ayer D, Rodriguez E, Ronchi F, Sallusto F, Dinh H, Sims JE, Gabay C. IL-36R ligands are potent regulators of dendritic and T cells. Blood 118, 5813-5823, 2011.

124) Vinsonneau C, Girshovich A, Ben M'Rad M, Perez J, Mesnard L, Vandermersch S, Placier S, Letavernier E, Baud L, Haymann JP. Intrarenal urothelium proliferation: An unexpected early event following ischemic injury. Am J Physiol Renal Physiol 299, 479-486, 2010.

125) Wang C, Ross WT, Mysorekar IU. Urothelial generation and regeneration in development, injury, and cancer. Dev Dyn 246, 336-343, 2017.

126) Wang Y, Nose M, Kamoto T, Nishimura M, Hiai H. Host modifier genes affect mouse autoimmunity induced by the lpr gene. Am J Pathol 151, 1791-1798, 1997.

127) Washino S, Hosohata K, Miyagawa T. Roles played by biomarkers of kidney injury in patients with upper urinary tract obstruction. Int J Mol Sci 21, 1-18, 2020.

128) Watanabe M, Natsuga K, Nishie W, Kobayashi Y, Donati G, Suzuki S, Fujimura Y, Tsukiyama T, Ujiie H, Shinkuma S, Nakamura H, Murakami M, Ozaki M, Nagayama M, Watt FM, Shimizu H. Type XVII collagen coordinates proliferation in the interfollicular epidermis. Elife 6, e26635, 2017.

129) Webster AC, Nagler E V., Morton RL, Masson P. Chronic kidney disease. Lancet 389, 1238-1252, 2017.

130) Weinstein AM, Giraldo NA, Petitprez F, Julie C, Lacroix L, Peschaud F, Emile JF, Marisa L, Fridman WH, Storkus WJ, Sautès-Fridman C. Association of IL-36γ with tertiary lymphoid structures and inflammatory immune infiltrates in human colorectal cancer. Cancer Immunol Immunother 68, 109-120, 2019.

131) Wilson DR, Wilson DDR. Pathophysiology of obstructive nephropathy. Kidney Int 18, 281-292, 1980.

132) Xu D, Mu R, Wei X. The roles of IL-1 family cytokines in the pathogenesis of systemic sclerosis. Front Immunol 10, 2025, 2019.

133) Xu W-D, Su L-C, Fu L, Lan Y-Y, Liu X-Y, Huang Q, Wu Q, Zhou J, Huang A-F. IL-38, a potential therapeutic agent for lupus, inhibits lupus progression. Inflamm Res 71, 963-975, 2022.

134) Xu W, Su L, Liu X, Wang J, Yuan Z, Qin Z, Zhou X, Huang A. IL-38: A novel cytokine in systemic lupus erythematosus pathogenesis. J Cell Mol Med jcmm 24, 12379-12389, 2020.

135) Yacoub W-SZ. Gender differences in systemic lupus erythematosus. Gend Med 1, 12-17, 2004.
136) Yamaguchi N, Chiba M, Mitani H. The induction of c-fos mRNA expression by mechanical stress in human periodontal ligament cells. Arch Oral Biol 47, 465-471, 2002.
137) Yamamoto S, Yanagita M. A novel pathological mechanism of tertiary lymphoid structure formation in the renal pelvis. J Am Soc Nephrol 33, 4-6, 2022.
138) Yin Z, Bahtiyar G, Zhang N, Liu L, Zhu P, Robert ME, McNiff J, Madaio MP, Craft J. IL-10 regulates murine lupus. J Immunol 169, 2148-2155, 2002.
139) Yu C, Gershwin ME, Chang C. Diagnostic criteria for systemic lupus erythematosus: A critical review. J Autoimmun 48-49, 10-13, 2014.
140) Zhang J, Wong CC, Leung KT et al. FGF18–FGFR2 signaling triggers the activation of c-Jun–YAP1 axis to promote carcinogenesis in a subgroup of gastric cancer patients and indicates translational potential. Oncogene 39, 6647-6663, 2020.